Nature and sources of Röntgen radiation

Jan T. Bonarski

Instytut Metalurgii i Inżynierii Materiałowej
im. Aleksandra Krupkowskiego
POLSKIEJ AKADEMII NAUK w Krakowie

Lectures course for Ph.D. studies at the IMIM PAN
in the summer semester of the 2011/2012 academic year

Subject: ………. Characterization of materials structure by X-ray diffraction techniques

Lecturer: ……… Jan Bonarski, Ph.D, D.Sc., professor at Polish Academy of Sciences

Internet survey of the lectures: http://anizo.imim.pl/wiki/dl/jan_bonarski_wyklad_i_mmn_2009.pdf
http://anizo.imim.pl/wiki/dl/jan_bonarski_wyklad_ii_mmn_2009.pdf

1. Nature and sources of the X-rays

2. Diffraction phenomenon of X-ray

3. Crystallography and diffraction

4. Crystallographic texture

5. X-Ray Texture Tomography

6. Texture analysis of polycrystalline materials

7. Using X-ray diffraction in materials engineering

8. X-ray phase analysis, other useful methods and the newest achievements in the field of X-ray diffraction

9. Demonstration of experimental set up and measurement procedures in the X-ray Laboratory

10. Final colloquium

Bibliography

Bojarski, Z., Łągiewka, E. (1988). Rentgenowska analiza strukturalna, PWN, Warszawa.

Bonarski, J. (2001). Rentgenowska Tomografia Teksturowa, IMIM PAN, Kraków.

Bunge, H.J. (1982). Texture Analysis in Materials Science. Mathematical Methods. Butterworths Publ. London.

James, R.W. (1954). The Optical Principles of the Diffraction of X-Rays. London: Bell and Sons Ltd.

Cullity, B.D. (1978). Elements of X-Ray Diffraction. 2nd Ed., Addison Waseley Publ.Comp.Inc., London, Amsterdam, Don Mills, Sydney, Podstawy dyfrakcji promieni rentgenowskich. tłum z j. ang., PWN (1964), Warszawa.

LaboTex. (2000). The Texture Analysis Software. by LaboSoft s.c.

Luger, P. (1989). Rentgenografia strukturalna monokryształów. PWN Warszawa, tłum. Z ang. Ed. by Walter de Gruyter, Berlin - New York, Modern X-Ray Analysis on Single Crystals

Przedmojski, J. (1990). Rentgenowskie metody badawcze w inżynierii materiałowej, WNT. Warszawa.

Sonin, A.S. (1982). O krystalografii, PWN, Warszawa.

Visible range
of
electromagnetic
radiation

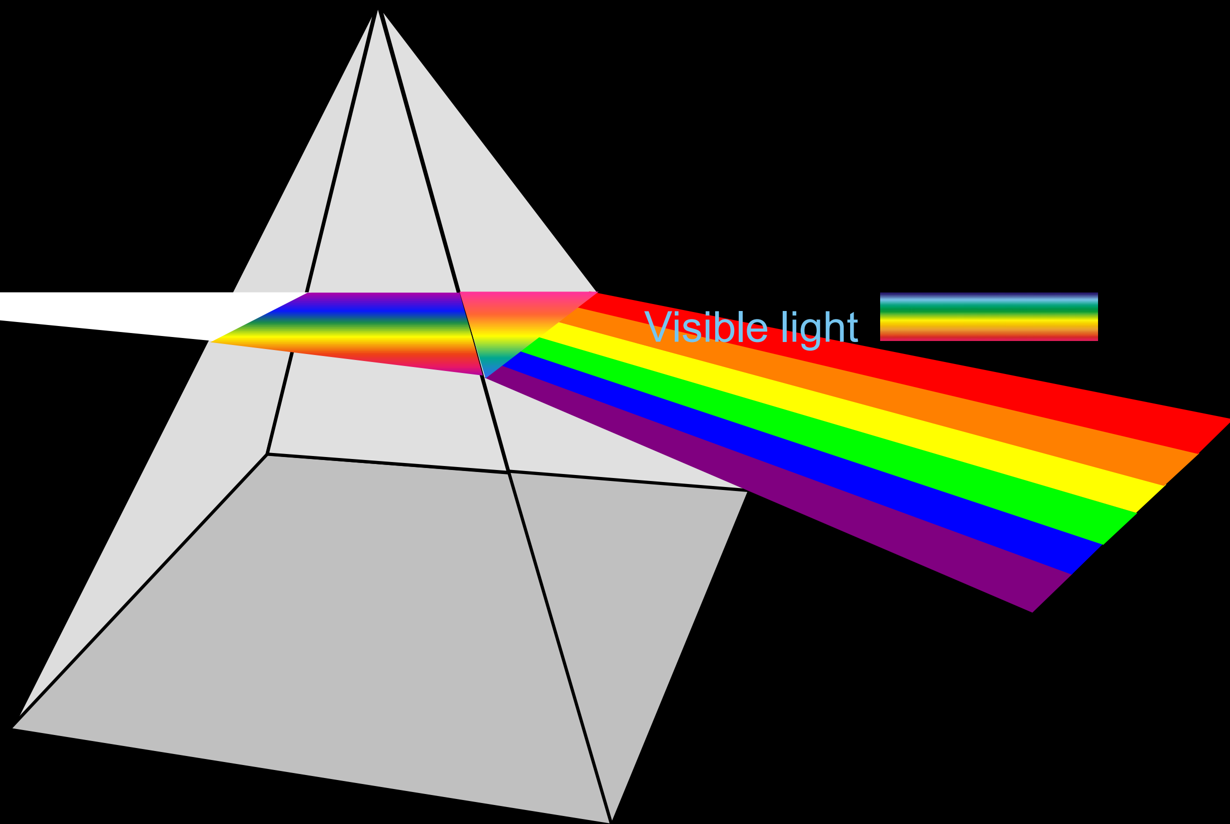

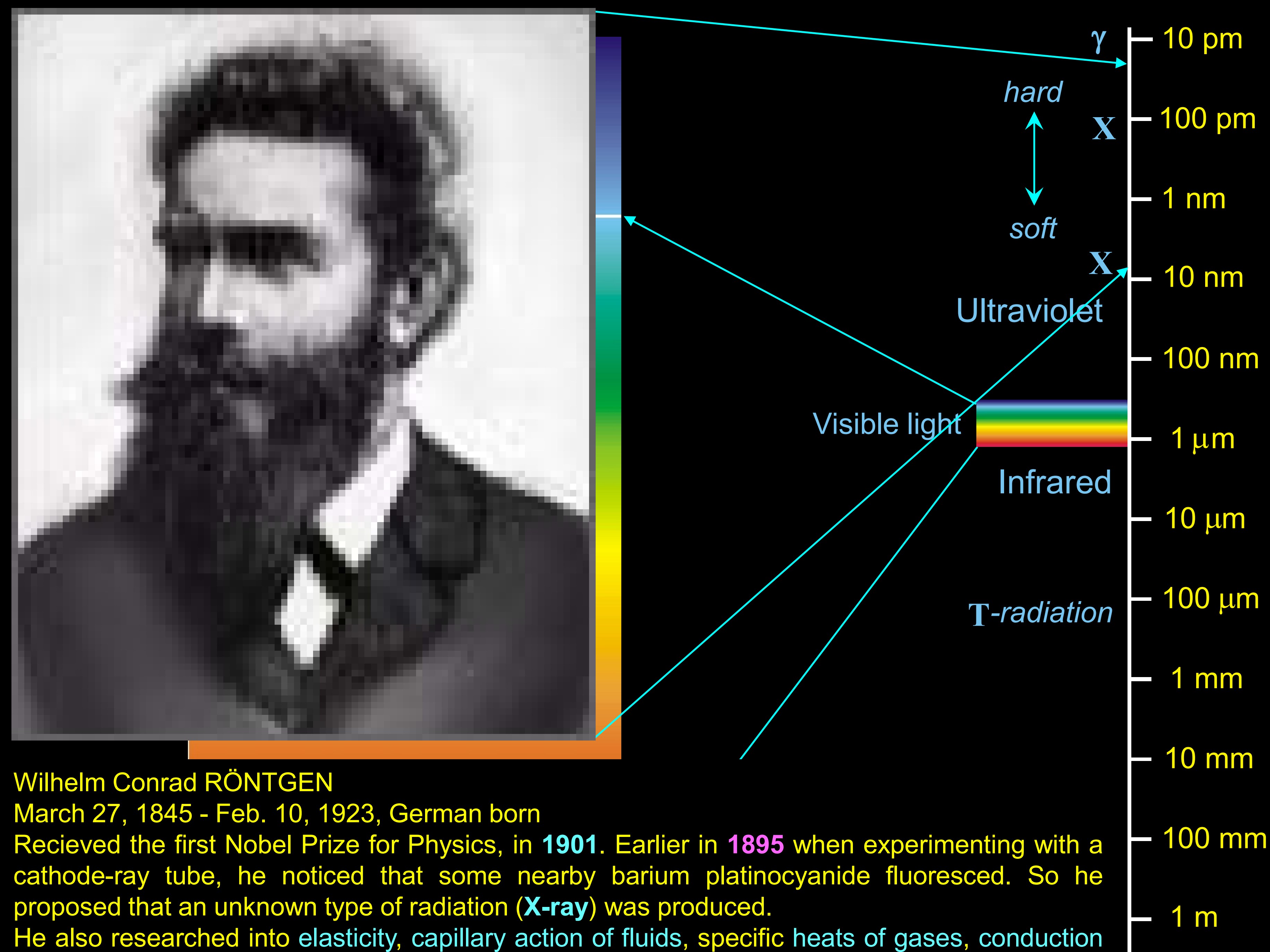

Wilhelm Conrad RÖNTGEN

March 27, 1845 - Feb. 10, 1923, German born

Recieved the first Nobel Prize for Physics, in **1901**. Earlier in **1895** when experimenting with a cathode-ray tube, he noticed that some nearby barium platinocyanide fluoresced. So he proposed that an unknown type of radiation (**X-ray**) was produced.

He also researched into elasticity, capillary action of fluids, specific heats of gases, conduction of heat in crystals, absorption of heat by gases, and piezoelectricity.

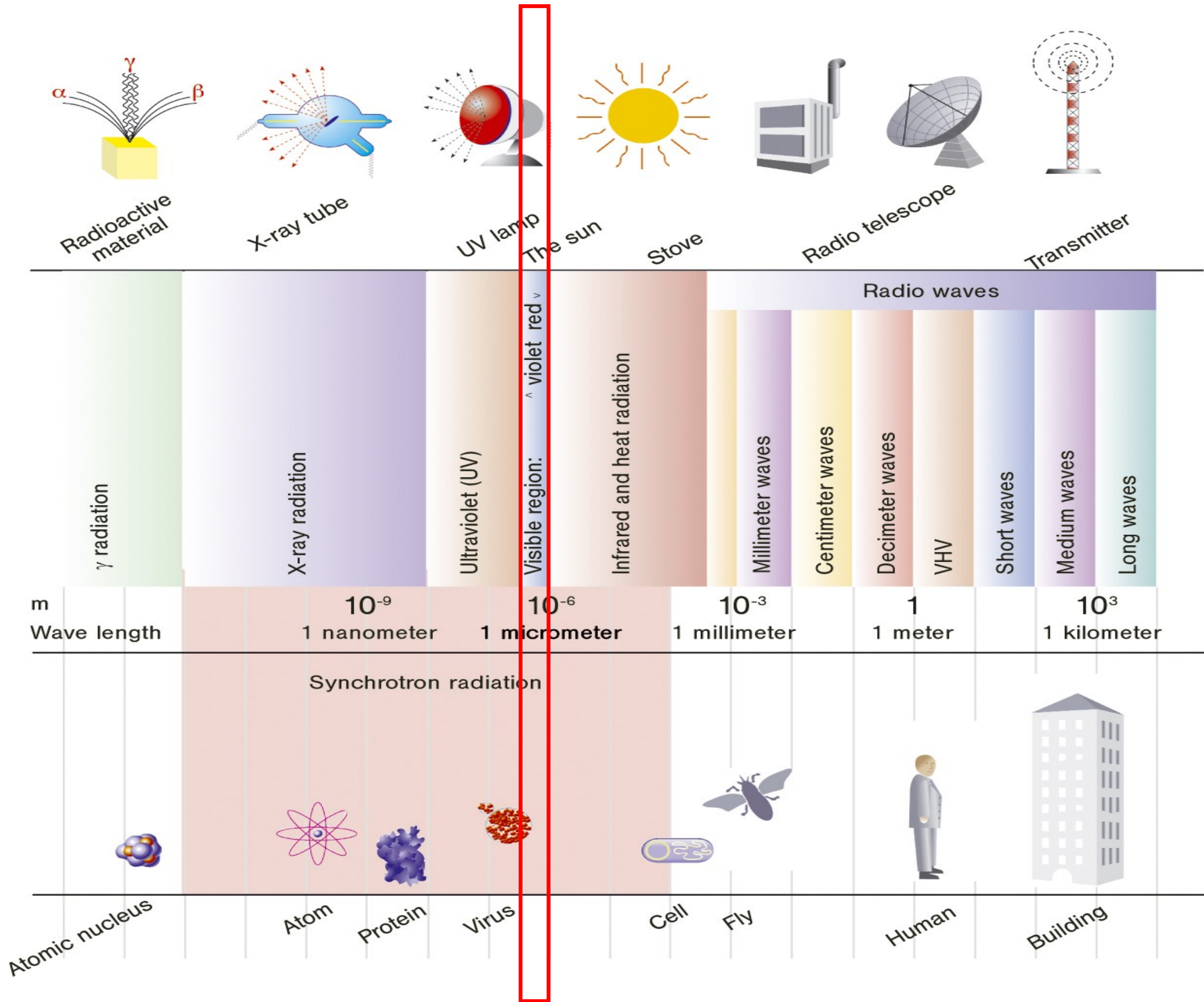

α
γ
β
Radioactive material
X-ray tube
UV lamp
The sun
Stove
Radio telescope
Transmitter
γ radiation
X-ray radiation
Ultraviolet (UV)
Visible region: < violet red >
Infrared and heat radiation
Radio waves
Millimeter waves
Centimeter waves
Decimeter waves
VHV
Short waves
Medium waves
Long waves
m
Wave length
10^-9
1 nanometer
10^-6
1 micrometer
10^-3
1 millimeter
1
1 meter
10^3
1 kilometer
Synchrotron radiation
Atomic nucleus
Atom
Protein
Virus
Cell
Fly
Human
Building

Sources of Röntgen radiation

two phenomena which generate the X-rays:

[1] Electron transitions

[2] Change of momentum of the elementary particles (electrons)

Universum [1 + 2 + black holes]

Environment of plasma generation [1]

Thermo-nuclear reactions [1 + 2]

X-ray tubes [1]

Synchrotron [2]

X-ray tubes

- traditional way of inducing the Röntgen radiation

X-ray tube

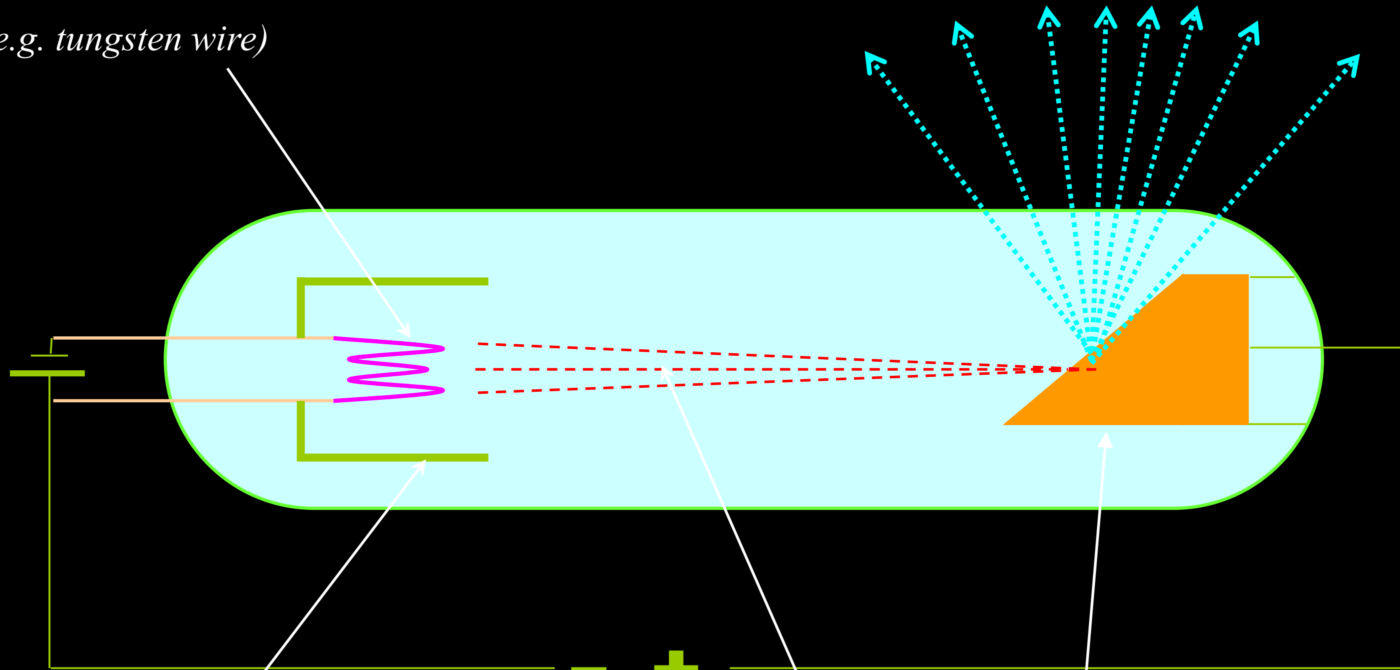

Characteristics:

- white radiation
- tube output
- focus (point/line)
- cooling system

04 kwiecień april
2012

www.po.opole.pl

05 maj may
2012

www.po.opole.pl

06 czerwiec june
2012

www.po.opole.pl

07 lipiec july
2012

www.po.opole.pl

08 sierpień august
2012

www.po.opole.pl

09 wrzesień september
2012

www.po.opole.pl

10 październik october
2012

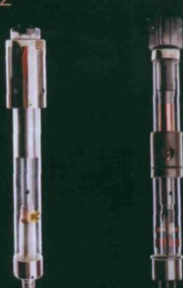

11 listopad november
2012

12 grudzień december
2012

diffraction X-ray tubes FK61 are featured by a high pri
intensity distribution, spectral purity, and a long lifetime.

X-ray tubes

, focus size, and output data can be taken from the tables. Th
tation of the elements (in brackets) contained in the sample, has

ds of application:

e Cu (Co, Fe, Mn)
ures for X-ray analysis with film chambers or diffractomet
ode W (-)
es owing to the high intensity covering the entire white spe
Anode Mo (Y, Sr, Rb)
f heavily absorbing samples
e Co (Mn, Cr, V)
ferruginous samples, such as upon stress analysis
Fe (Cr, V, Ti)
minerals
ode Cr (Ti, Sc, Ca)
f substances with large lattice constants, or for stress a

ode long anode
30.3 mm
34 mm
118 mm
207 mm

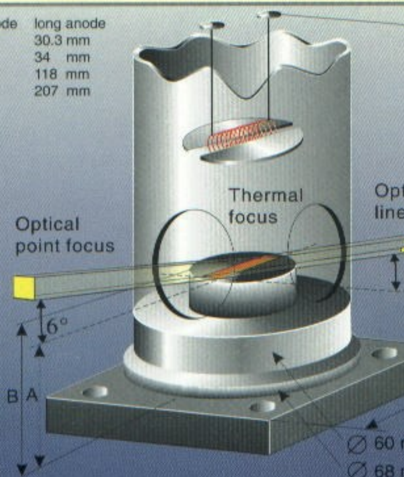

l Data

: maximum 60 kV
nt: maximum 3.8 amps
(2.8 amps micro focus)
at approx. 10 volt
0.25 mm (Cr: 0.1 mm)
diameter: 16 mm

minimum 3.5 liters/min

maximum 35 °C
e: maximum 8 bar

EIFERT & CO.
Freiberger Präzisionsmechanik GmbH
Am St. Niclas Schacht 13
D - 09599 Freiberg
eMail:SEIFERT-FPM@t-online.de
807189 Tel.:+49(03731)781266, Fax:+49(03731)781265

01 styczeń january
2012

www.po.opole.pl

02 luty february
2012

www.po.opole.pl

03 marzec march
2012

Electron configuration of ***Cu****-atom*:

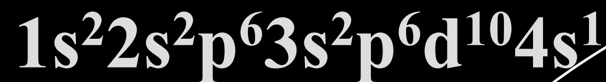

Quantum numbers describing the electron configuration are the result of description its movement by a wave equation. Non-zero solution (non-zero amplitude of electron) in the wave equation for the electron needs a complete number of its wave length for the defined orbit. For that reason the sequential numbers (quantum numbers) accurating the orbitals have been introduced: e.g. ……….. 8 states (2-"s" and 6-"p") for the electron quantum number n = 2,
……… 18 states (2-"s", 6-"p" and 10-"d") for the electron quantum number n = 3, and so on.

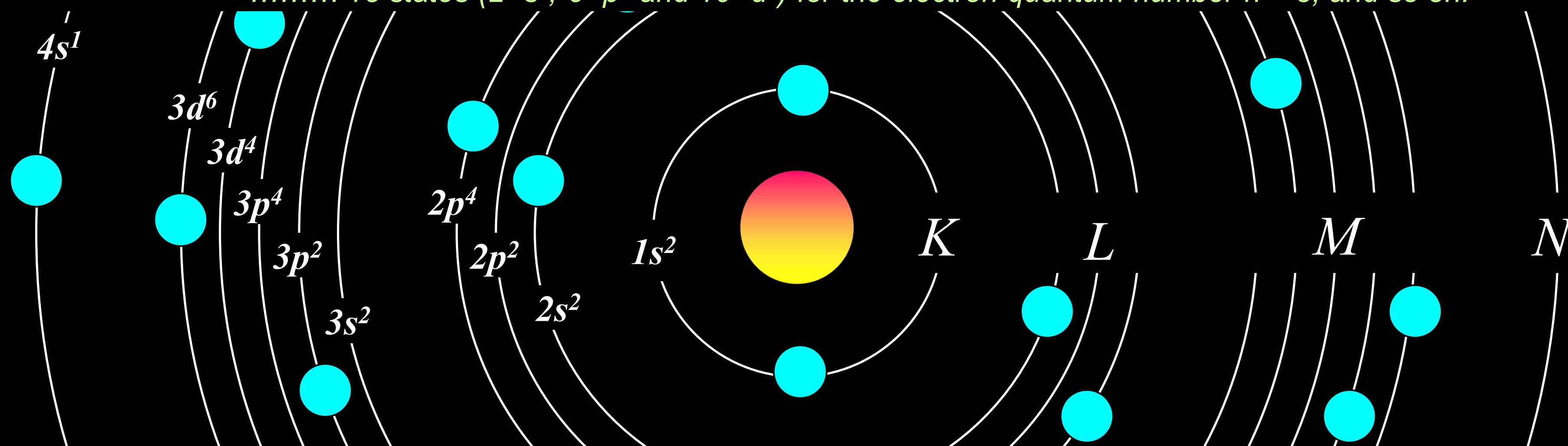

***n* (1, 2, 3…)** principal quantum number (reflects the complete wave length of the electron on its orbit with r-radius) using to estimate the electron energy.

***l* (s, p, d…)** marginal quantum number (introduced for non-circular orbits) reflects the orbital moment of momentum: *s* - relates to *l* = 0, *p* – to *l* = 1, *d* – to *l* = 2,...). *l* = 0, 1, 2, 3… n-1

Additional two quantum numbers ***m*** and ***s*** are required for a complete description of the electron state in the atom:

m - magnetic quantum number regards a various orientation of the orbital which corresponds to specific movement state: *m* = -l, (-l+1), …, 0, +1, +2, …, +*l*.

s - spin quantum number of electrons: *s* = ±½

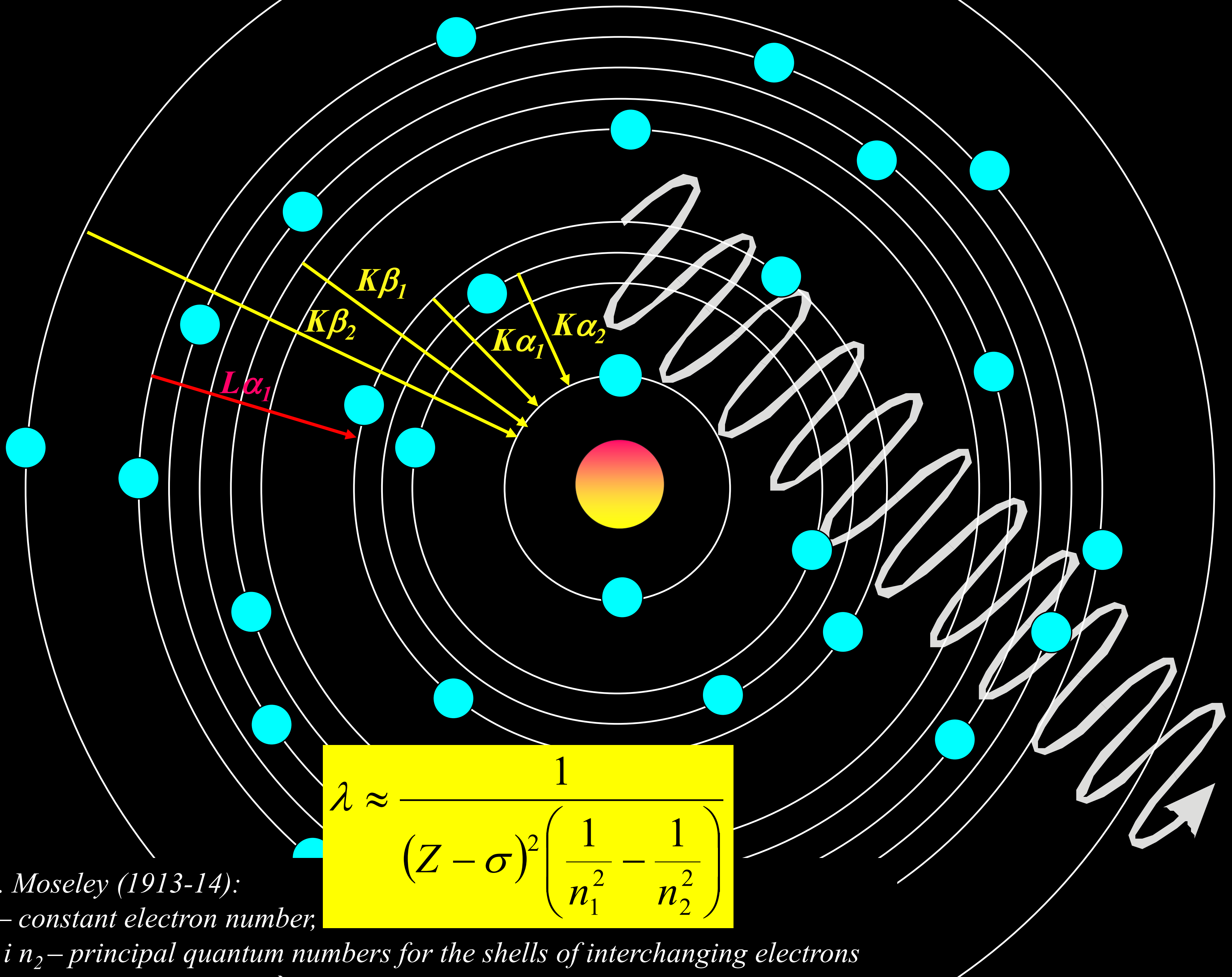

$$\lambda \approx \frac{1}{(Z-\sigma)^2\left(\frac{1}{n_1^2}-\frac{1}{n_2^2}\right)}$$

by. Moseley (1913-14):
σ – constant electron number,
n_1 i n_2 – principal quantum numbers for the shells of interchanging electrons

Characteristics:

- white radiation
- tube output (actual)
- focus (point/line)
- cooling system

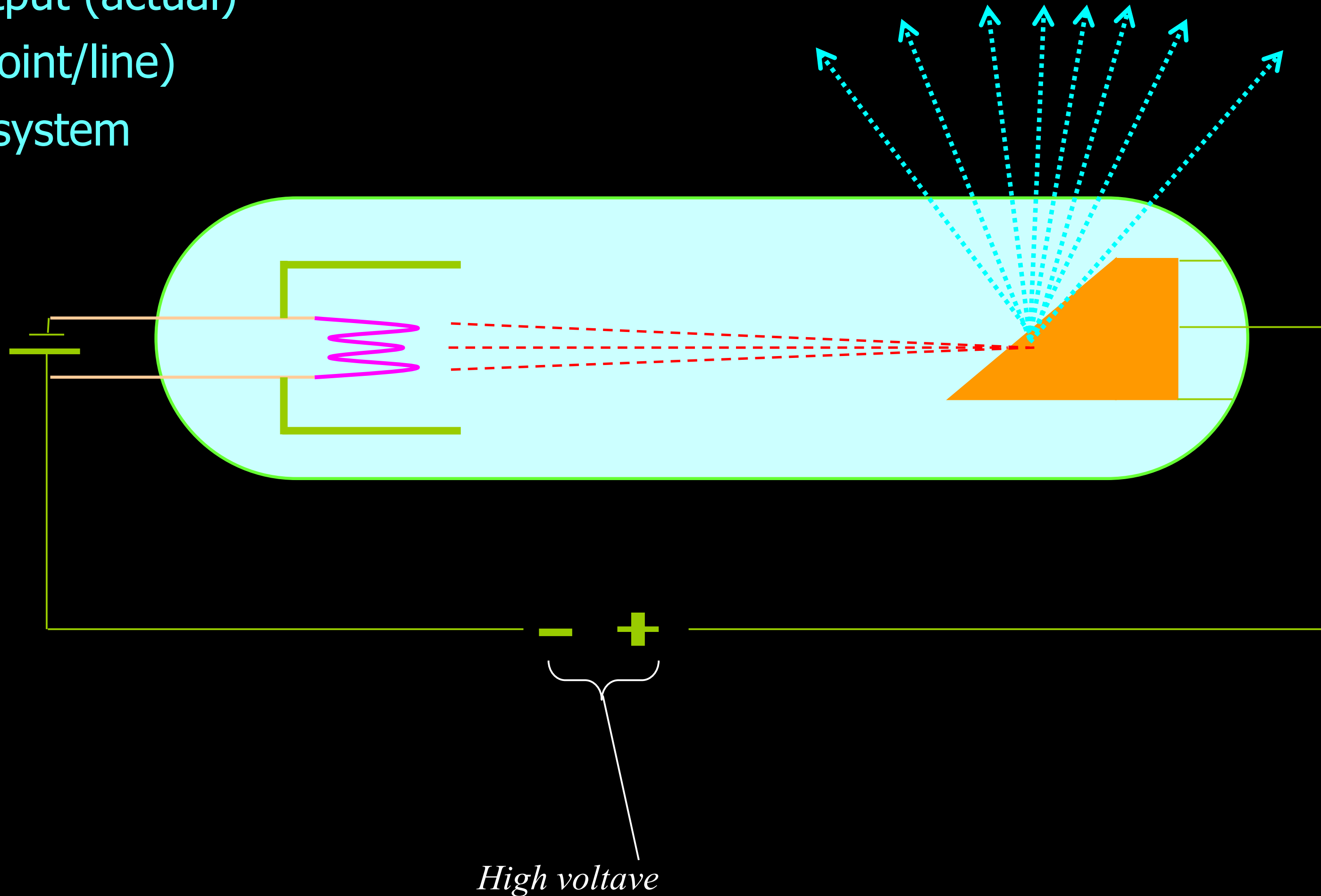

$$kinetic \quad enery \ of \quad elektron = eV = \frac{1}{2}mv^2$$

$$kinetic\ \ enery\ of\ \ elektron = eV = \frac{1}{2}mv^2$$

$$extremal\ \ case : eV = h\nu_{\max}$$

$$\lambda = \frac{c}{\nu}$$

$$\lambda_{\min} \equiv \lambda_{SwLS(KGW)} = \frac{c}{\nu_{\max}} = \frac{hc}{eV}$$

$$\lambda_{SwLS(KGW)} = \frac{(6.626 \times 10^{34})(2.998 \times 10^{8})}{(1.602 \times 10^{-19})V}\ \text{[m]}$$

$$\lambda_{SwLS(KGW)} = \frac{12.4 \times 10^{3}}{V}\ \text{[Å]}$$

Short-wave limit of spectrum
(krótkofalowa granica widma)

$$\lambda_{KGW} = \frac{12.4 \times 10^3}{V} \quad [\text{Å}]$$

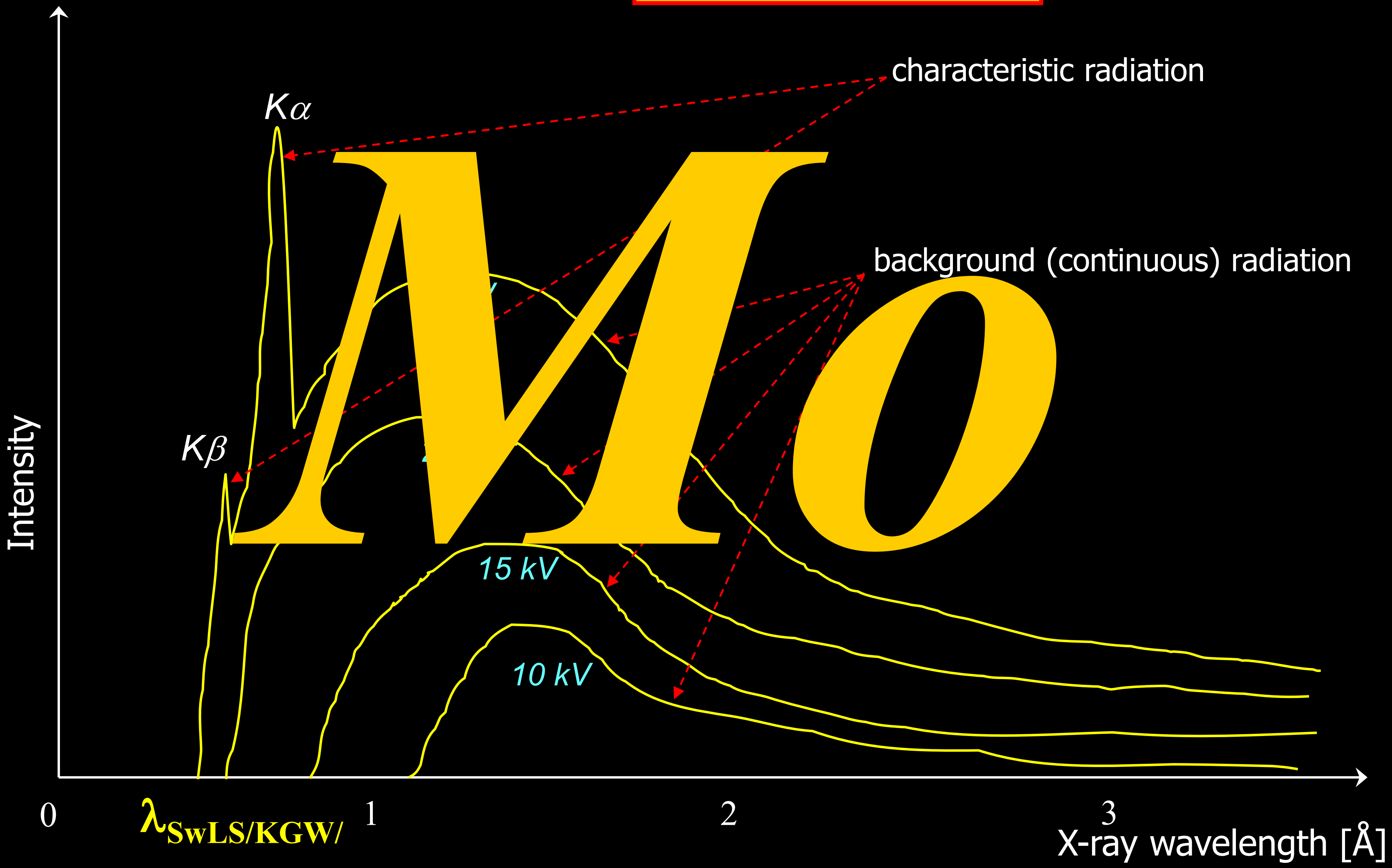

$$I_{\text{background spectrum}} = AiZV^{m}$$

W (medicine)

Intensity of the characteristic X-ray of ***i-th* element**, generated by electrons in excited, micro-volume area of massive material is proportional to contcentration of the element and depends on a depth-distribution of the emission effect

$$I_i = n_0 C_i \int_0^{\infty} \varphi_i(\rho z) d(\rho z)$$

n_0 – number of electrons falling down on sample,
C_i – concentration of *i-th* element in sample,
$\varphi_i(\rho z)$ – induction distribution function of X-ray of the *i-element* in materials

Base of X-ray microanalysis

Moseley law ($\lambda \sim 1/Z$) allow to explain the sequence of elements in periodic system which is based on the atomic number (Z) not mass number (M). For that reason, eg. cobalt (Z_{Co}=27) proceeds nickel (Z_{Ni}=28), in spite of M_{Co} (58.93) > M_{Ni} (58.69)

X-ray absorption

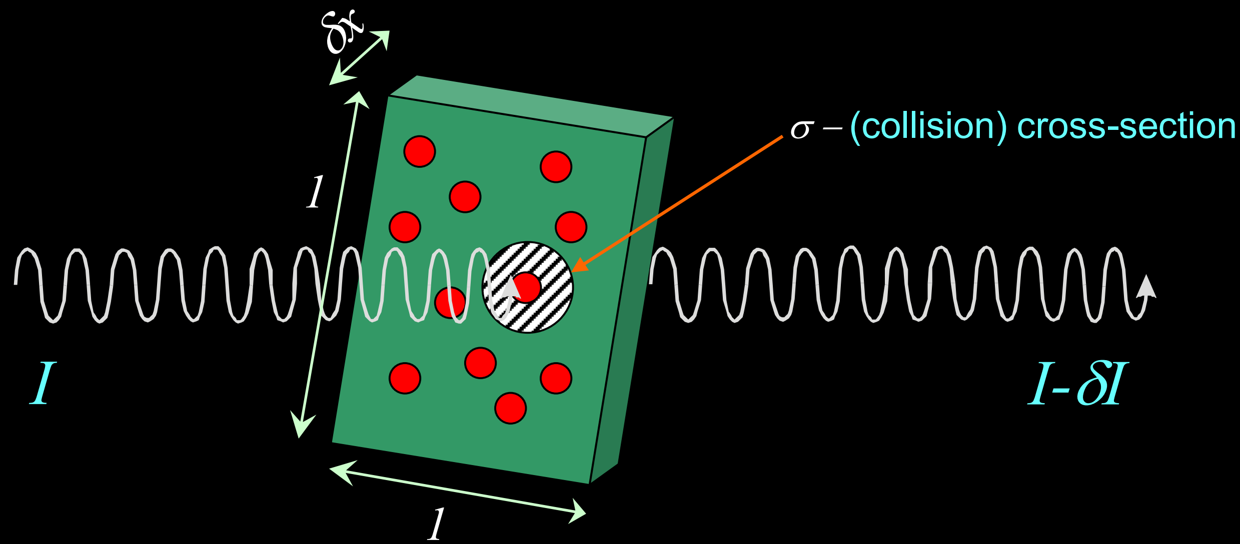

$$-\frac{\delta I}{I} = \sigma n \delta x$$

$$I = I_0 e^{-\sigma n x}$$

$\sigma n \equiv \mu$: **linear** absorption coefficient

σ – (collision) cross-section for scattering and absorption of fotons is independent of material density and thats why the **mass absorption coefficient** can be easily expressed in a form: σN/A or μρ

X-ray source

absorber

$$I = I_0 e^{-\mu x}$$

detector

Absorption edge

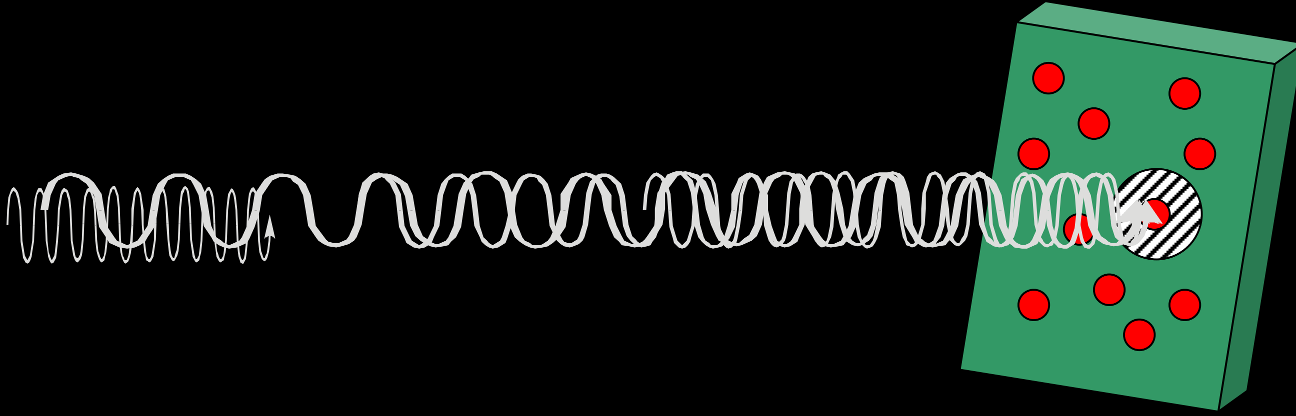

σ – (collision) cross-section for scattering and absorption of fotons <u>depends</u> on the photon energy and thats why the **filtering** of the spectrum components is possible, e.g. filter of *Kβ-component* (Ross's filter $K\alpha_1$-$K\alpha_2$)

Absorption edge

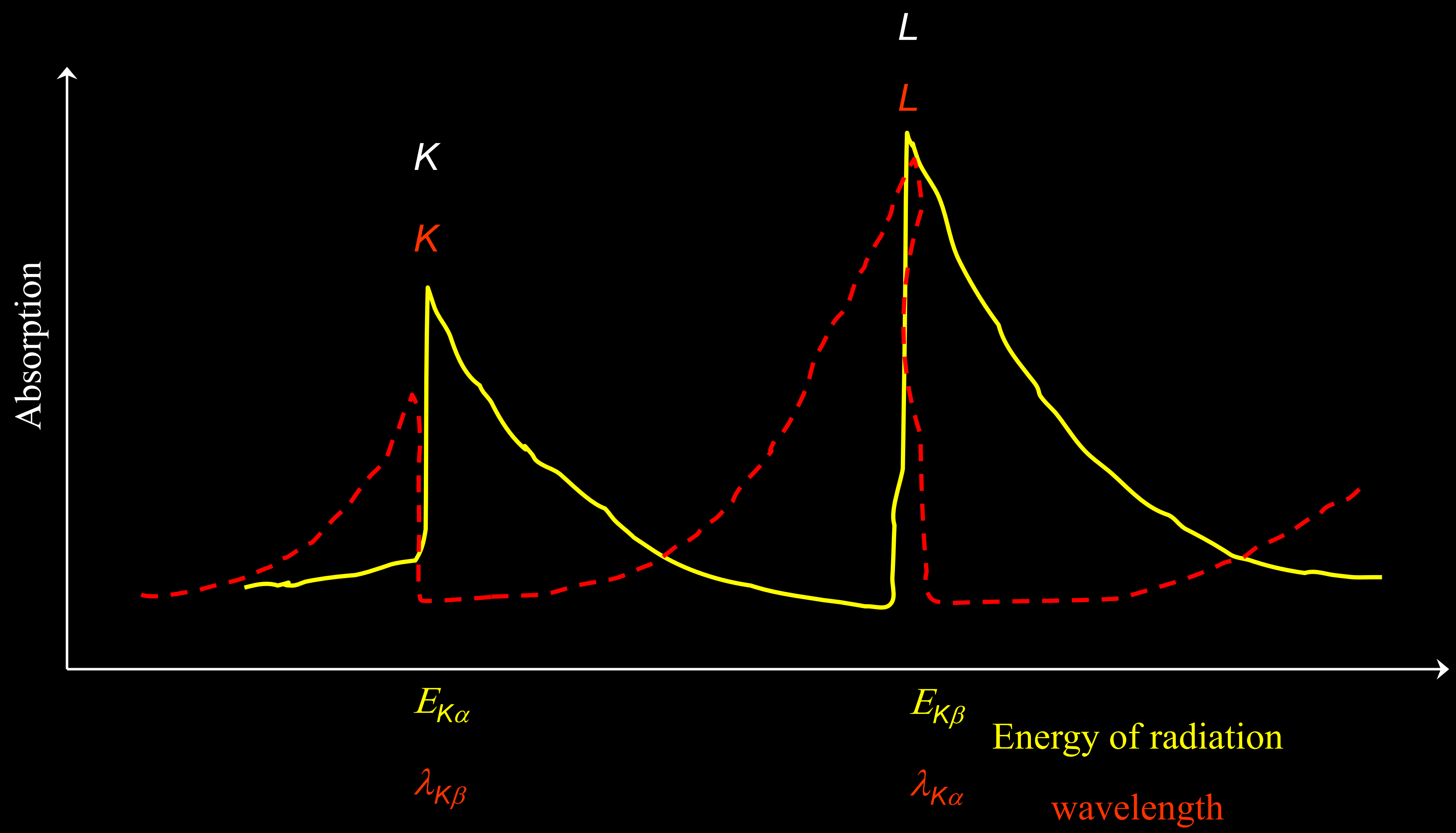

Principle of filtering the Kβ-component , ***Kα* : *Kβ* z** *5:1 do 600:1*

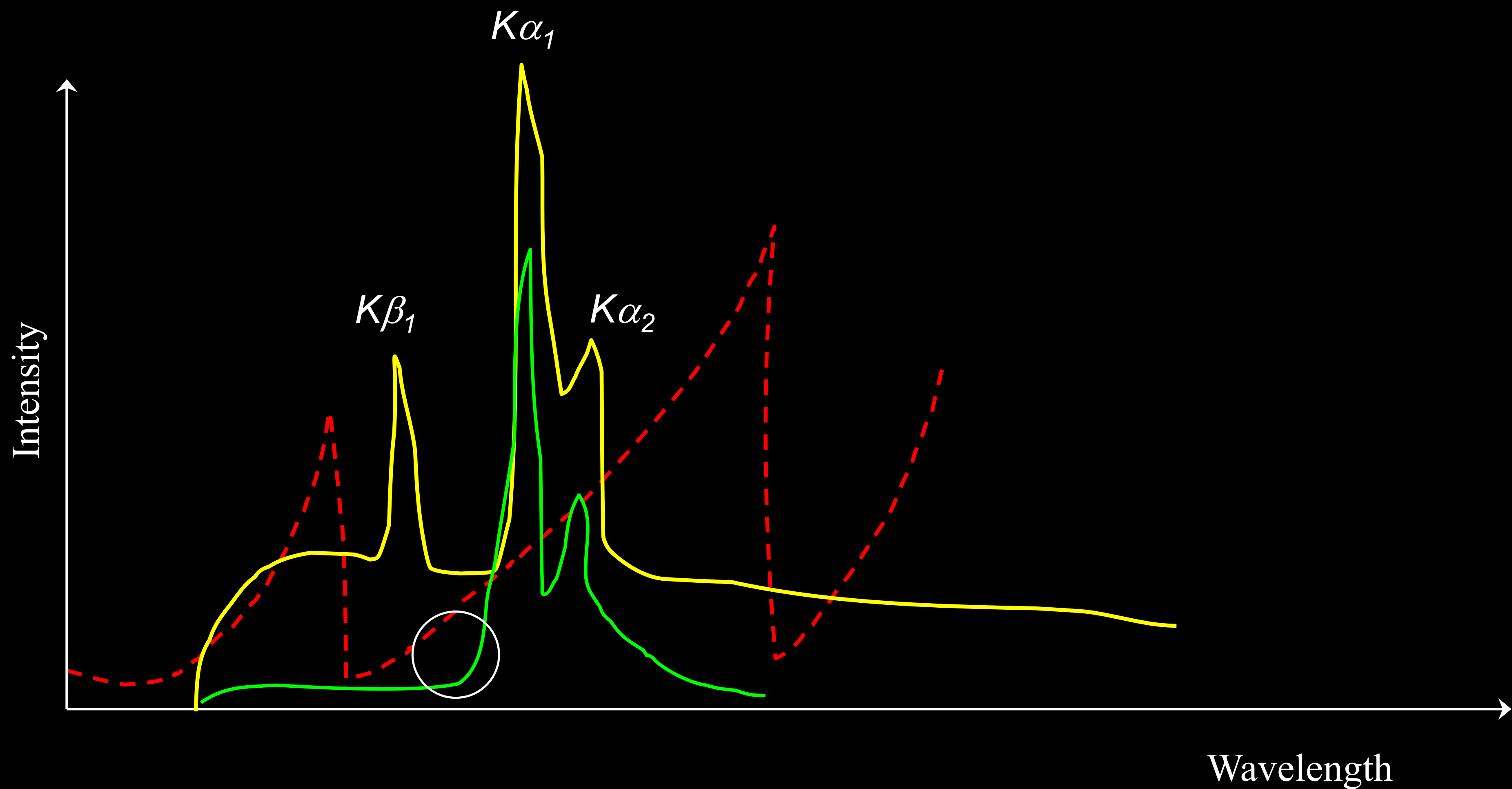

Ross’s filters

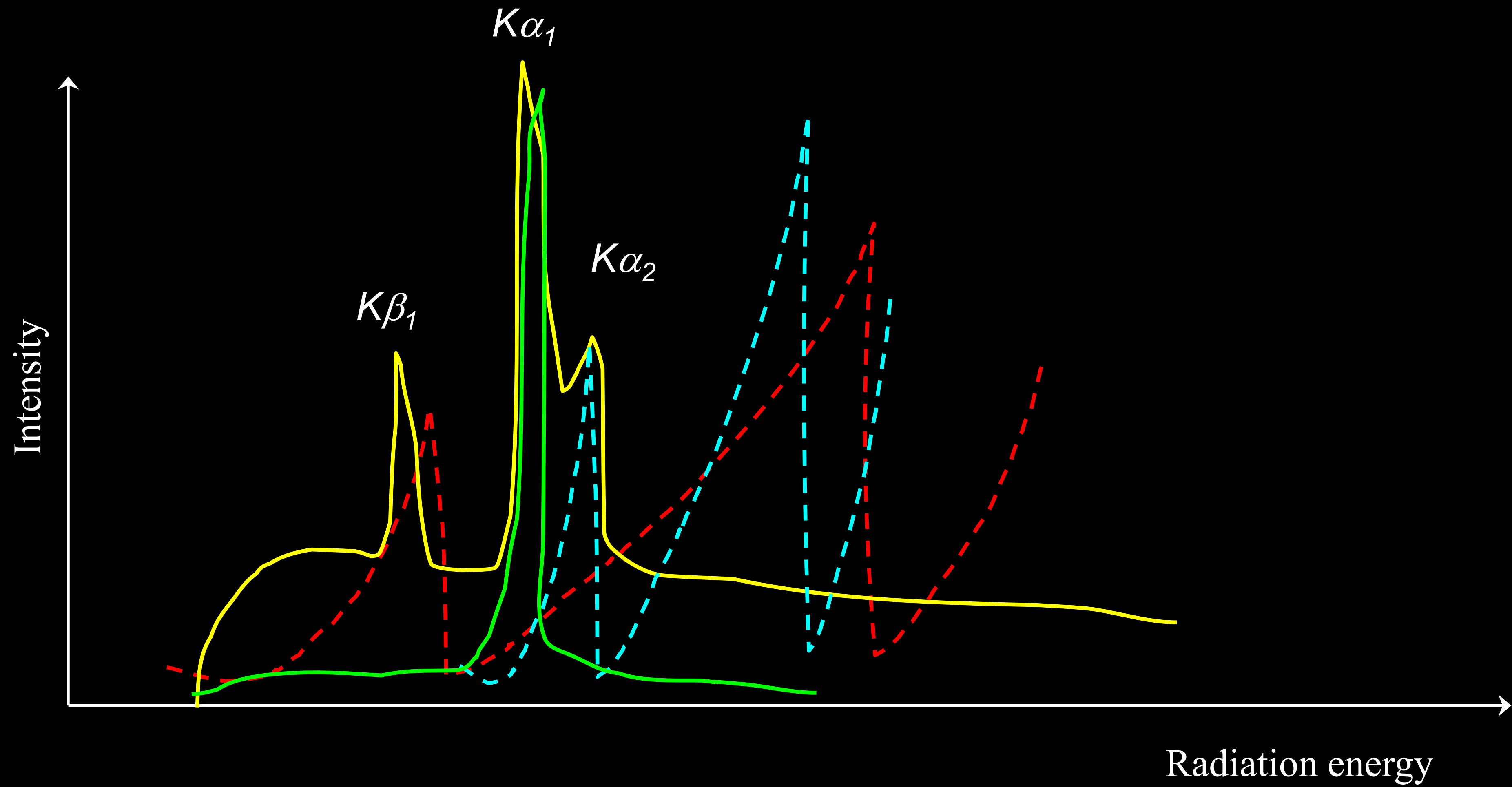

Exemplar wavelengths of the characteristic lines [Å] (by. Int. Tabl. Cryst. V. III):

Material	$K\alpha_2$	$K\alpha_1$	$K\beta_1$	***filter of*** $K\beta_1$ ***comp.***
Cr (24)	2.29351	2.28962	2.08480	*wanadium* (23)…… [0.016 mm]
Fe (26)	1.93991	1.93597	1.75653	*manganese* (25)….. [0.016 mm]
Co (27)	1.79278	1.78892	1.62075	*iron* (26)………….. [0.018 mm]
Cu (29)	1.54433	1.54051	1.39217	*nickel* (28)……….. [0.021 mm]
Mo (42)	0.71354	0.70926	0.63225	*zirconium* (40)……. [0.108 mm]

Properties of X-ray (Röntgen radiation)

(electromagnetic wave)

- scattering (coherent and fluorescent)
- absorption (attenuation in material medium)
- refraction (air - solid body; $1-n = 10^{-6}$) (załamanie)
- total reflection ($q = 10' \div 30'$)
- magneto-”optical” Kerr effect

Miniature X-Ray Generator with Pyroelectric Crystal

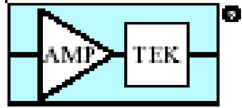

AMPTEK INC. 6 De ANGELO DRIVE, BEDFORD, MA 01730-2204 U.S.A.
Tel: +1 (781) 275-2242 ***Fax:*** +1 (781) 275-3470 ***email:*** sales@amptek.com **www.amptek.com**

Battery Operated

World's Smallest

APPLICATIONS

- Portable X-Ray Instrumentation
- Teaching Laboratories
- Instrument Calibration
- Research

FEATURES

- Miniature size - 0.6” dia x 0.4”

15 mm dia x 10 mm

- Low Power: <300 mW
- Runs on a standard 9 V battery
- Variable end point energy: up to 35 kV
- Peak X-Ray flux: 108 photons per second

(equivalent to a 2 mCi source)

- Solid state: Pyroelectric Crystal
- No radioactive sources

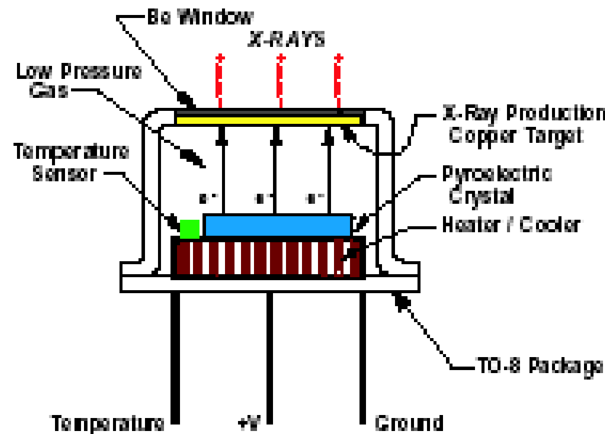

The COOL-X is a novel, miniature X-ray generator which uses a pyroelectric crystal to generate energetic electrons that produce X-rays in the target material (Cu). The hermetically sealed package has a thin beryllium window which allows the X-rays to be transmitted. The COOL-X does not use radioisotopes or high power X-ray tubes. It is a self contained, solid state system which generates X-rays when the crystal is thermally cycled.

The COOL-X is unique, and should not be compared with other X-ray tubes. It is thermally cycled between 2 to 5 minutes, and does ***not*** produce a constant flux of X-rays. The X-ray flux varies throughout the cycle and may vary from cycle to cycle, see Figure 4.

The use of the COOL-X in practical applications will challenge the user’s imagination!

Miniature X-Ray Generator with Pyroelectric Crystal

COOL-X Output Spectrum from Cu Target

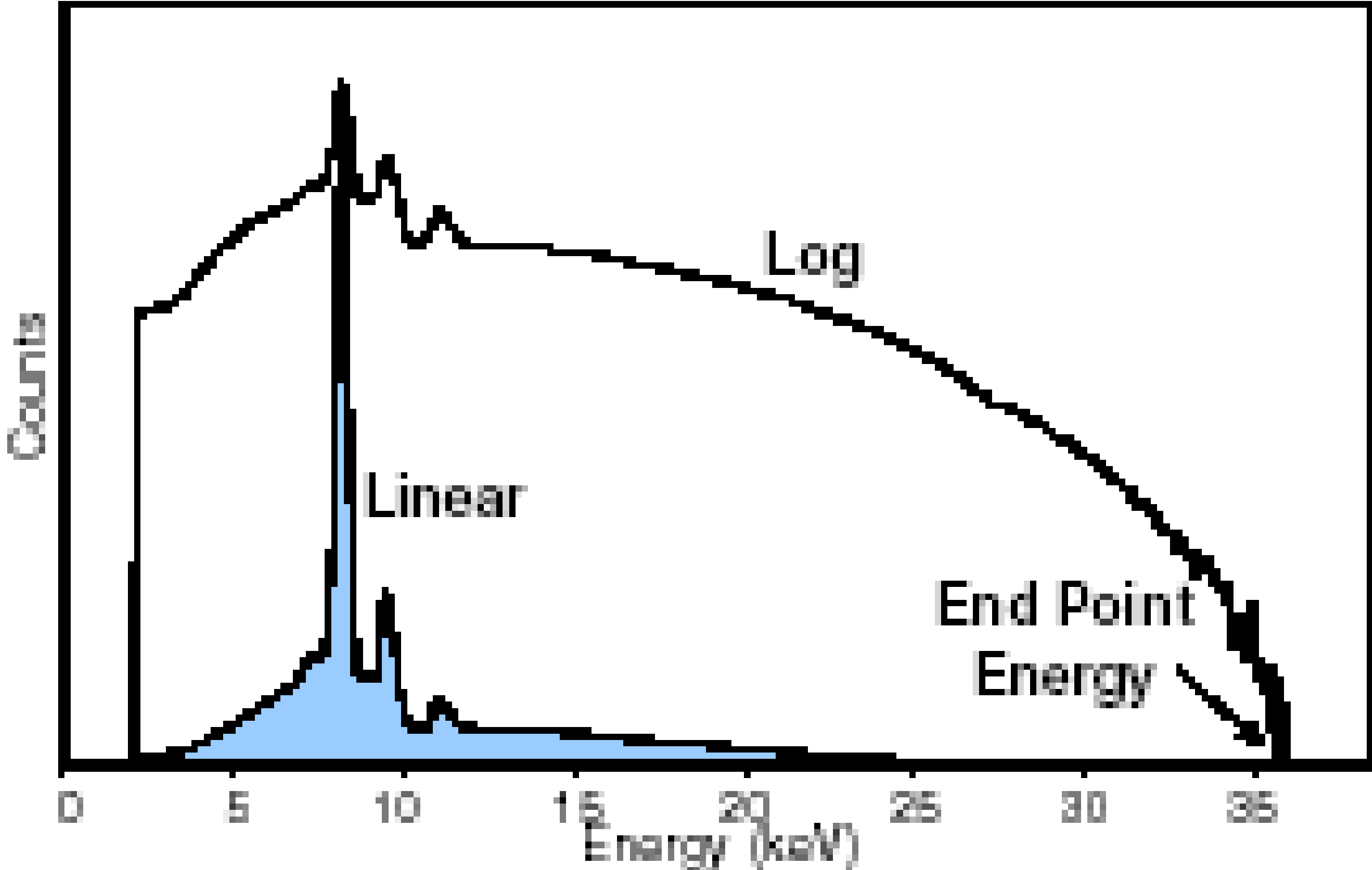

Miniature X-Ray Generator with Pyroelectric Crystal

XRF Applications

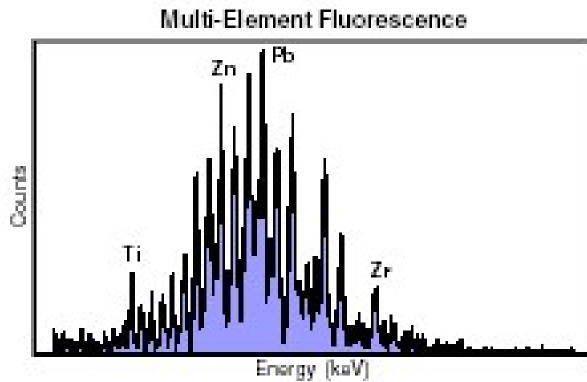

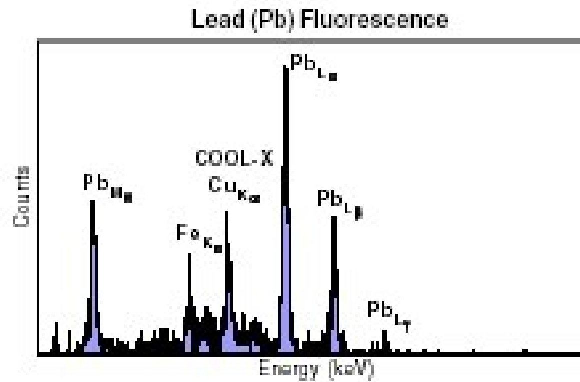

COOL-X shown with the Amptek XR-100CR
X-Ray Detector in an XRF application

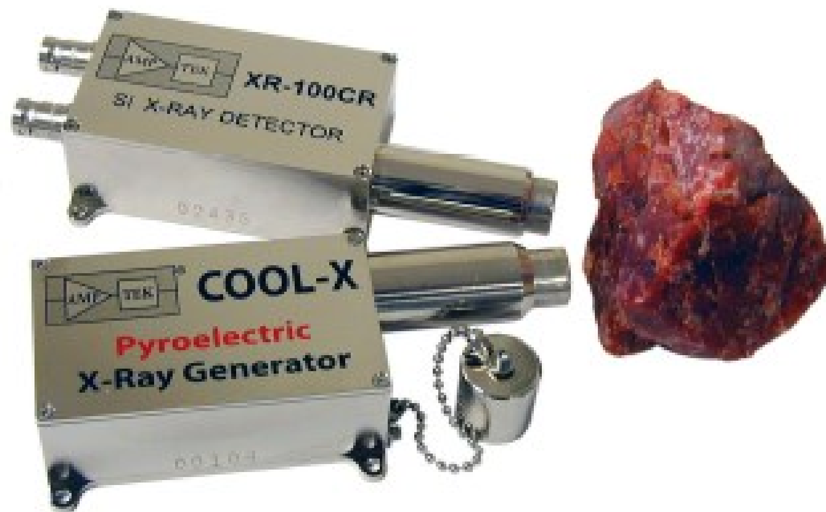

Metal-Jet X-ray Source – How does it work?

Ga (95%)/In/Sn alloy liquid metal jet, 200 µm wide, 50 m/s velocity

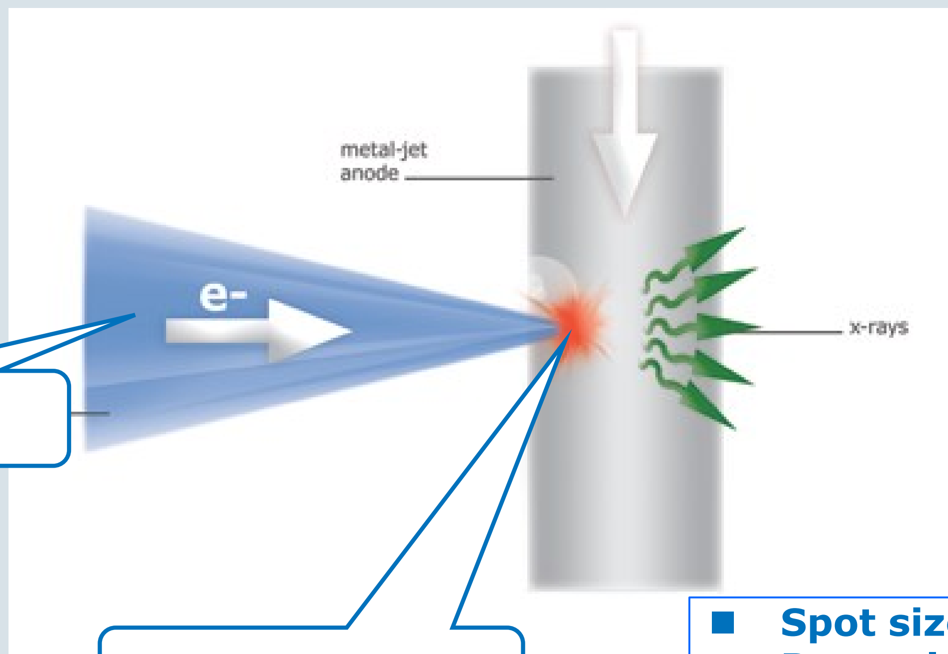

Electron beam

Target spot

- **Spot size: 5 - 20 µm**
- **Power load: up to 200 W**
- **Emission: Ga kα, 9.25 keV**

08940886(2011)24(3)

World-wide localization of synchrotron laboratories

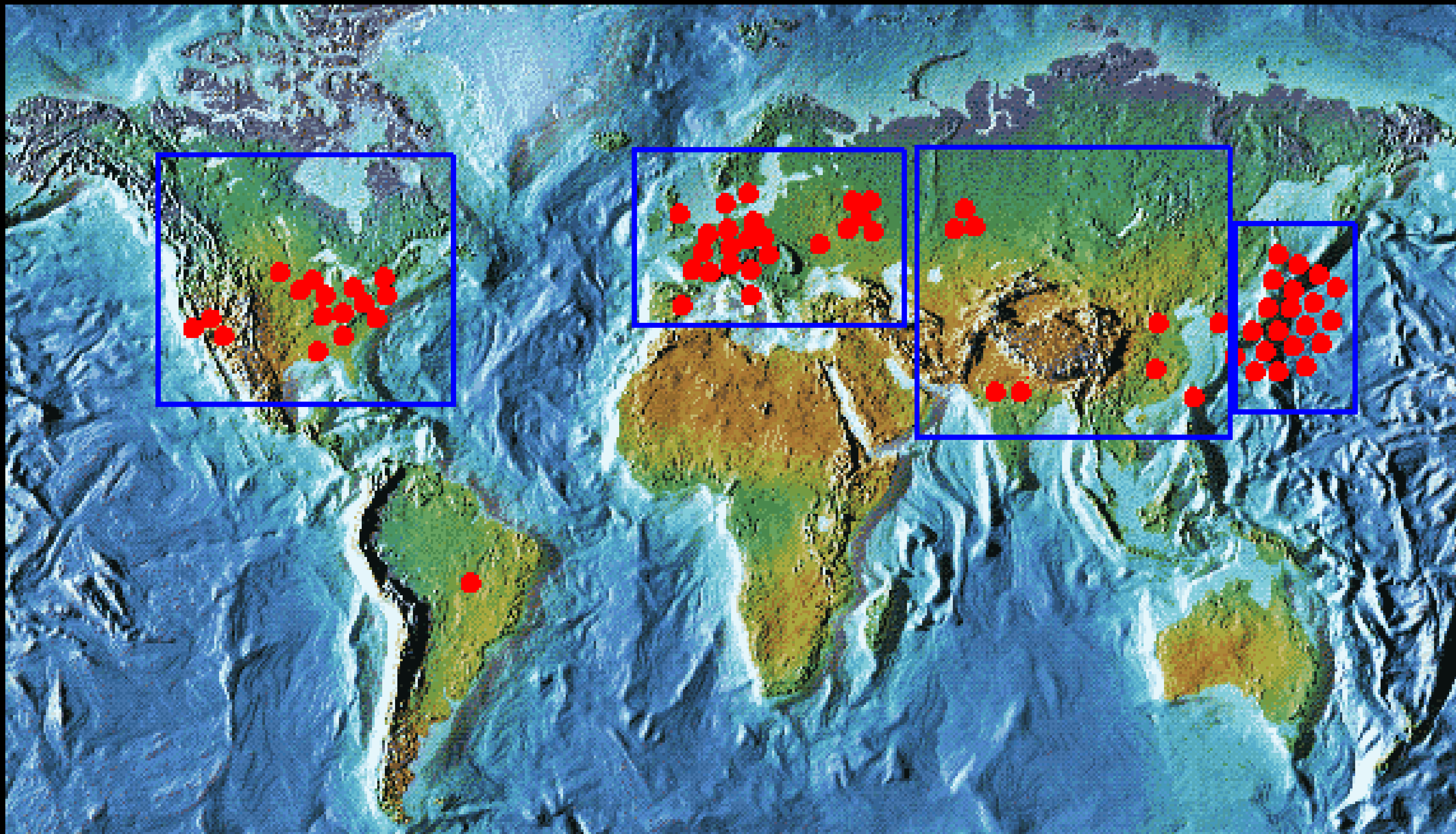

TNK
Siberia 1
Siberia 2
VEPP2
VEPP3
VEPP4
Siberia AS
Siberia SM
ASTRID
Lund
SRS
ELSA
DESY
Bessy I
AmPSMEA
Bessy II
EUTERPE
DELTA
BONN2
LURE
ANKA
ESRF
SLS
ELETTRA
LSB

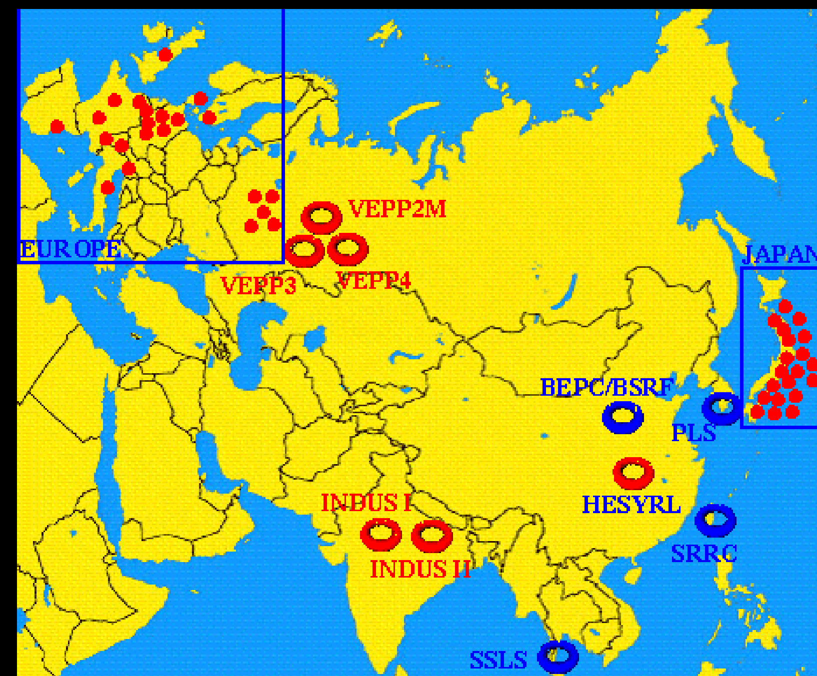
EUROPE
VEPP2M
VEPP3
VEPP4
JAPAN
BEPC/BSRF
PLS
HESYRL
INDUS I
INDUS II
SRRC
SSLS

CLS
CESR/CHESS
SXLS
APS
ALADDIN
NSLS/VUV
HELIOS
LANL
NSLS/XRAY
ALS
PEP
SPEAR / SLAC / SSRL
SURF2
DUKE FEL
LOS ALAMOS
CAMD

SORTEC
NIJI 4
NIJI 3
NIJI 2
TSSR
KEK, TSUKUBA
SPRING 8
AURORA
HISOR
KANSAI-SR
SOR KYUSHU
UVSOR Okasaki
MELCO2 AMGASAKI
SUPER ALIS Atsugi
NAR ATSUGI
SOR Ring ?

TNK
Siberia 1
Siberia 2
Lund
ASTRID
VEPP2
VEPP3
VEPP4
Siberia AS
Siberia SM
SRS
ELSA
DESY
Bessy I
AmPS
MEA
EUTERPE
Bessy II
DELTA
BONN2
ANKA
LURE
SLS
ELETTRA
ESRF
LSB

Diffractometry
recognizing the internal structure of matter

Medical diagnostic/therapy
human/animal treating, life elongation/comfort

Spectrometry
identification of chemical composition

Industrial radiography
safety of exploitation, quality control

Scientific research
modification of genetic structure by irradiation

Investigation of fast phenomena
flash inspection in synchrotron

Metrology
thickness of coatings, keeping the horizontal level

Food production
detection of forein bodies, preservation

X-ray litography
patterns on Si-plates

Sterilisation
medical tools/materials

Neutralization of electrostatic charges
in manufacturing the paper and plastics

Public security
ilumination of passangers/baggage, terrorism prevention

X-ray Astronomy
observation of universum

Archeology
non-destructive inspection of historic objects

Based on „Kalendarz Politechniki Opolskiej", 2012

Radiogram lilii oraz anturium wykonany przez D. Taskera w 1937 r. (zaczerpnięto z http://www.flickr.com)

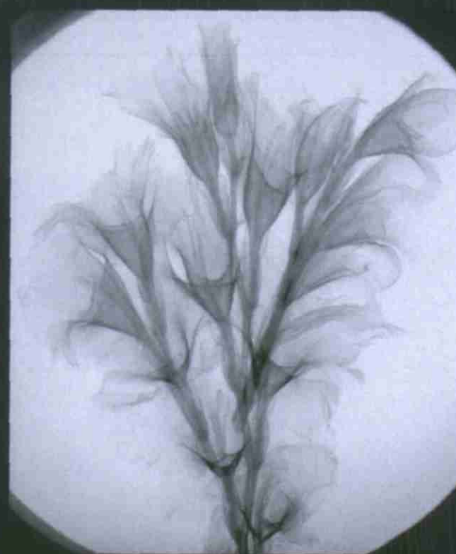

Radiogramy kwiatów Merrilla C. Raikesa [15]

Radiogramy kwiatów Alberta Richardsa: yucca (1993), begonia (1996) oraz azalia (1990); (zaczerpnięto z http://www.luminous-lint.com/app/vexhibit/_PHOTOGRAPHER_Albert__Richards_01/4/0/0/)

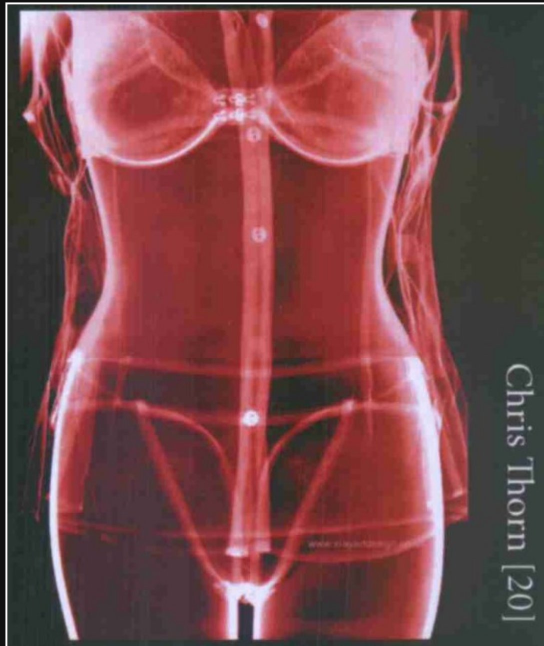

Chris Thorn [20]

Wybrana strona (kwiecień) z kalendarza 2011 firmy Eizo [36]

Wybrane grafiki Yrija Szapakowskiego

Wybrane radiogramy dużych obiektów technicznych - Nick Veasey [22]

Aracor's Eagle[2]

[2]www.aracor.com

Cocaine hidden near rear window well and quarter panel

Stowaways hidden amongst cargo

Bibliography

- **Study of the Author**
- **Original publications**
- **Internet websites: HASYLAB, *http://srdweb2.dl.ac.uk/srs/srworld/***
- **Reports: *European Science Foundation***
- **Presentations: Leszek Tarkowski (2001), Bartosz Górka (2001)**
- **Popular journals: Świat Nauki (Scientific American)**
- **Books:**

James, R.W. (1954).
The Optical Principles of the Diffraction of X-Rays. London: Bell and Sons Ltd.

Cullity, B.D. (1978).
Elements of X-Ray Diffraction. 2nd Ed., Addison Waseley Publ.Comp.Inc., London, Amsterdam, Don Mills, Sydney,
Podstawy dyfrakcji promieni rentgenowskich. tłum z j. ang., PWN (1964), Warszawa

Bunge, H.J. (1982).
Texture Analysis in Materials Science. Mathematical Methods. Butterworths Publ. London

Bibliography (cont.)

Sonin, A.S. (1982).
O krystalografii, PWN, Warszawa.

Bojarski, Z., Łągiewka, E. (1988).
Rentgenowska analiza strukturalna, PWN, Warszawa.

Luger, P. (1989).
Rentgenografia strukturalna monokryształów. PWN Warszawa, tłum. Z ang. Ed. by Walter de Gruyter, Berlin - New York, *Modern X-Ray Analysis on Single Crystals*

Przedmojski, J. (1990).
Rentgenowskie metody badawcze w inżynierii materiałowej, WNT. Warszawa.

LaboTex. (2000).
The Texture Analysis Software. by LaboSoft s.c.

Bonarski, J. (2001).
Rentgenowska Tomografia Teksturowa, IMIM PAN, Kraków.

X-ray scattering by a free atom

Thomson factor
(mass of nucleus can be neglected)

$$I_0 = I_0 \left(\frac{e^2}{mc^2} \right)^2 \frac{1}{R^2} \frac{1+\cos^2 2\theta}{2}$$

Size of atom <u>can not be neglected</u>; electrons are not concentrated in one point!
For that reason the scattered wave is summarized over all electrons in atom, regarding amplitudes and phases of individual waves

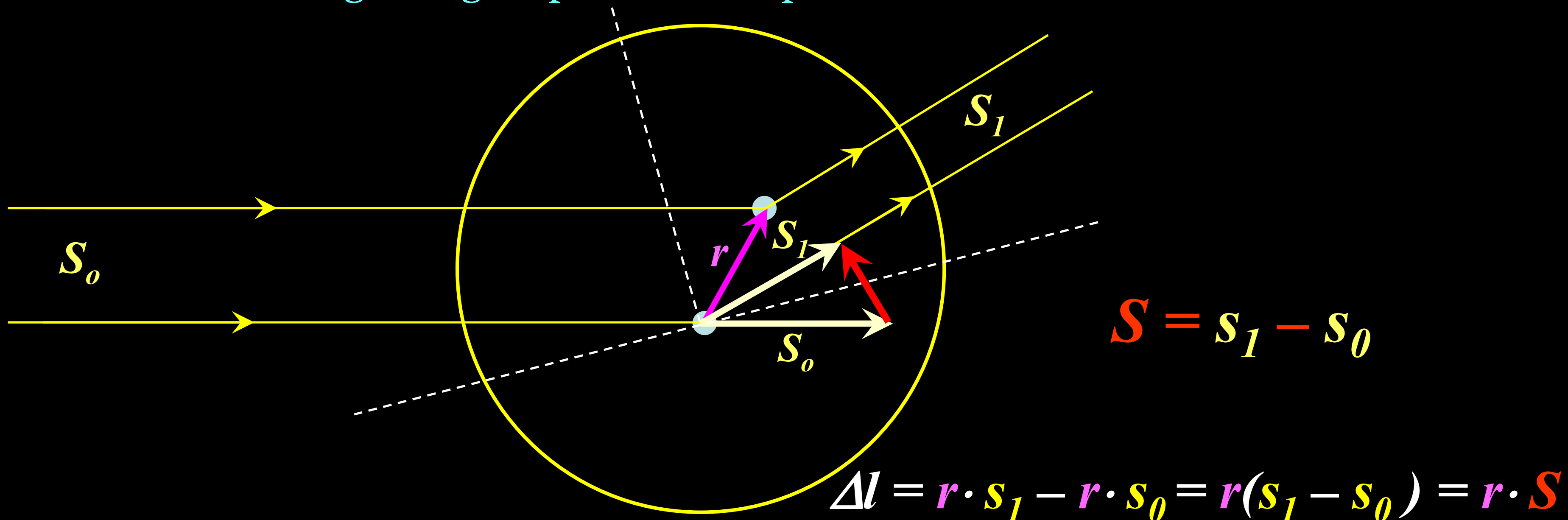

Fine-Structure Constant

Arnold Sommerfeld: $\alpha = \frac{e^2}{\hbar c \, 4\pi\varepsilon_0} = 7,2973525698(24) \times 10^{-3} = \frac{1}{137,035999074(44)}$

e – electron charge
$\hbar = h/(2\pi)$ – Planck constant
c – light velocity
ε_0 – permitivity of free space (przenikalność elektryczna próżni)

$\alpha \approx 1/137$ ($\alpha \approx 1/128$ for energy = particle mass)

By watching the far distant quasars the astronoms can to register a primeval light

The world-largest radiotelescope (∅40m) with moving focusing cap:

Green Bank (West Virginia,USA)

New project:
summarized area of the focusing cap = **1 km²**
(Australia, 2012-2015):

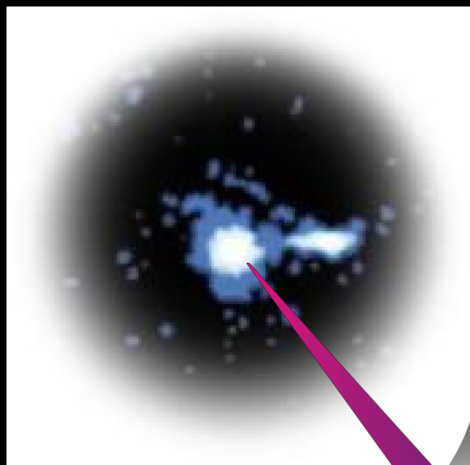

Absorption spectrum

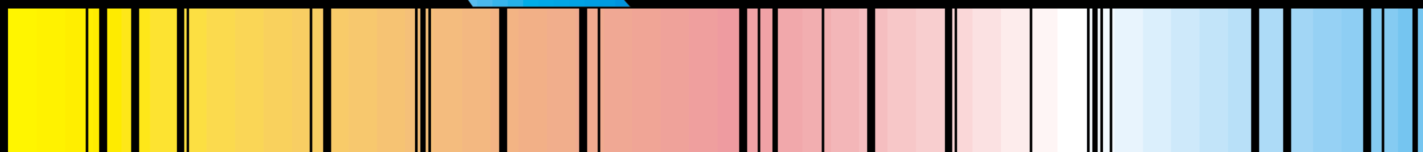

Diagnostics of microstructure

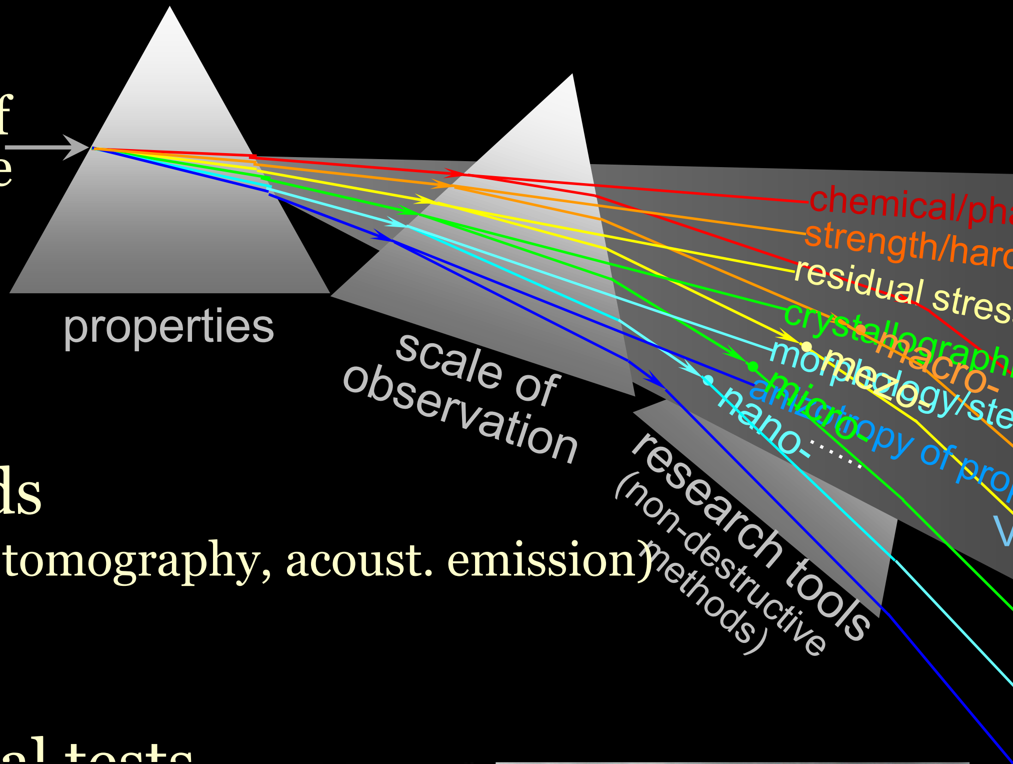

...Ultrsounds

(defctoscopy, tomography, acoust. emission)

...Mechanical tests

(strength, har

...Chemical

(corrosion pr

γ-ray
Electron beam
Hard X-ray
Soft X-ray
Ultra-violet
Visible light
Infra-red
Thermal rad.
Microwave

10 pm
100 pm
1 nm
10 nm
100 nm
1 µm
10 µm
100 µm
1 mm
10 mm
100 mm
1 m

Microstructure inhomogeneity

...distinguishing feature of FGM

X-ray diffraction phenomenon. Part I

Jan T. Bonarski

Instytut Metalurgii i Inżynierii Materiałowej
im. Aleksandra Krupkowskiego
POLSKIEJ AKADEMII NAUK w Krakowie

Diffraction theories of X-ray on condensed matter

Various extent of generality

geometrical → describes **only directions**, in which the diffracted rays are observed (no intensity predictions)

kinematical → describes (among others) **intensity** of radiation and is correct in the case of defected and relatively fine-grained materials to fulfil relation: $I_{(scattered)} << I_{(diffracted)}$. No extinction is regarded

dynamical → Describes diffraction on materials with enough large areas of coherent scattering with L dimmension ($\mu L > 0.01$)

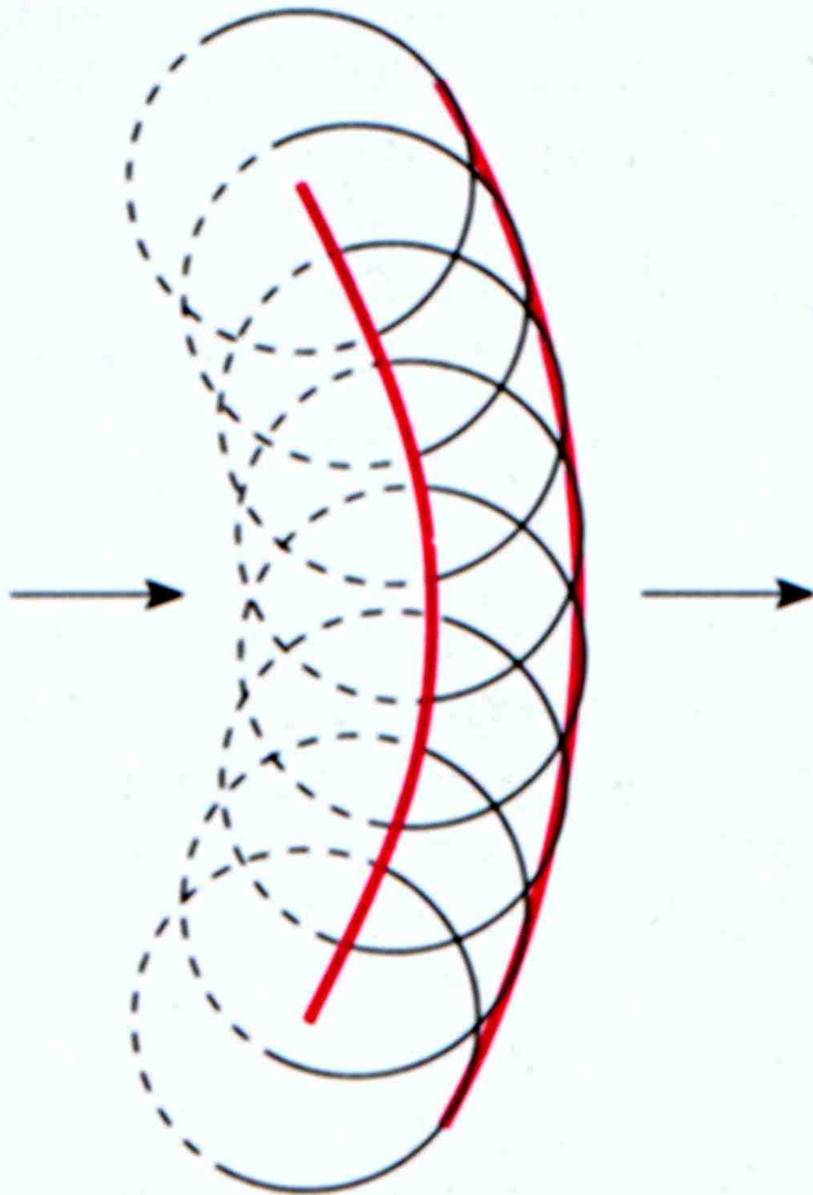

Powstawanie nowej powierzchni falowej jako obwiedni fal cząstkowych

Christian **HUYGENS**
(1629-1695),
1678: outline of light theory

HUYGENS explained mechanizm of waves propagation

FRESNEL
1818: perturbation in any point is a result of interference of elementary waves regarding its amplitude and phase

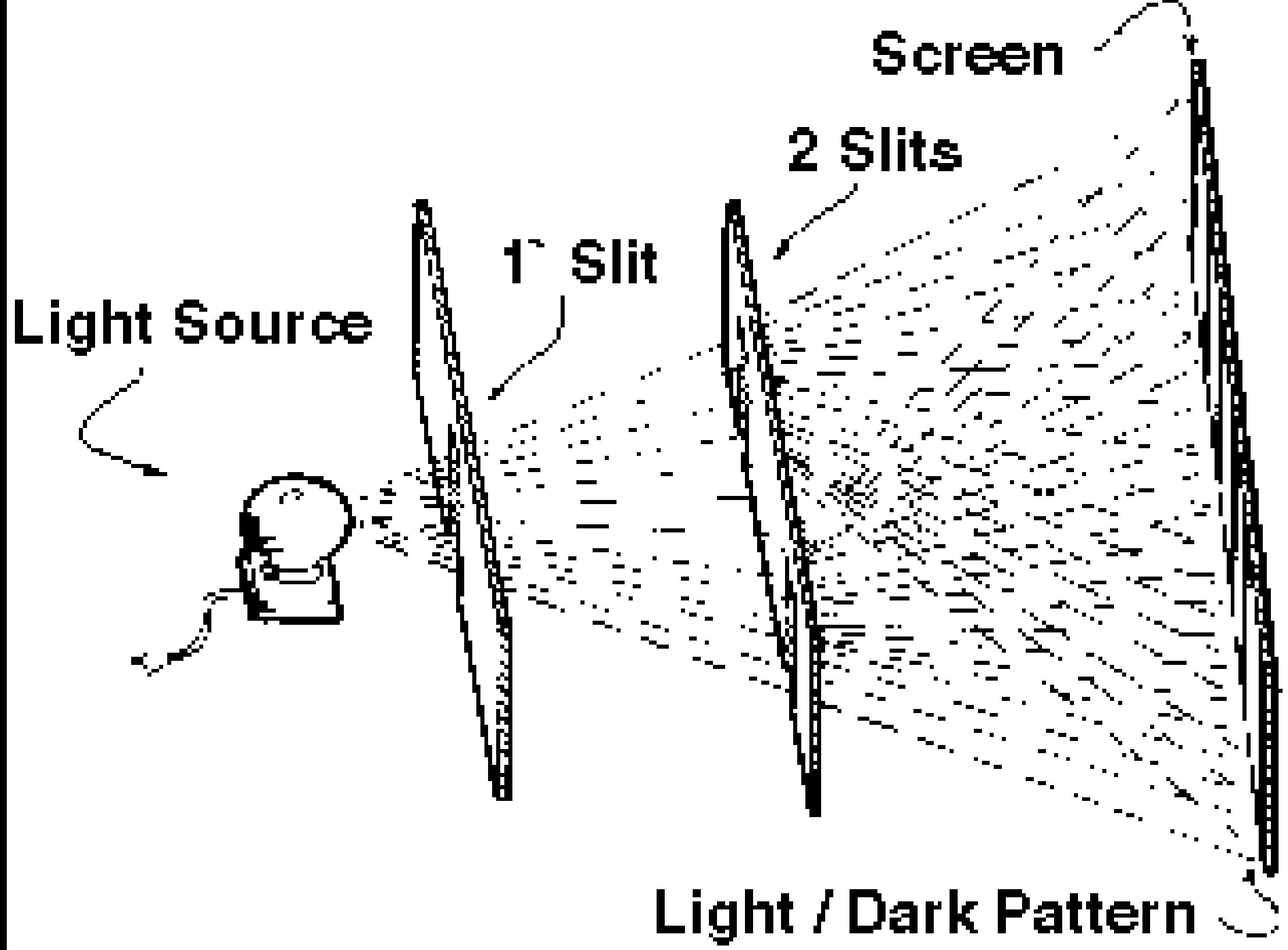

Thomas **YOUNG** (1773-1829),

1802 carried out and explained the interference phenomena

Estimated wavelength.

Other interests: elasticity of solid bodies (E modulus)

- for steel   E = 2.0 x 100 000 MPa
- for bronze E = 1.0 x 100 000 MPa
- for glass E = 0.6 x 100 000 MPa

Interference

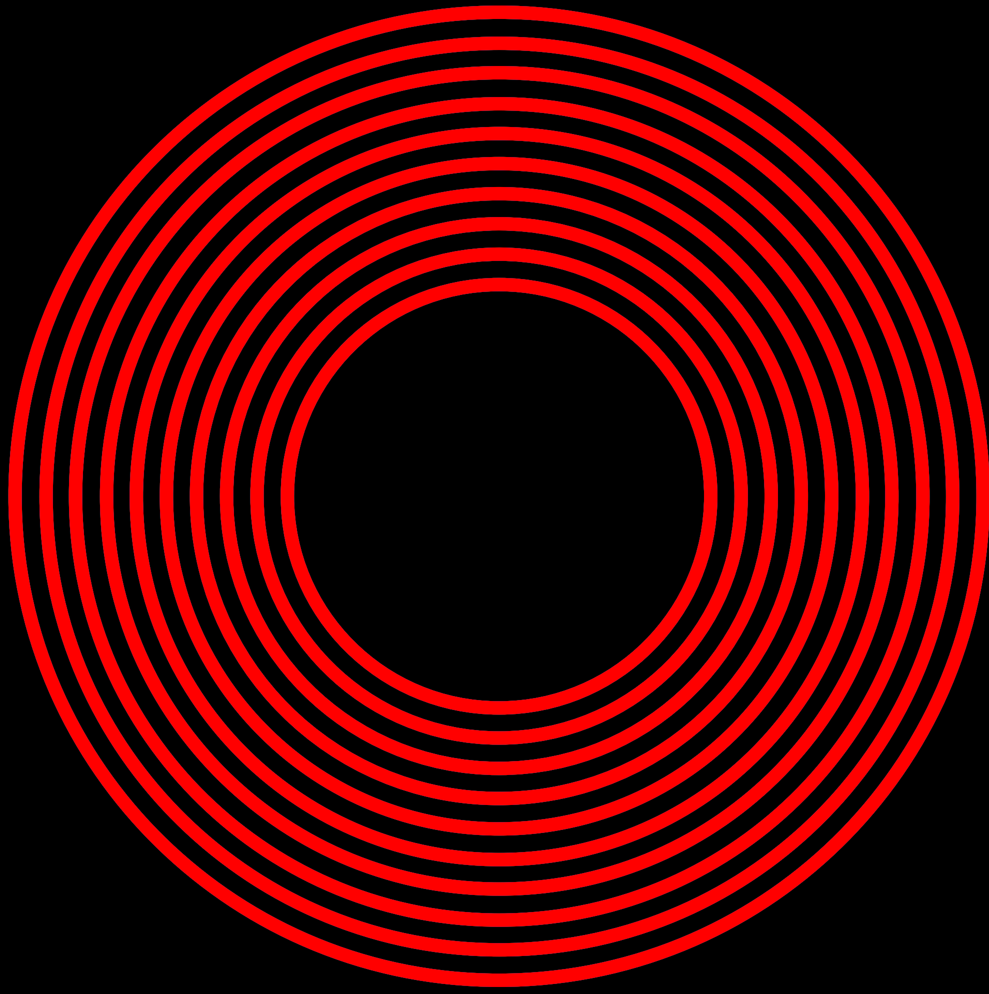

Effect of laser light diffraction on two slits

Scattered coherent waves:

Interference constructive **Interference destructive**

Mathematical formulae: von Laue* (1912)

Diffraction$_{\text{ugięcie, odbicie}}$ = … g + *interference*

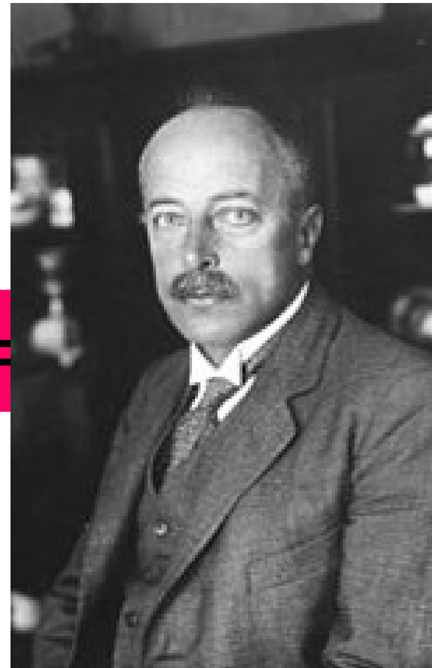

Max von **LAUE** *(1879–1960), physiker, prof. univ. Zurich and Berlin,*

Discoverer of X-ray diffraction*, Nobel Prize, 1914*

Scattering on many atom layers in crystalline materials

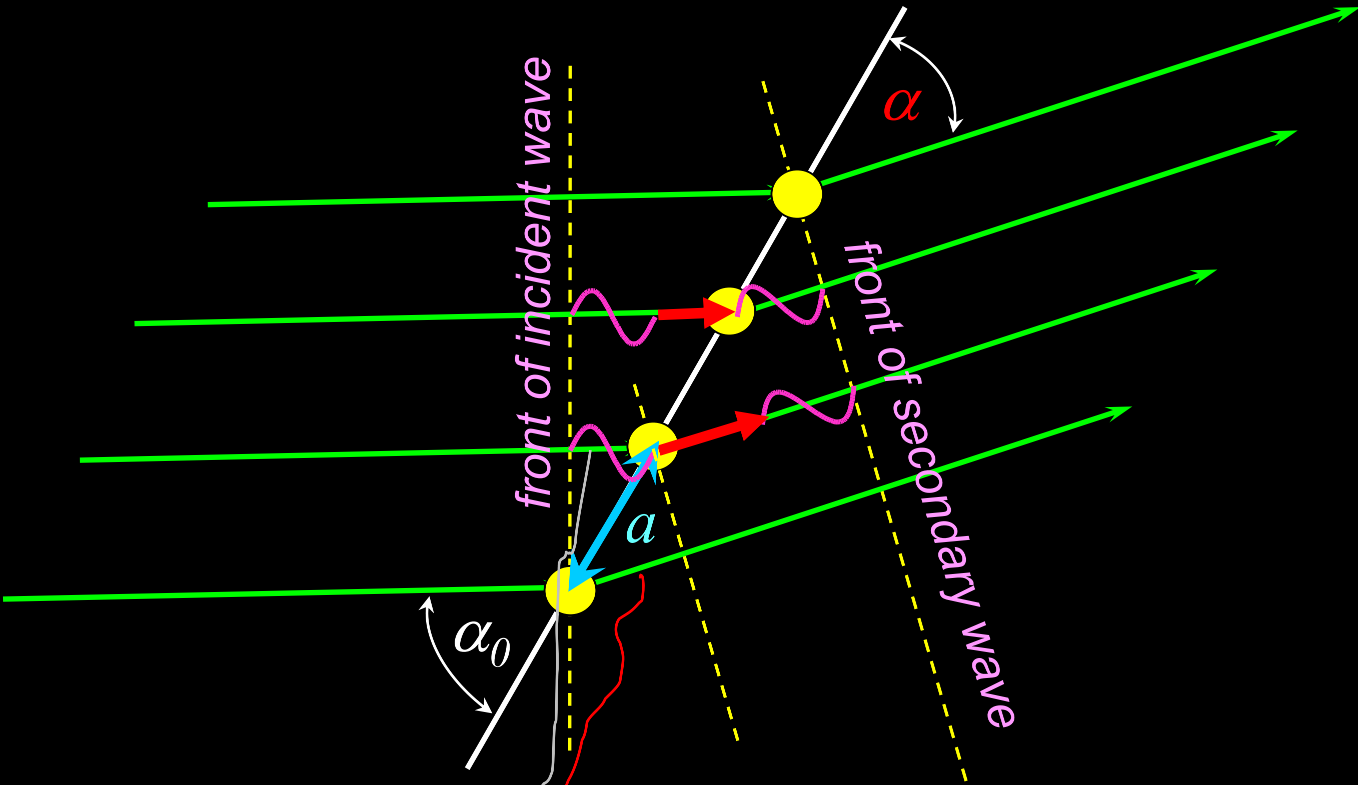

Condition of X-ray diffraction on a lattice axis: $\Delta S = a(\cos\alpha - \cos\alpha_0) = H\lambda$

$$a(\cos\alpha - \cos\alpha_0) = H\lambda$$
$$b(\cos\beta - \cos\beta_0) = K\lambda$$
$$c(\cos\gamma - \cos\gamma_0) = L\lambda$$

LAUE's equations (condition of X-ray diffraction on a space lattice of crystal)

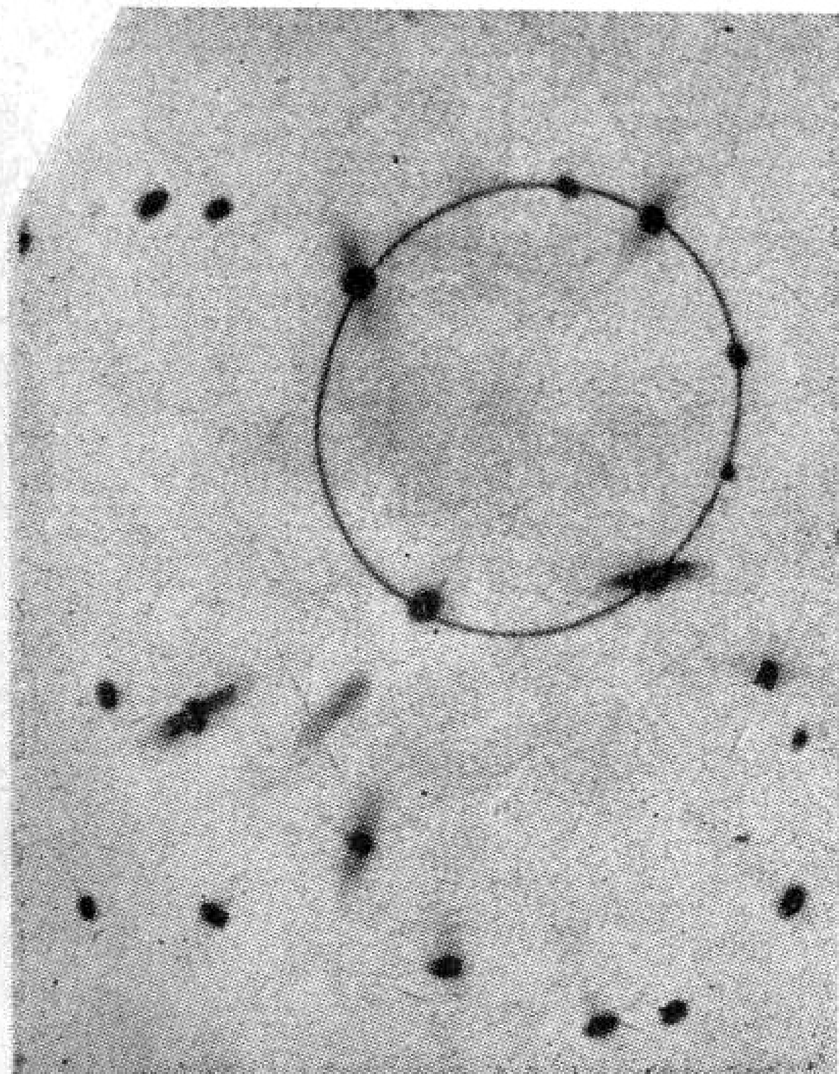

a)

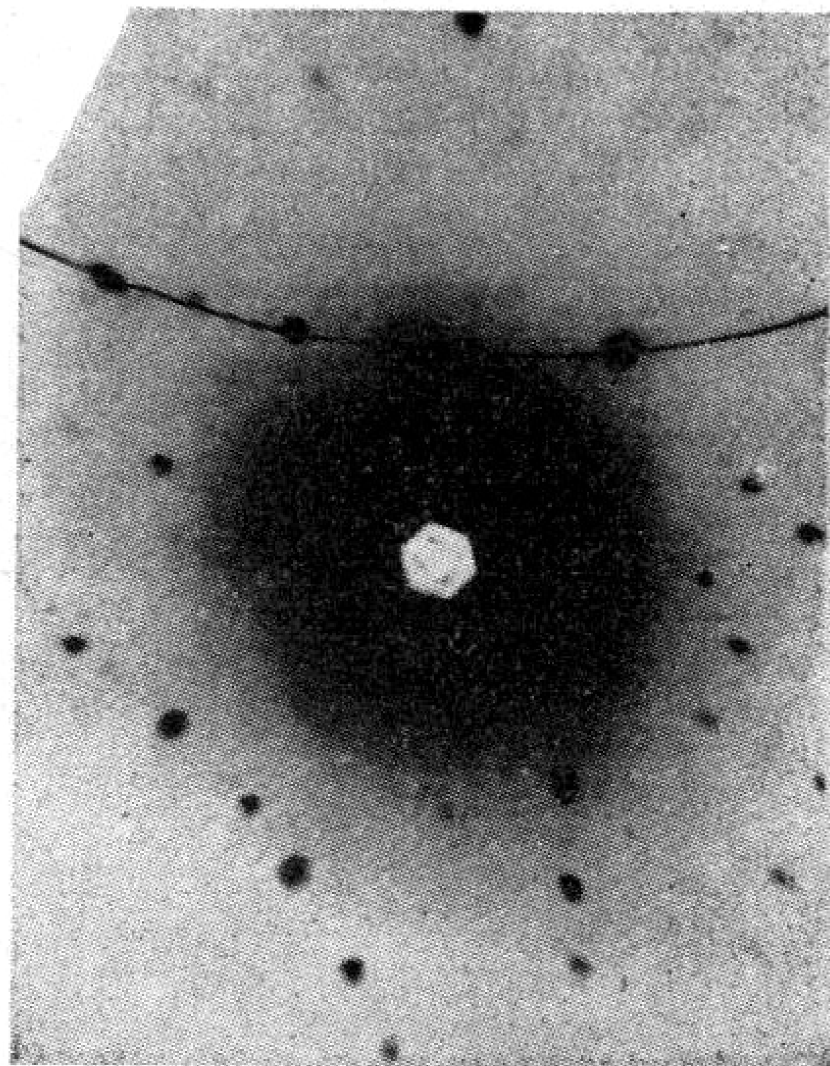

b)

Rys. 3.6. Lauegramy wykonane metodą: a) promieni przechodzących i b) promieni zwrotnych. Promieniowanie anody wolframowej 30 kV, 19 mA

X-ray scattering by a free electron

Kinematical theory of interference
(Max von LAUE [1879 - 1960, discovered diffraction of X-ray on crystals)

Electromagnetic, polarized/unpolarized waves → free electron → secondary source of vibration:

Thomson factor

Lorentz-polarization factor

$$I_0 = I_0 \left(\frac{e^2}{mc^2} \right)^2 \frac{1}{R^2} \frac{1 + \cos^2 2\theta}{2}$$

X-ray scattering by a free atom

Thomson factor
(mass of nucleus can be neglected)

Lorentz-polarization factor

$$I_0 = I_0 \left(\frac{e^2}{mc^2} \right)^2 \frac{1}{R^2} \frac{1+\cos^2 2\theta}{2}$$

Size of atom can not be neglected; electrons are not concentrated in one point! For that reason the scattered wave is summarized over all electrons in atom, regarding amplitudes and phases of individual waves

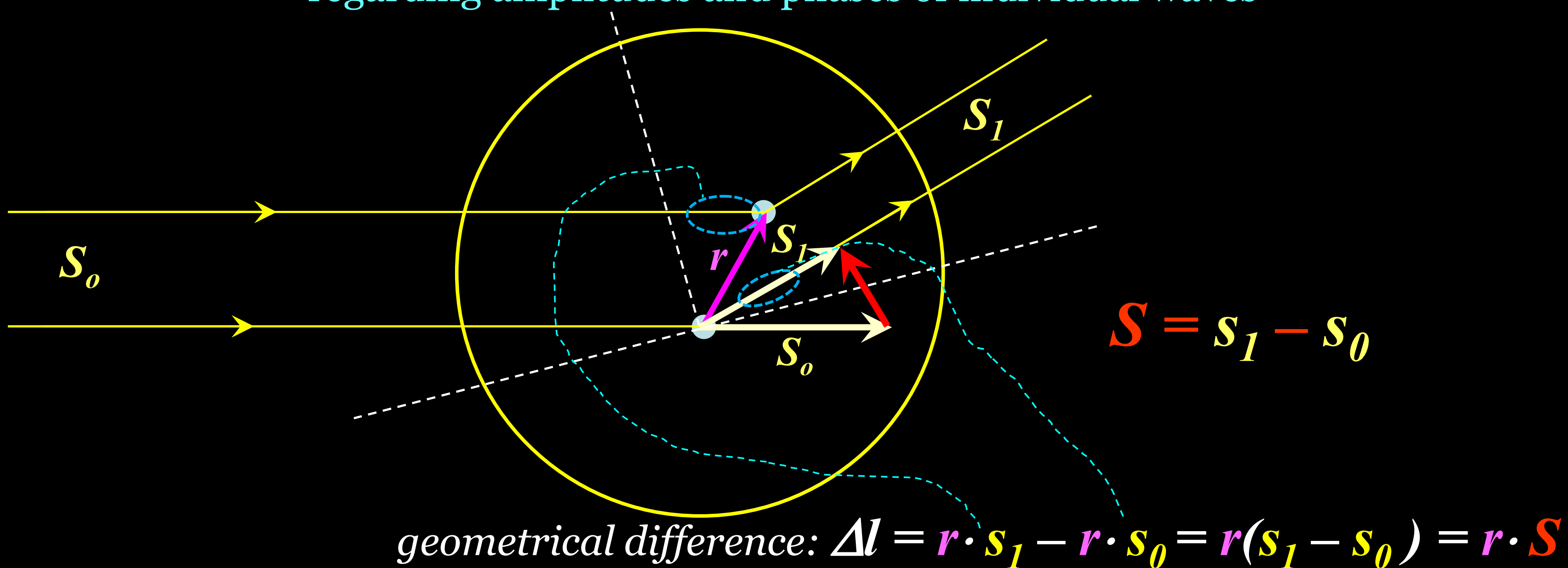

geometrical difference: $\Delta l = \mathbf{r} \cdot \mathbf{s_1} - \mathbf{r} \cdot \mathbf{s_0} = \mathbf{r}(\mathbf{s_1} - \mathbf{s_0}) = \mathbf{r} \cdot \mathbf{S}$

Difference of waves scattered on A i B electrons: $\Delta\varphi = \frac{2\pi}{\lambda}\Delta l \quad \Rightarrow \quad \Delta\varphi = \frac{2\pi}{\lambda}\vec{r} \cdot \vec{S}$

X-ray scattering by a free atom

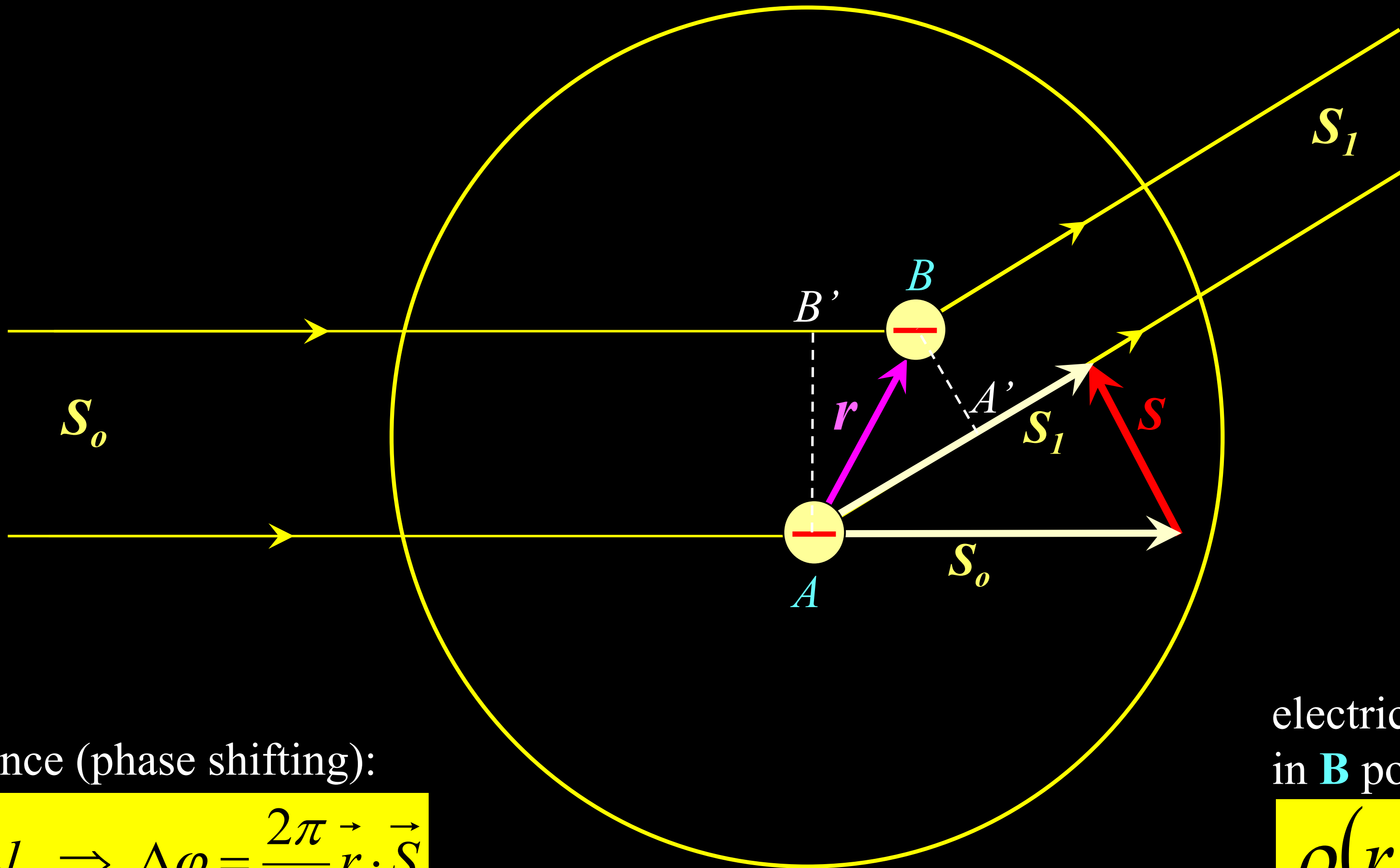

electrical charge in **B** point:

$$\rho(r)dv$$

Phase difference (phase shifting):

$$\Delta\varphi = \frac{2\pi}{\lambda}\Delta l \quad \Rightarrow \quad \Delta\varphi = \frac{2\pi}{\lambda}\vec{r}\cdot\vec{S}$$

Finally, amplitude of wave scattered in B point:

$$\rho(r)dve^{\frac{2\pi}{\lambda}i\bar{r}\cdot\bar{S}}$$

Amplitude of wave scattered in all points (electrons) in **S** direction (**atomic** scattering amplitude):

$$f(S) = \int_V \rho(r)e^{\frac{2\pi}{\lambda}i\vec{r}\vec{S}}dv$$

Let's assume the coordinate system in point **A**; then, charge in point **B**: **ρ(r)dv**

where **ρ(r)** is a charge density in voxal **dv** located in **r** distance

X-ray scattering by a free atom

characterizes an ability of atom to scattering X-rays.
*In other words: the numerical value **f** exhibits how many times the amplitude of wave scattered by an atom is greater than one of scatterd by a singular electron*

$$f(\vec{S}) = \int_V \rho(r) e^{\frac{2\pi}{\lambda} i \vec{r}\vec{S}} dv$$

$$f = \frac{\text{amplitude scattered by atom}}{\text{amplitude scattered by elektron}}$$

atomic *scattering amplitude for a spherical distribution of charge in atom:*

$$f(\vec{S}) = \int_0^\infty 4\pi r^2 \rho(r) \frac{\sin(\vec{r}\cdot\vec{S})}{\vec{r}\cdot\vec{S}} dv$$

The greater atomic number of element, the greater atomic amplitude.
That's why,
*e.g. X-ray scattering by **hydrogen** is very poor*

$$for\ \vec{S} \to 0,\ f(0) = \int_0^\infty 4\pi r^2 \rho(r) dv \approx Z$$

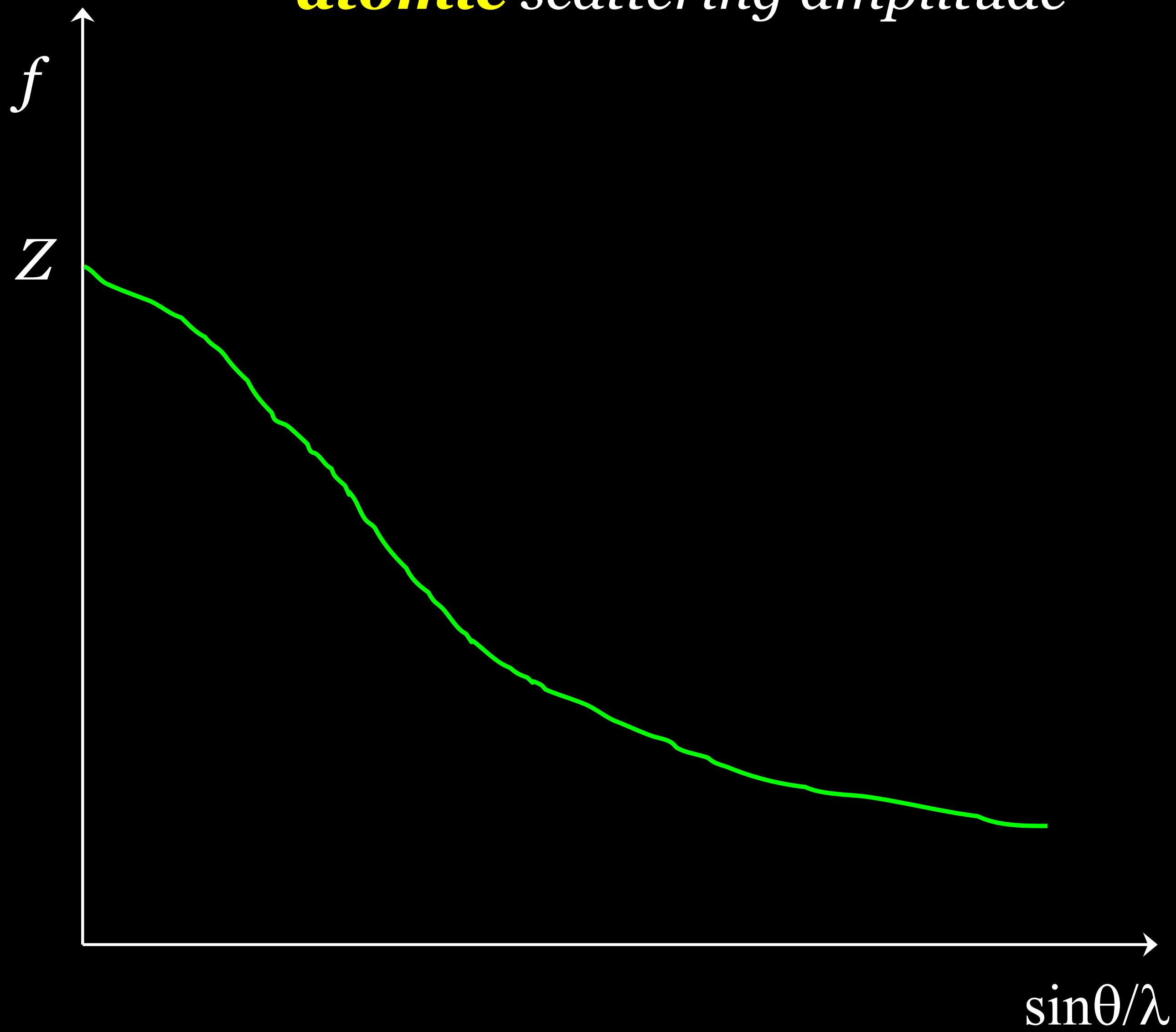
atomic scattering amplitude
f
Z
sinθ/λ

atomic scattering amplitude

Regarding the thermal oscillation of atoms (possible maximal ampl. ≈ **0.1 Å**):

$$f = f_0 e^{-M}$$

$$M = 8\pi^2 \overline{u}^2 \frac{\sin\theta}{\lambda}$$

$\overline{u}^2$ *- mean square oscillation of the atom from a balance position*

Geometry of diffraction (but not intensities)
can be expressed relatively clearly
using the Bragg (Wulf-Braggs) low:

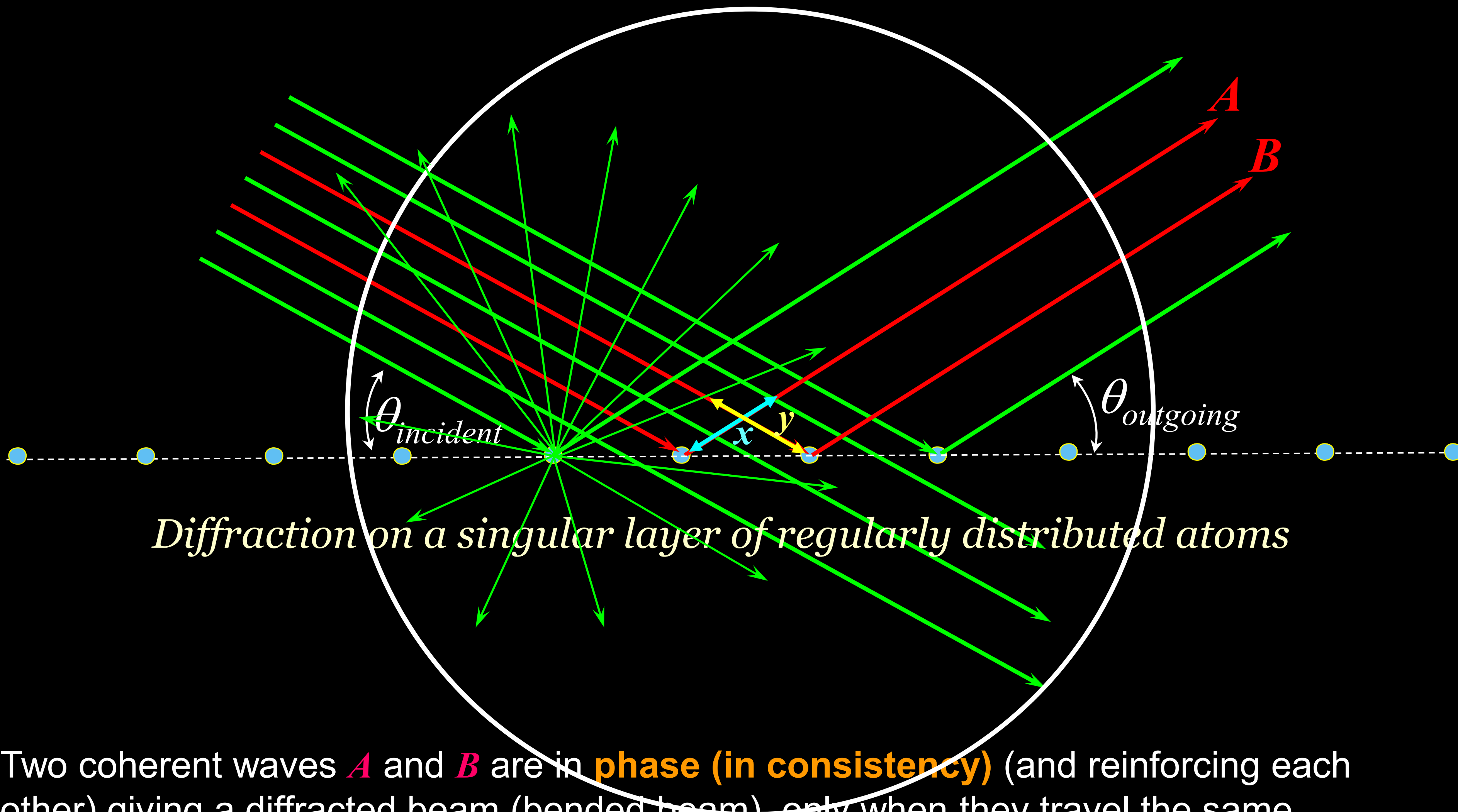

Two coherent waves *A* and *B* are in **phase (in consistency)** (and reinforcing each other) giving a diffracted beam (bended beam), only when they travel the same distance, i.e. when x and y are equal:

$$x = y$$

This only occurs for scattered waves with an outgoing angle of:

$$\theta_{outgoing} = \theta_{incident}$$

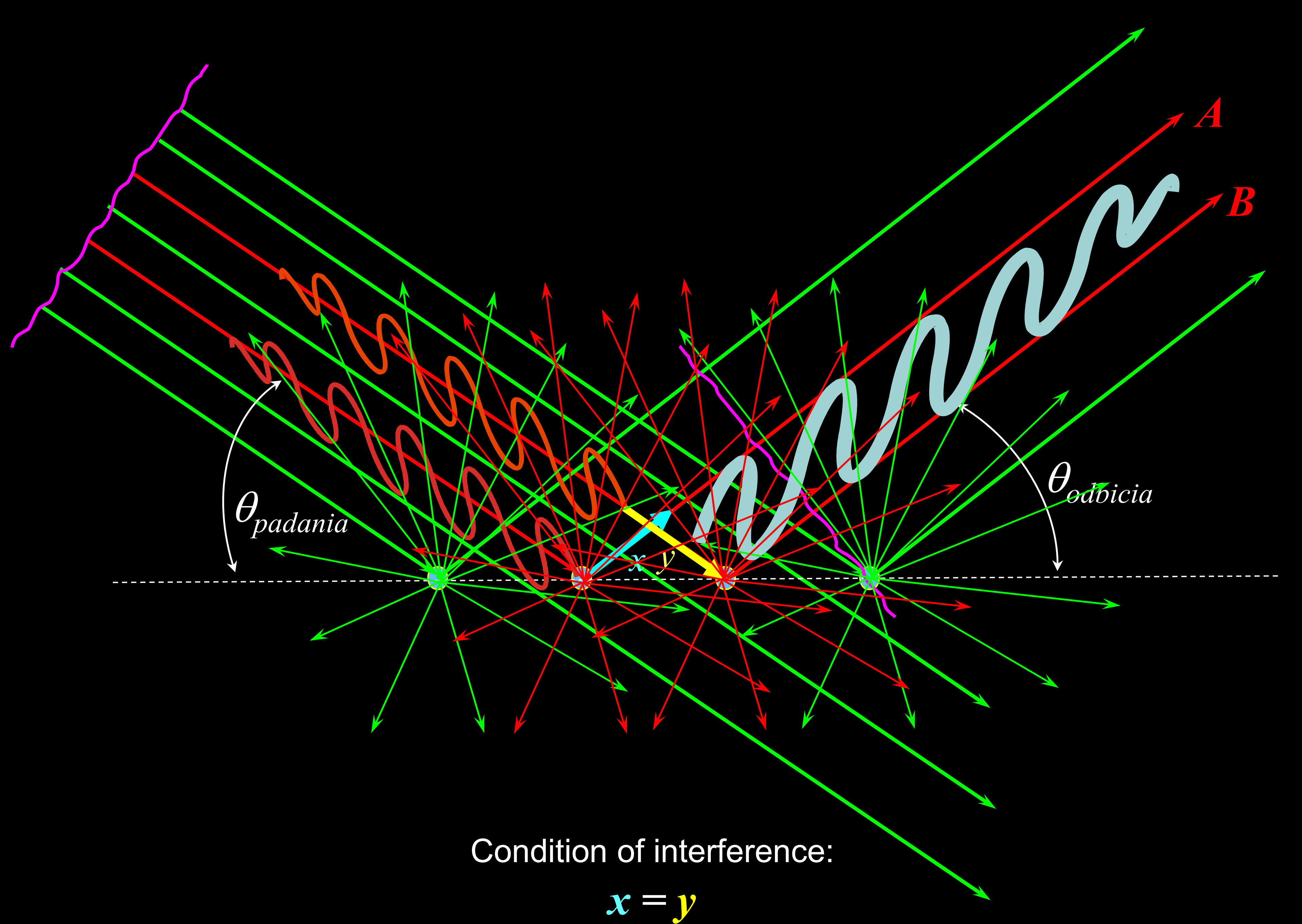
A
B
$\theta_{padania}$
$\theta_{odbicia}$
x
y
Condition of interference:
$x = y$

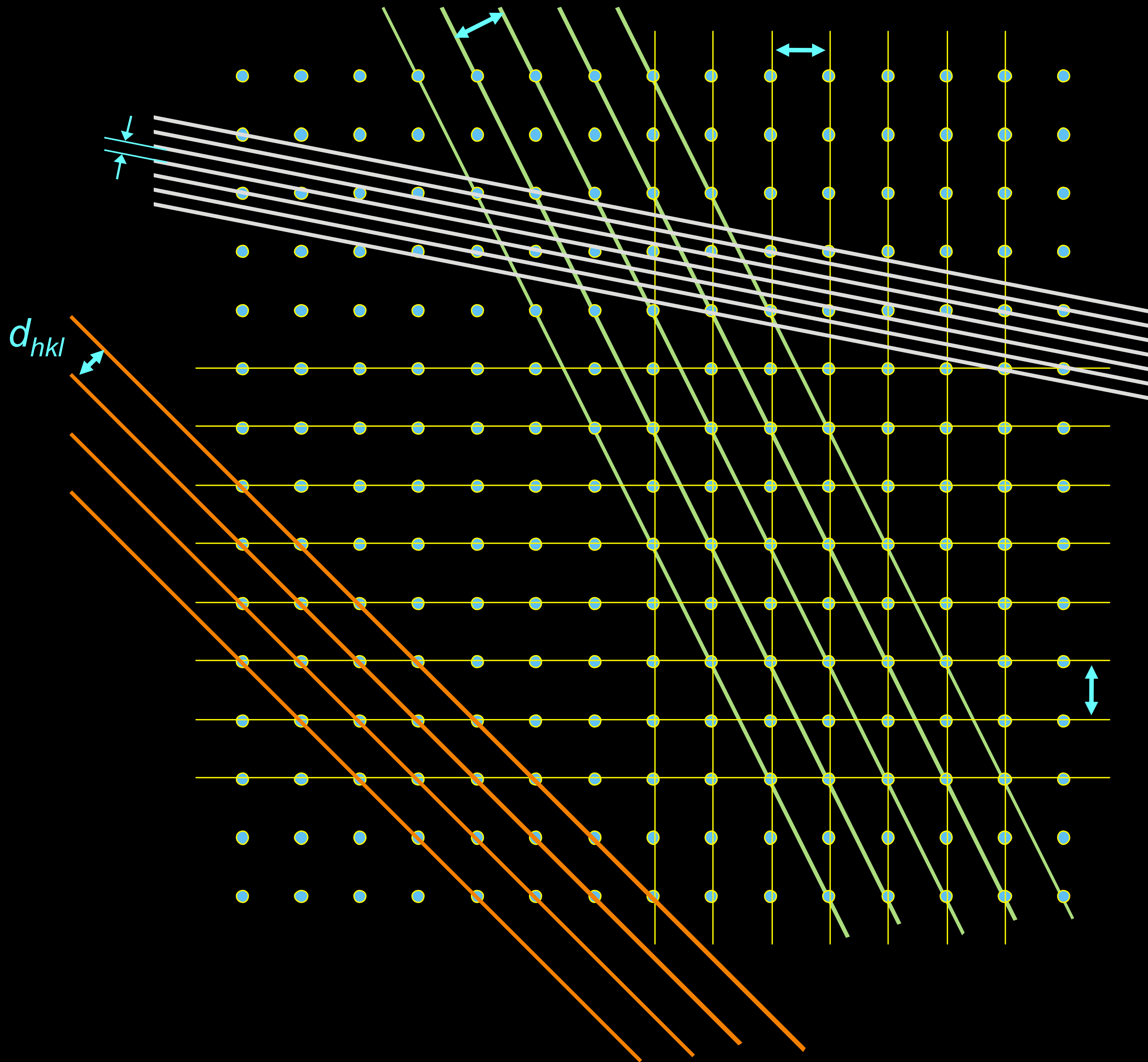

d_{hkl}

Case of many layers of regularly spaced atoms – as in crystal

As we alredy known: $\theta_{incidence} = \theta_{outgoing}$

How the coherent waves are scattered on many atomic layers?

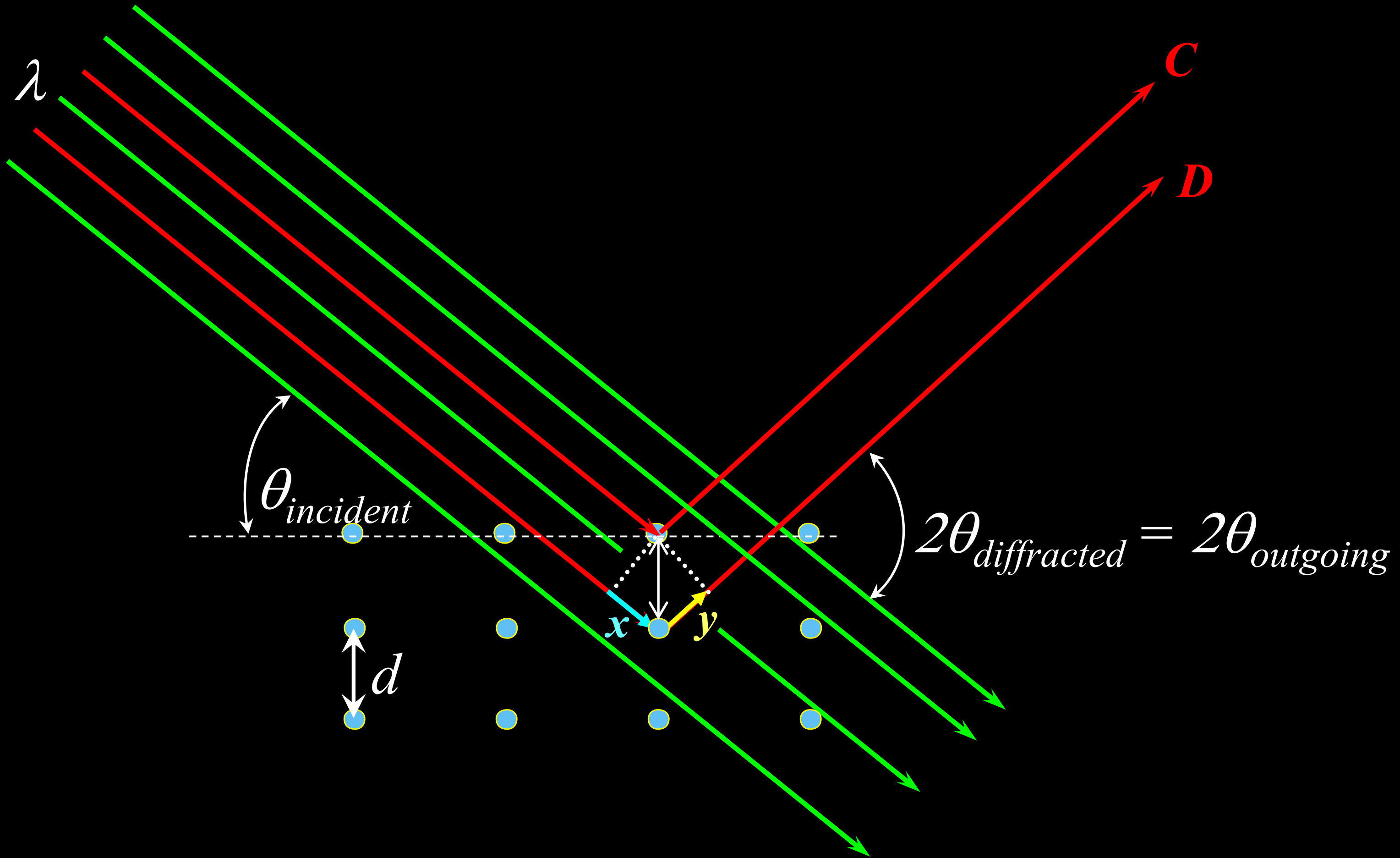

Difference of routes for scattered **C** and **D** waves: $x + y = 2d\sin\theta = n\lambda$

$$n\lambda = 2d_{hkl}\sin\theta_B$$

Scattering on many atomic layers in crystal

For defined pair of $\mathbf{d_{hkl}}$ and λ there are a few values of diffraction angle θ_{hkl} predicted by the ….. law (quite so!)

$$n\lambda = 2d_{hkl}\sin\theta_B$$

Bragg equation ?

A basi… …tion

• in Anglo-Saks…
• in Russian lite…

PROCEEDINGS OF THE ROYAL SOCIETY A MATHEMATICAL, PHYSICAL & ENGINEERING SCIENCES

The Reflec…

By W. H. Bragg, M.A., …
University of Leeds; …
Cambridge.

(Received …

In a discussion of the La…
may conveniently be interpr…
planes within the crystal as …
attempt to use cleavage pla…
gives a reflected pencil fro…
visible impression on a pho…
has also been observed tha…
ionisation method.†

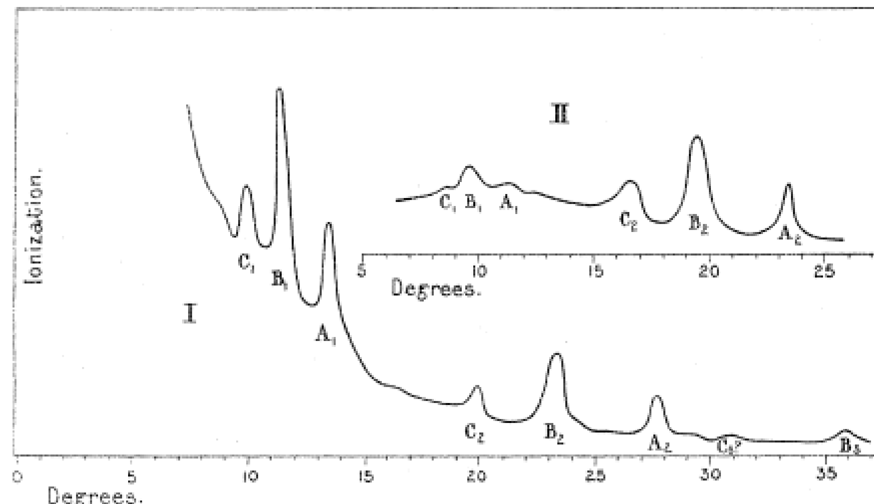

Fig. 3.—Reflection (I) from face (100) and (II) from face (111) of rock-salt. The curves show the variation of strength of reflected beam with angle of incidence.

William Henry…
Univ. of Lond…
1915 (along wi…

William Lawra…

…reflection of X-rays in …spectrometer in form, …ope. The collimator is …n be stopped down to the centre carries the …n. long and 5 cm. in …nstrument, to which its …ur dioxide in order to …l iodide have also been …cteristics of the gas in

…Part I, p. 43.

It is of great interest to attempt to find the exact wave-length of the rays to which these peaks correspond. On considering Curve I, fig. 3, it seems evident that the peaks $A_1 B_1 C_1$, $A_2 B_2 C_2$ are analogous to spectra of the first and second orders, because of the absence of intervening sets of peaks. The value of n in the equation

$$n\lambda = 2d \sin\theta$$

seems clear. The difficulty of assigning a definite wave-length to the rays arises when we attempt to determine the value of d, the distance of plane from plane.

* We learn that Messrs. Moseley and Darwin have lately been making experiments similar to some of those recorded here. Their results, which have not been published, agree with ours.

…aphist, prof.
1915 (along

…. of Kazań,
the Science
…3 returned to

...by **Bragg**:

$$n\lambda = 2d_{hkl} \sin\theta_B$$

[Proceedings of the Royal Society, 1913, 88, 428]

Adnotation at the end of the work of H.W & W.L. Braggs from 1913: „Received April 7, 1913"

Gieorgij W. **Wulf** – two his works from beginning 1913 in Russian [Fizika, 1913, zesz. 1, s. 10 and Priroda, 1913, s. 27] concerned to interference of X-rays and its behaviour in passing through the crystals. *He known the earlier works of W.L. Bragg from 1912r.*

....by ***Wulf***:

$$\frac{\lambda}{2} = \frac{\delta\varepsilon}{m}$$

„Ueber die Kristallroentgenogramme" [Physikalishe Zeitschtrift, **1913**, z. 6, s. 217]

where $\delta = d_{hkl}$, $\varepsilon = \cos\psi$ (ψ – angle between incident beam and normal to diffracting lattice plane), m – order of reflection)

$$m\lambda = 2d_{hkl} \cos\psi$$

Adnotation at the end of the work of G.W. Wulf (sent from Russia) from 1913: „Eingegangen 3 Februar 1913"

Base law (equation) of diffraction theory:

$$n\lambda = 2d_{hkl}\sin\theta_B$$

$$\frac{\lambda}{2} = \frac{\delta\varepsilon}{m}$$

$$m\lambda = 2d_{hkl}\cos\psi$$

Bragg *law (equation)*

Braggs *law (equation)*

Wulf *law (equation)*

Braggs – ***Wulf*** *law (equation)*

Wulf – ***Braggs*** *law (equation)*

Scattering on many atomic layers in crystalline materials

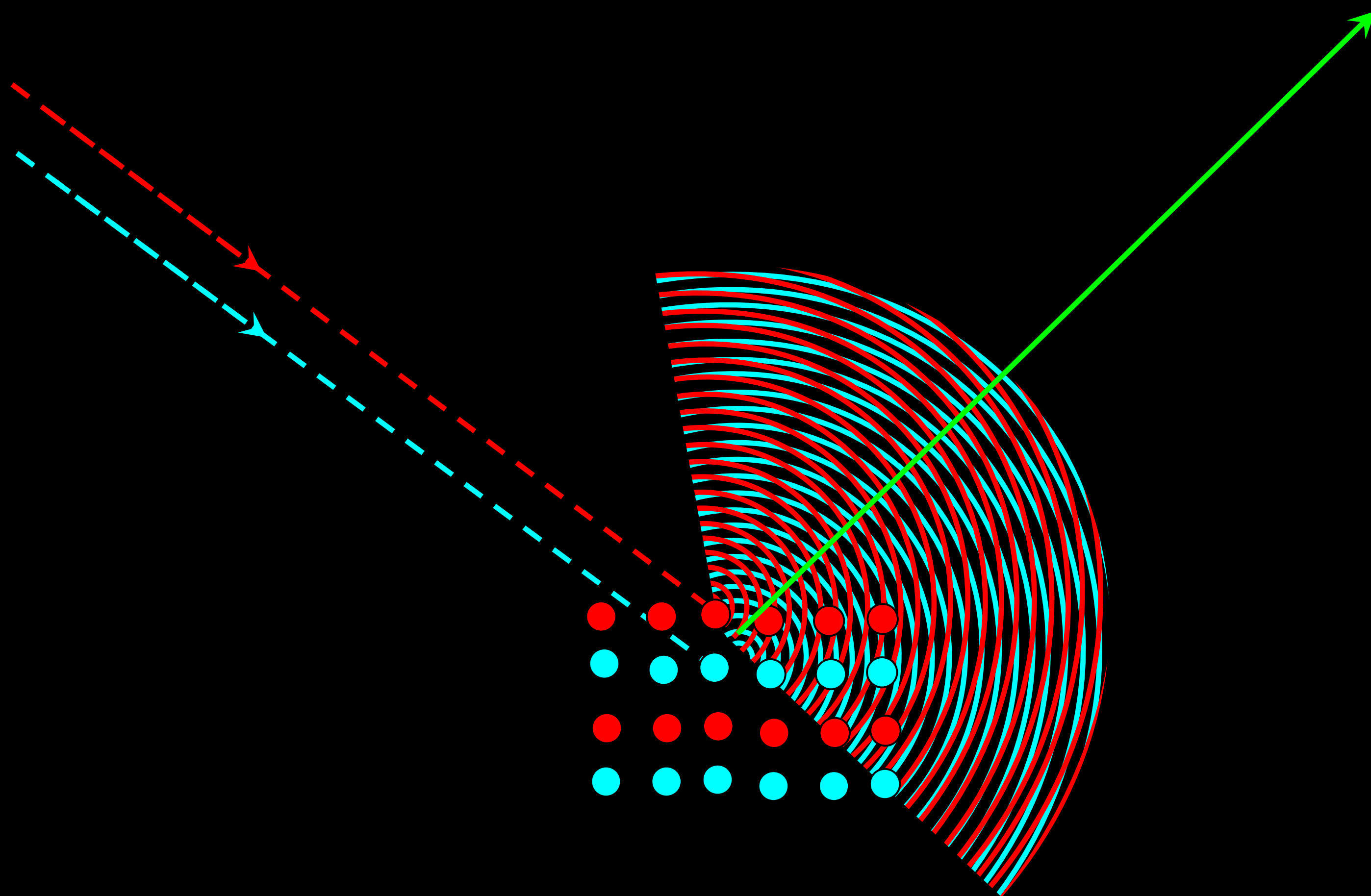

X-ray diffraction on polycrystalls

Polycrystal – definition

Debye cones

Petrus Josephus Wilhelmus Debije
(after change: Peter Joseph William Debye)
1884 (Maastricht) – 1966 (USA)

$2\theta_B$

$2\theta_B$

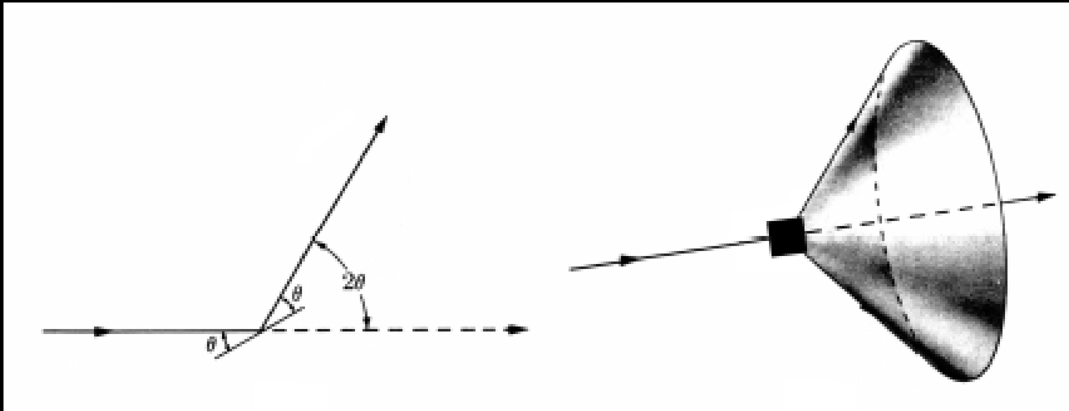

a)

film

2θ

próbka

b)

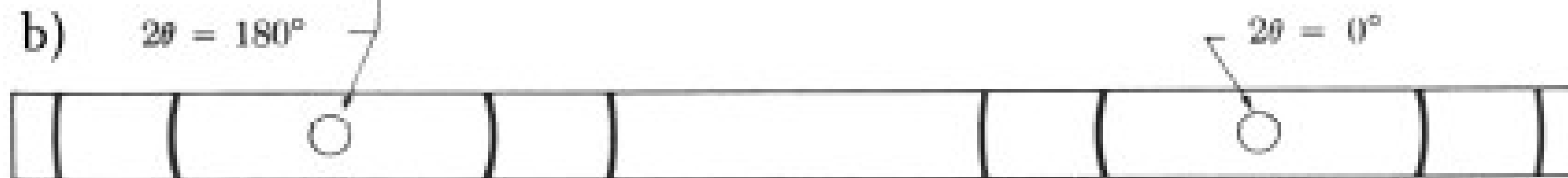

Metoda Debye'a – Scherrera (Cullity, 1959): (a) geometria pomiaru, (b) wygląd rozwiniętego filmu.

geometric

Summary of the **geometrical** theory of diffraction:

delivers two equivalent conditions of diffraction phenomena:

- scalar – **Bragg equation**: $n\lambda = 2d_{hkl} sin\theta_{hkl}$
- vector – **Laue conditions**: $a(cos\alpha - cos\alpha_0) = H\lambda$

$n \equiv H \longrightarrow order\ of\ reflection$

$$I_{hkl} = {}^{k}I_{hkl} + {}^{d}I_{hkl}$$

Kinematic component

- diffraction on polycrystals
- absorption

Dynamic component

- extinction (I- and II-order)
- anomalous absorption (Bormann effect)

Interaction of singular wave with a material particle (atom) - scattering

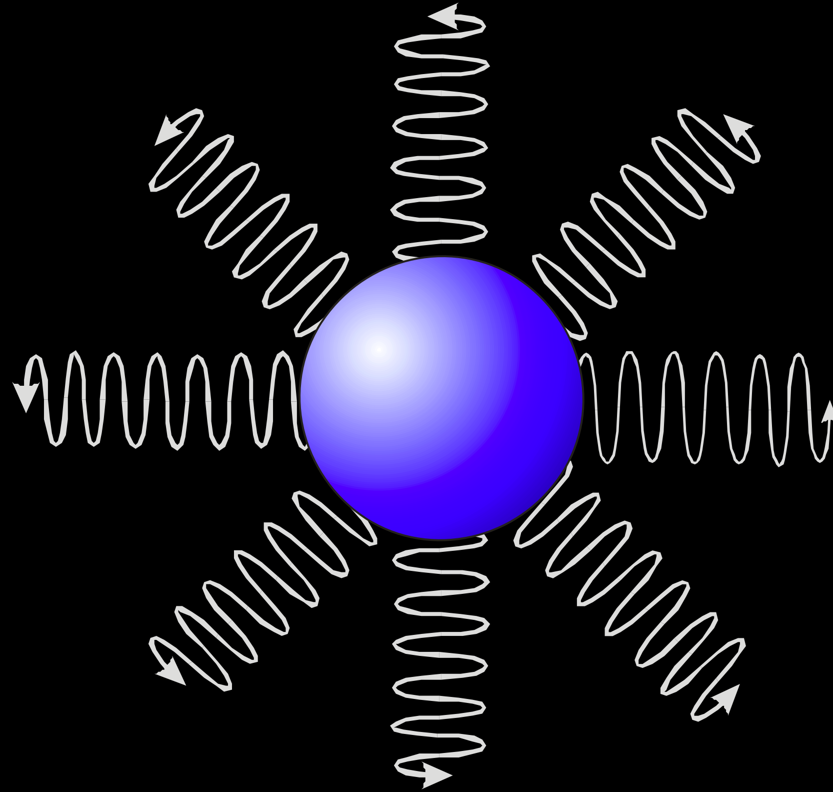

Interaction of singular wave with many material particles (atoms) – scattered waves interfering in a few directions, reinforcing each other = **diffraction**.

Its possible on a periodic structures only

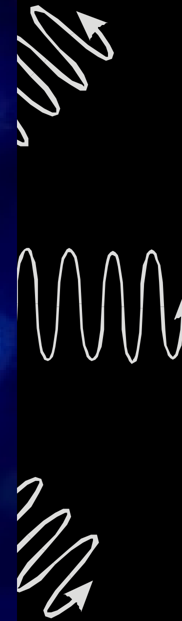

Remembrance: for understanding the diffraction geometry (λ =, amplitude =, φ ≠) (**superpozition**)

phase diff. = ½ π

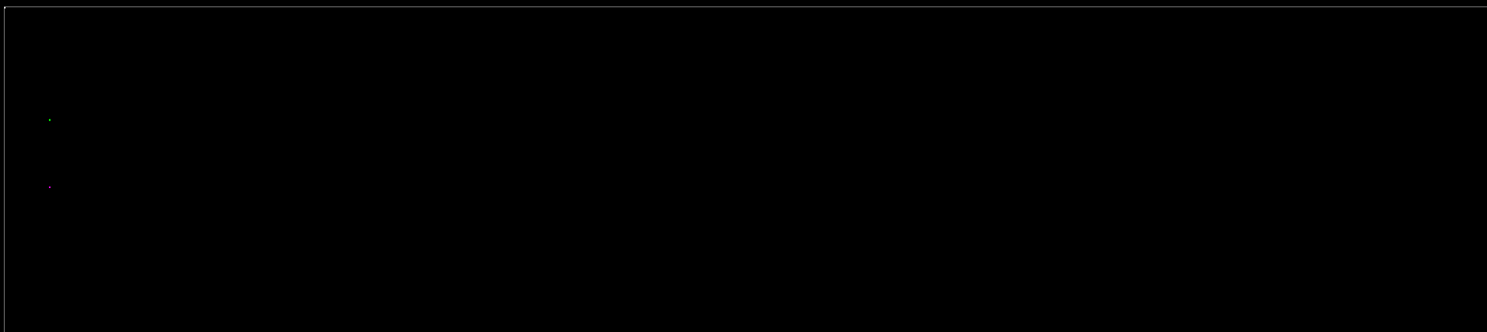

phase diff. = ¼ π

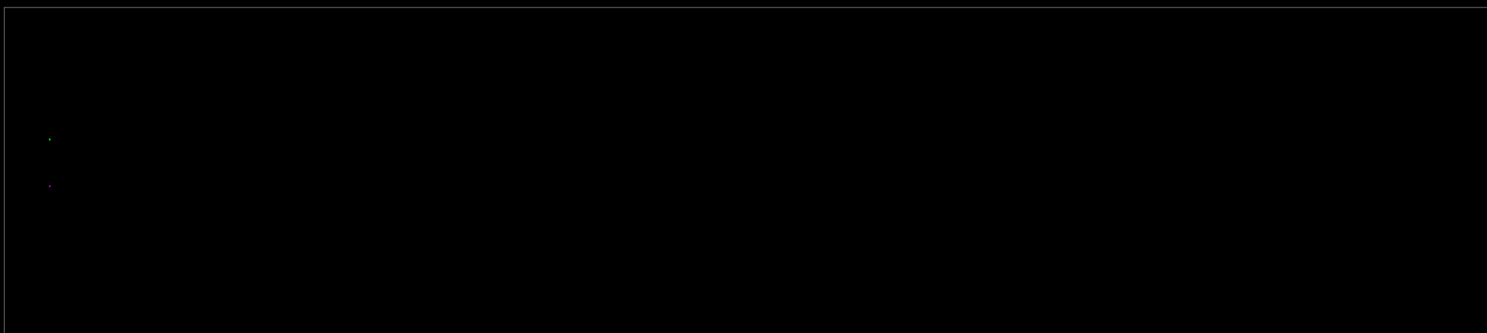

phase diff. = 0

or = $n \times 2\pi$

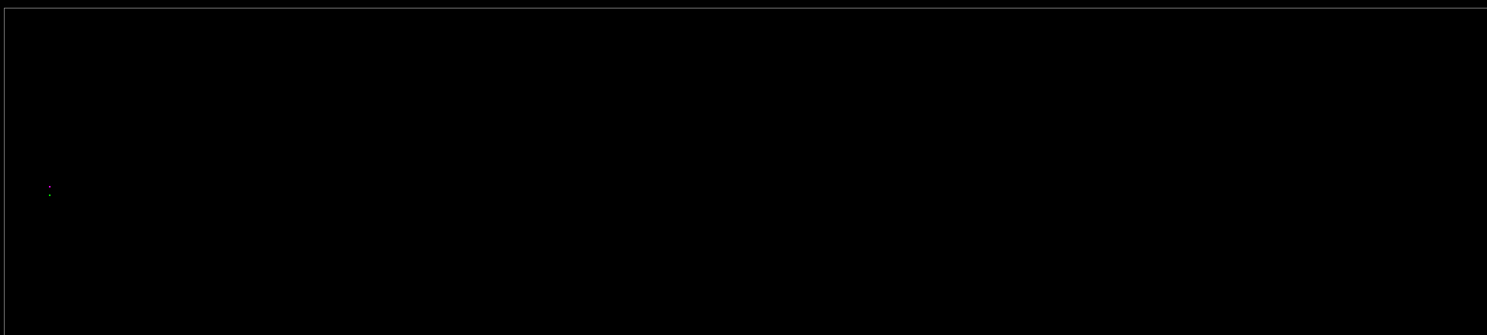

phase diff. = π

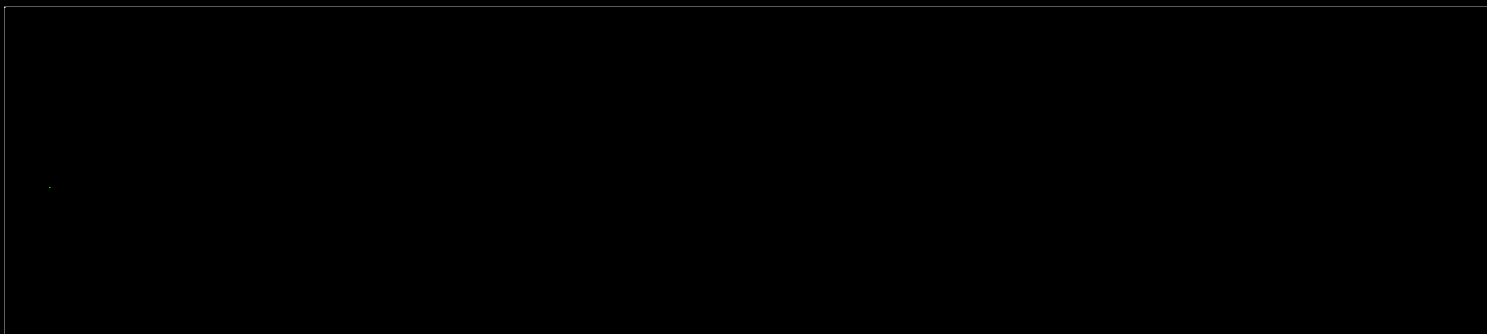

Interference of waves

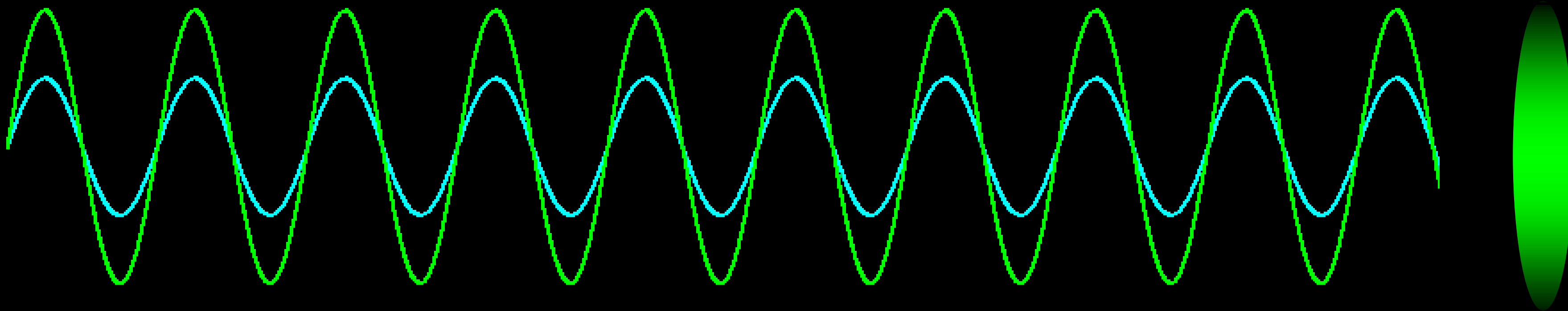

component wave
component wave
product wave

Scattering X-rays on crystal

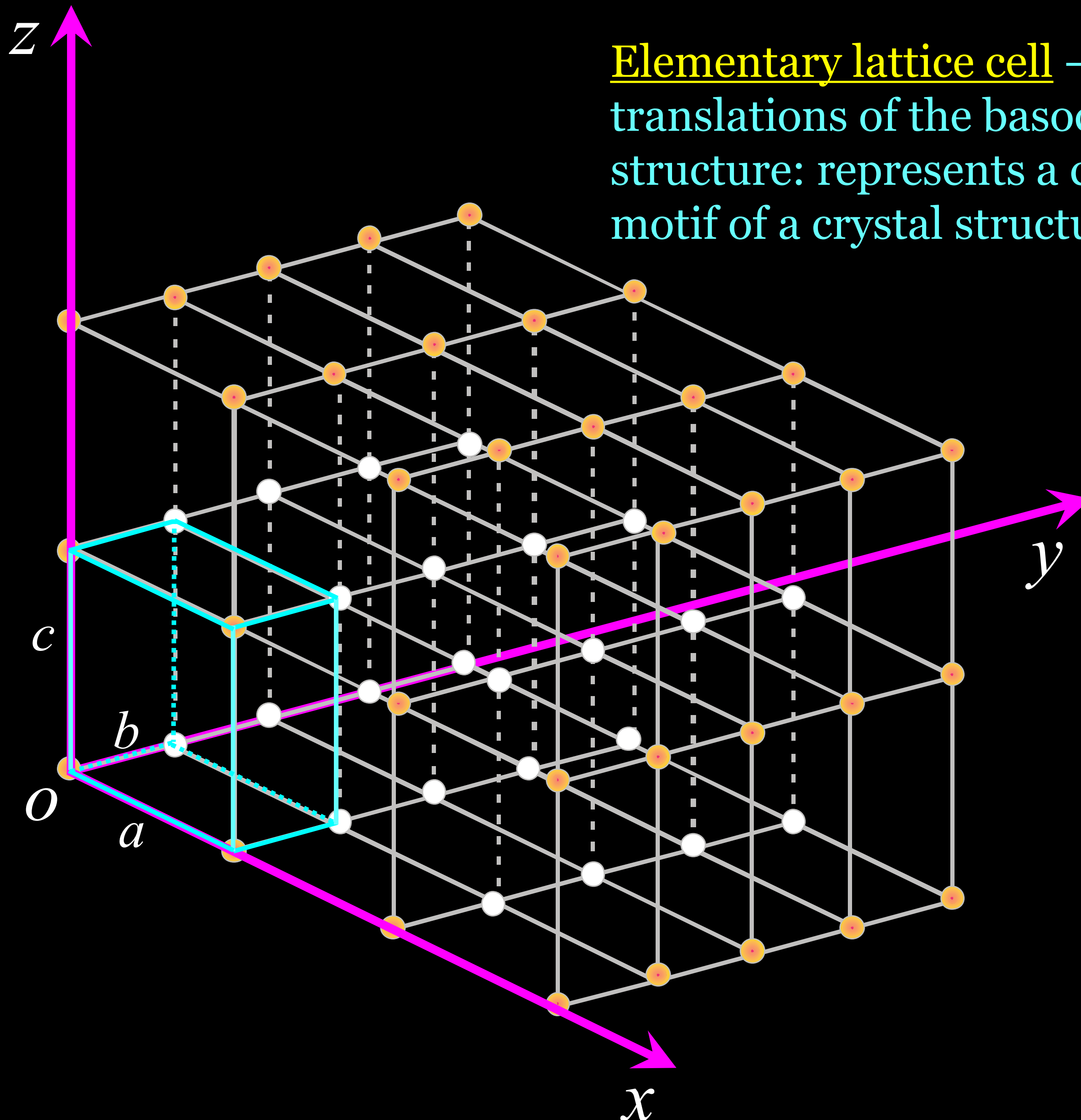

<u>Elementary lattice cell</u> – result of translations of the basoc elements of structure: represents a complete motif of a crystal structure

Scattering X-rays on crystal

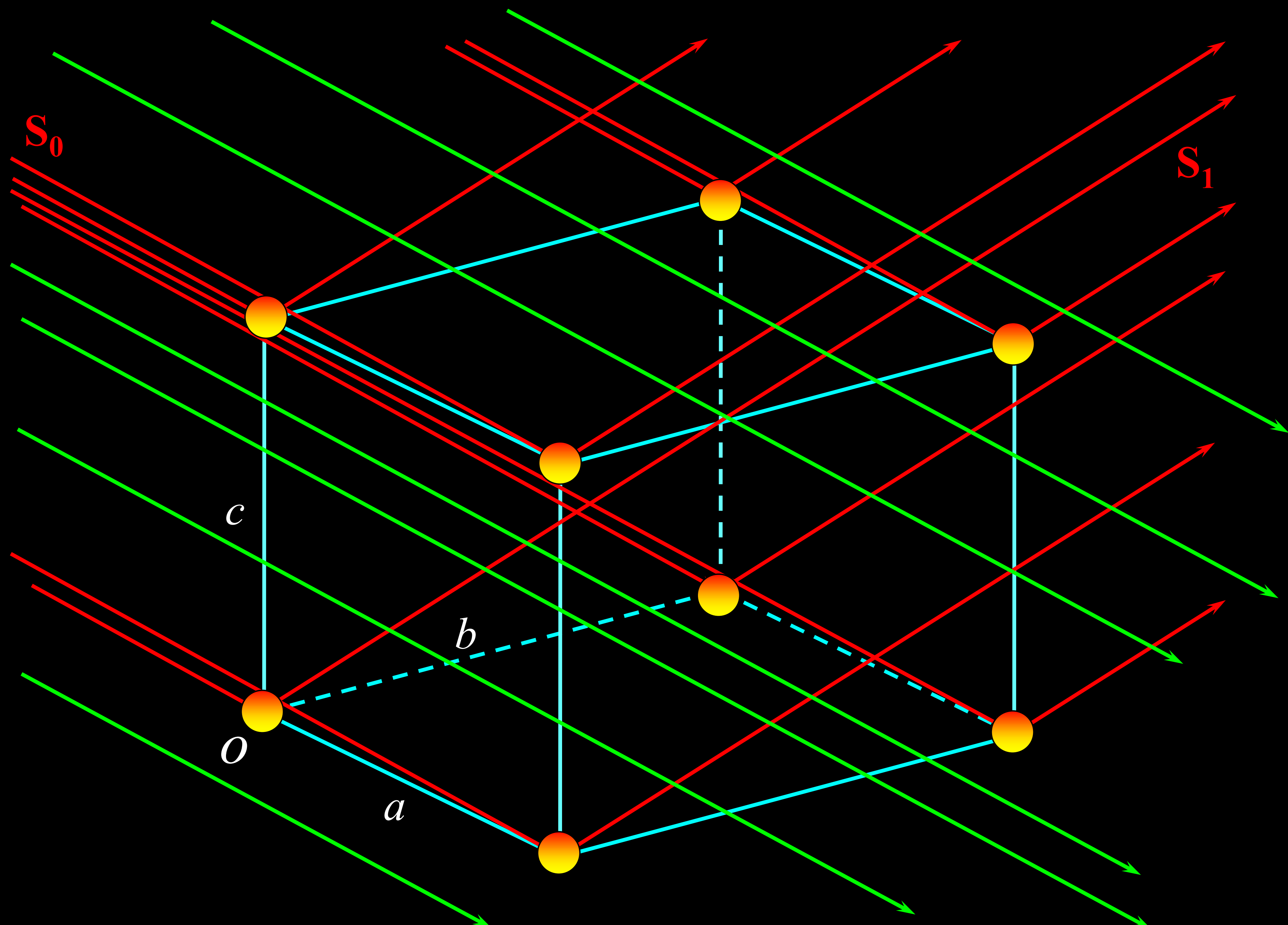

Scattering X-rays on crystal

*Difference of the wave phases scattered on **A** and **B** electrons:*

$$\Delta\varphi = \frac{2\pi}{\lambda}\Delta l \;\Rightarrow\; \Delta\varphi = \frac{2\pi}{\lambda}\vec{r}\cdot\vec{S}$$

Because $\mathbf{r} = x\mathbf{a} + y\mathbf{b} + z\mathbf{c}$ *(where x, y, z are coordinates of the atom in point **B** expressed in fractions of the lattice periods **a**, **b**, **c**) and* $\mathbf{S} = \lambda\mathbf{H}$ ($\mathbf{S_1} - \mathbf{S_0} = \lambda\mathbf{H}$)*, replacing:* $\mathbf{H} = h\mathbf{a}^* + k\mathbf{b}^* + l\mathbf{c}^*$*, (H – vector perpendicular to diffracting plane hkl) the following relation can be written:*

$$\Delta\varphi = 2\pi(hx + ky + lz)$$

Product amplitude from all atoms in the elementary lattice:

$$F = F_1 + F_2 + F_3 + \dots + F_n$$

***Structure** amplitude, non-measurable directly*

$$F = F_{hkl} = \sum_{j=1}^{n} f_j e^{2\pi i(hx_j + ky_j + lz_j)}$$

$$I_{hkl} \sim F_{hkl} \cdot F^*_{hkl}$$

$$I_{hkl} \sim F^2_{hkl}$$

$$F = \sum_{1}^{2} A_n = f_1 \exp\left(2\pi i\left(0+0+0\right)\right) + f_2 \exp\left(2\pi i\left(hu+kv+lw\right)\right)$$

exp(0) = 1

$$F = f_1 + f_2 \exp\left(2\pi i\left(hu+kv+lw\right)\right)$$

Various combinations of the *hkl* and *uvw* are possible which relfect in diversity of the *F* value:

F = 0 - *no diffraction effect (impossible to registering)*

F = $f_1 + f_2$ - *strong diffraction effect*

For ***bcc*** lattice, number of atoms deduces to TWO:

1 in 0,0,0 point (atomic scattering amplitude f),
2 in ½, ½, ½ point (amplitude f).

$$F = f + f\exp\left(2\pi i\left(\frac{h}{2}+\frac{k}{2}+\frac{l}{2}\right)\right)$$
$$= f\left(1+\exp\left(\pi i\left(h+k+l\right)\right)\right)$$

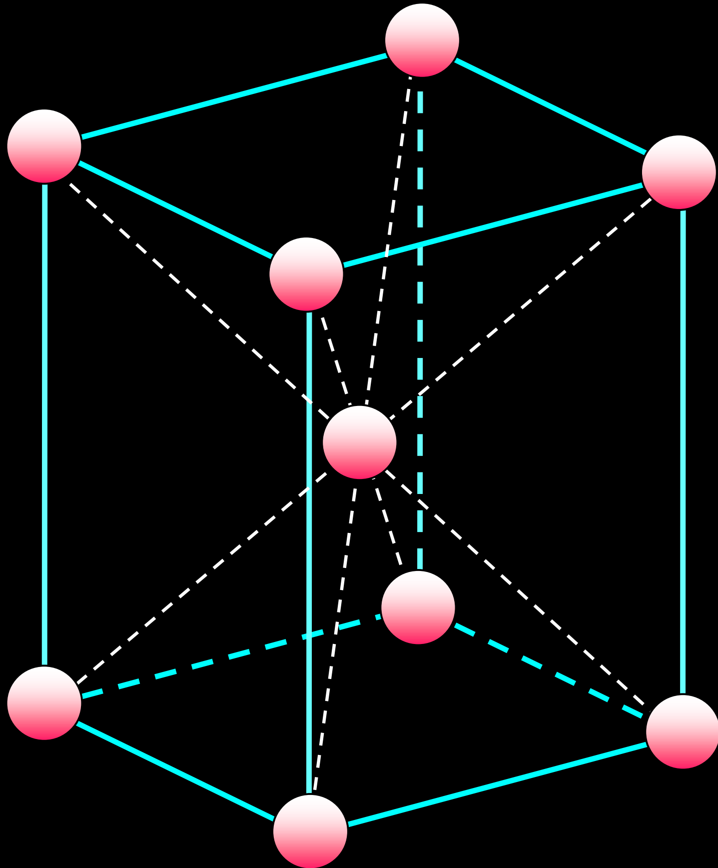

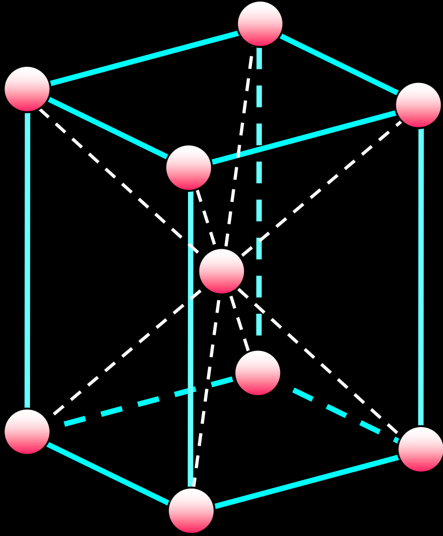

$$F = f + f\exp\left(2\pi i\left(\frac{h}{2}+\frac{k}{2}+\frac{l}{2}\right)\right)$$
$$= f\left(1+\exp\left(\pi i\left(h+k+l\right)\right)\right)$$

When diffraction occurs on the lattice for which *h+k+l* is odd (nieparzysta), the 2nd term = **-1**;

$$\mathbf{F}_{hkl(niep.)} = f(1-1) = 0$$

When *h+k+l* is even (parzyste), the 2nd term = **+1**;

$$\mathbf{F}_{hkl(parz.)} = f(1+1) = 2f$$

Conclusion: in the case of X-ray scattering on **bcc** lattice, diffraction is not observed for the planes which *h+k+l* is odd, (forbidden reflections)

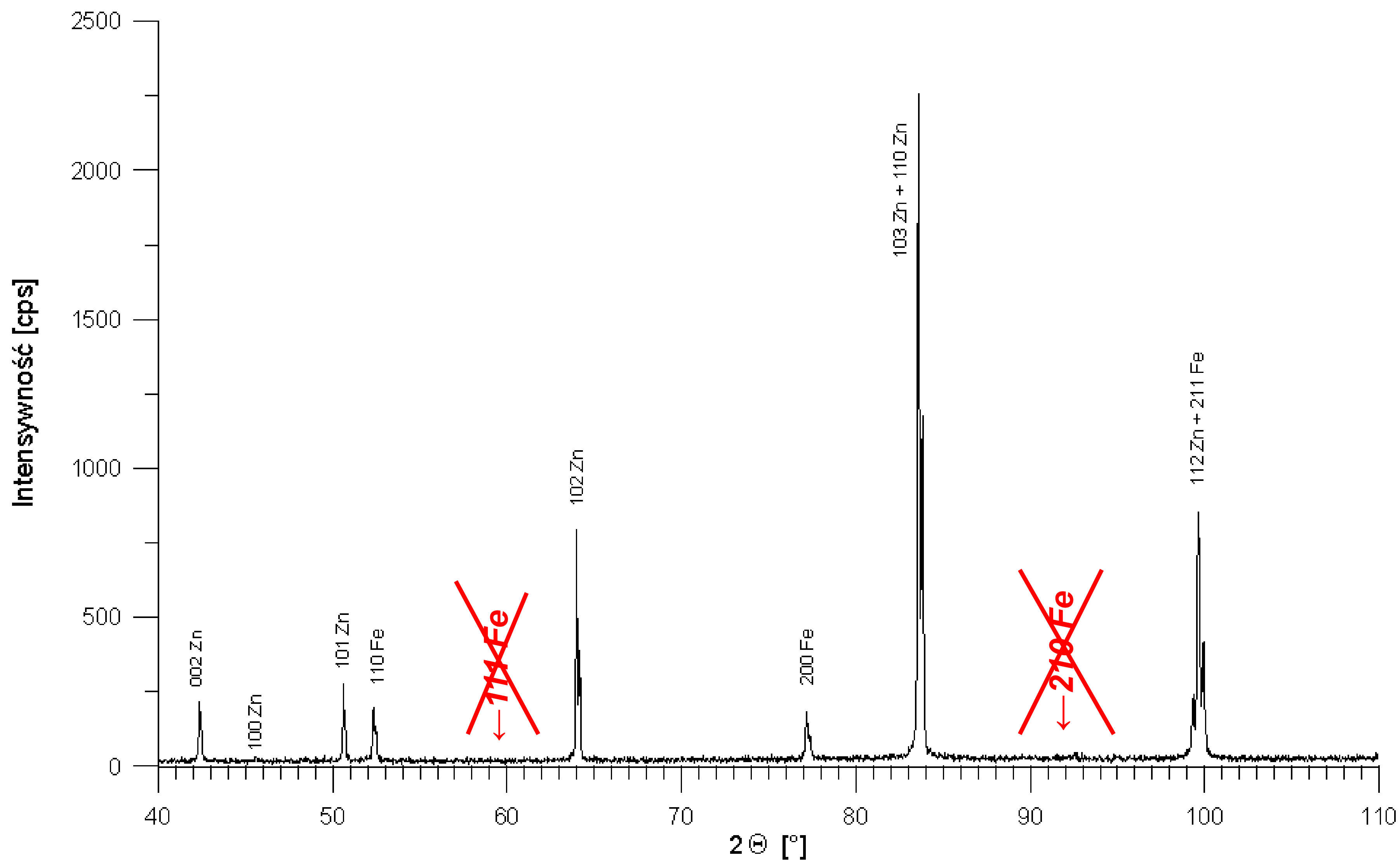
Dyfraktogram próbki stali głębokotłocznej pokrytej warstwą Zn (grubość ok. 7.5mikr.)
Użyte promieniowanie: CoK-alfa (śr.). IMIM-PAN, Kraków, Czerwiec 2000
Intensywność [cps]
2500
2000
1500
1000
500
0
40
50
60
70
80
90
100
110
2Θ [°]
002 Zn
100 Zn
101 Zn
110 Fe
111 Fe
102 Zn
200 Fe
103 Zn + 110 Zn
210 Fe
112 Zn + 211 Fe

Intensity of diffraction effect $I_{(hkl)}$ at defined Bragg angle $\theta_{(hkl)}$ for homogeneous phase of powdered sample:

$$I_{(hkl)} = \left(\frac{I_0 A \lambda^3}{32\pi r}\right)\left[\left(\frac{\mu_0}{4\pi}\right)^2 \frac{e^4}{m^2}\right]\left(\frac{1}{v^2}\right)\left[\left|F_{(hkl)}\right|^2 p_{(hkl)}\ LP_{(hkl)}\ \right]\left(\frac{e^{-2M}}{2\mu}\right)$$

where: I_0 - intensity of incident beam, A – cross-section of incident beamj [m^3], λ - wavelength [m],
r – radius of diffractometer, μ_0 – constant value, e- electric charge of electron [C], m – mass of electron [kg],
v – volume of elementary lattice cell [m^3], $F_{(hkl)}$ – structure amplitude (structure factor),
$p_{(hkl)}$ – multiplicity of lattice planes {*hkl*}, $LP_{(hkl)}$ – geometrical, (Lorenz-polarization) factor,
e^{-2M} - Debye-Waller factor, μ – liniear absorption coefficient [m^{-1}].

$$I_{(hkl)} = C\, I_0\, \lambda^3 \left|F_{(hkl)}\right|^2 p_{(hkl)}\ LP_{(hkl)} \left(\frac{e^{-2M}}{\mu}\right)$$

where:

$$C = \frac{A e^4 \mu_0{}^2}{1024\pi^2 m^2 v^2 r}$$

Indexing the crystallographic planes and directions

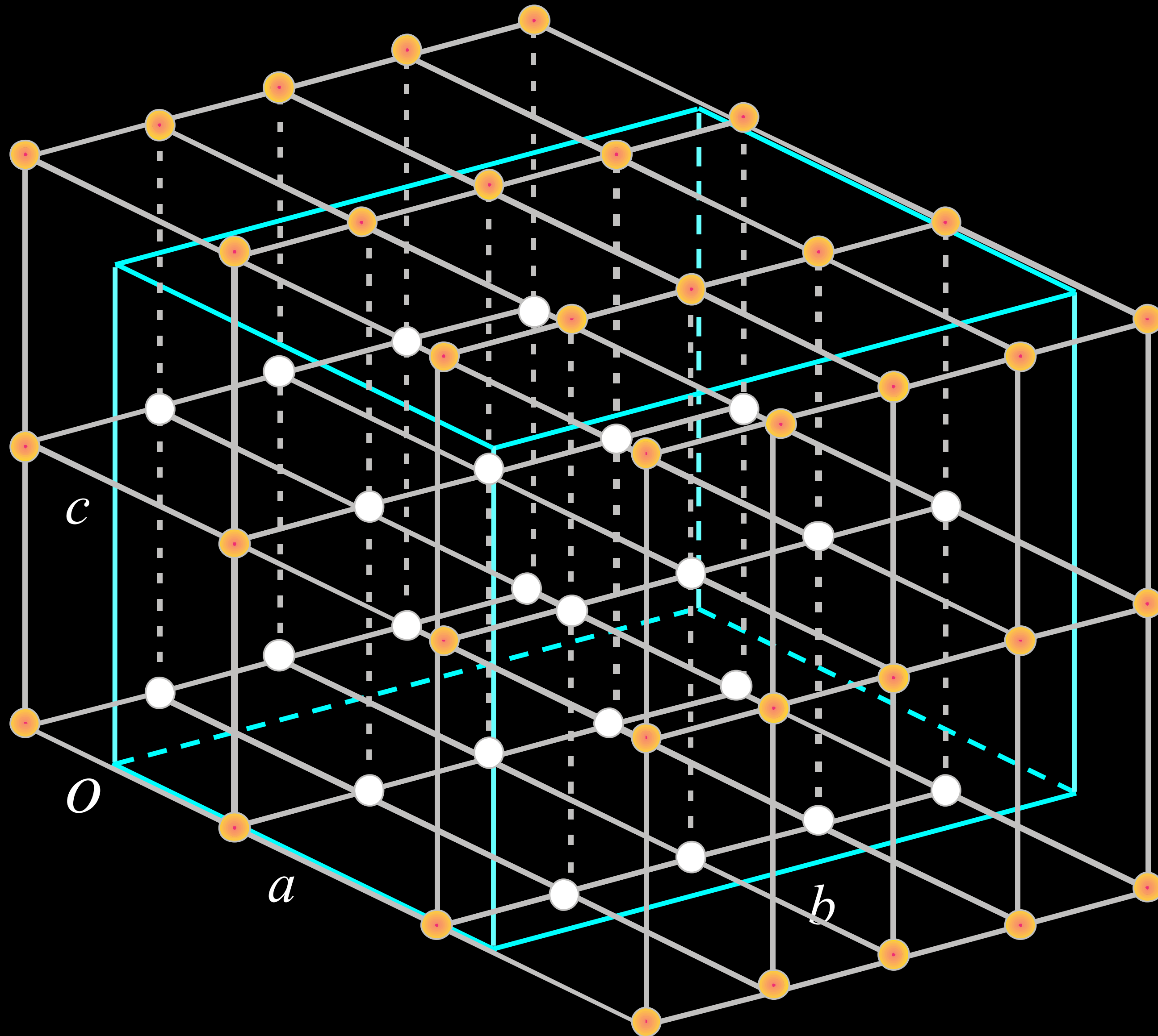

Miller indicies – are notation of the planes and directions defined in crystallographic lattice based on the elementary lattice cell.

Crystallographic **direction** – fractions of the basal vectors of the lattice cell [uvw], where u, v and w are complete numbers.
The family of directions crystallographically equivalent <uvw>.

Crystallographic directions in 2-D orthogonal lattice

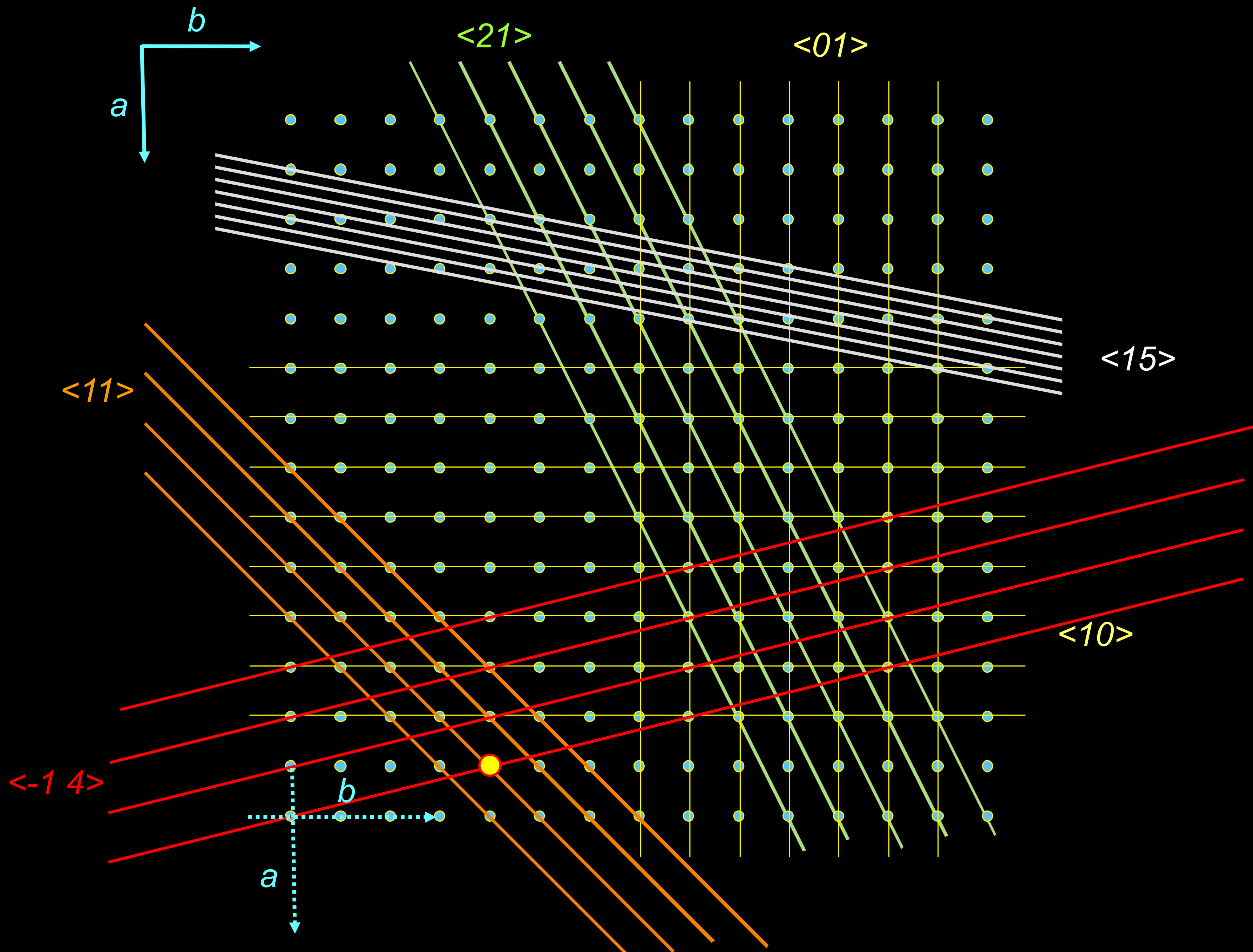

Miller indicies for **lattice planes** are expressed in form (hkl), where h, k, l are complete numbers indicate to how many parts of the basal periods a, b, c are divided by the plane

(na ile części dana płaszczyzna (najbliższa początku układu) dzieli podstawowe periody na osiach układu współrzędnych).

Family of crystallographically equivalent planes: {hkl}.

Miller indicies of a crystallographic plane

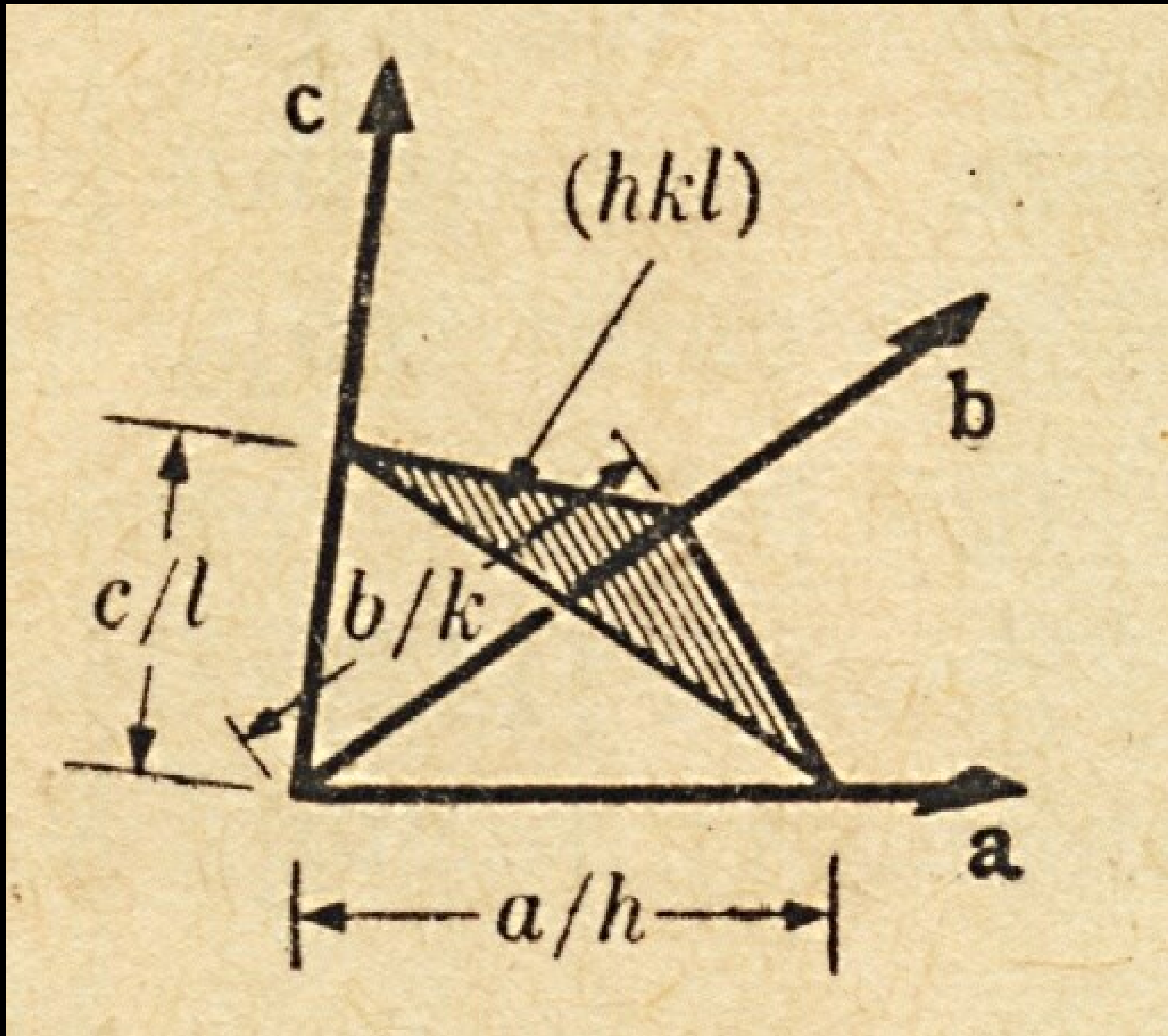

Basic families of the lattice planes

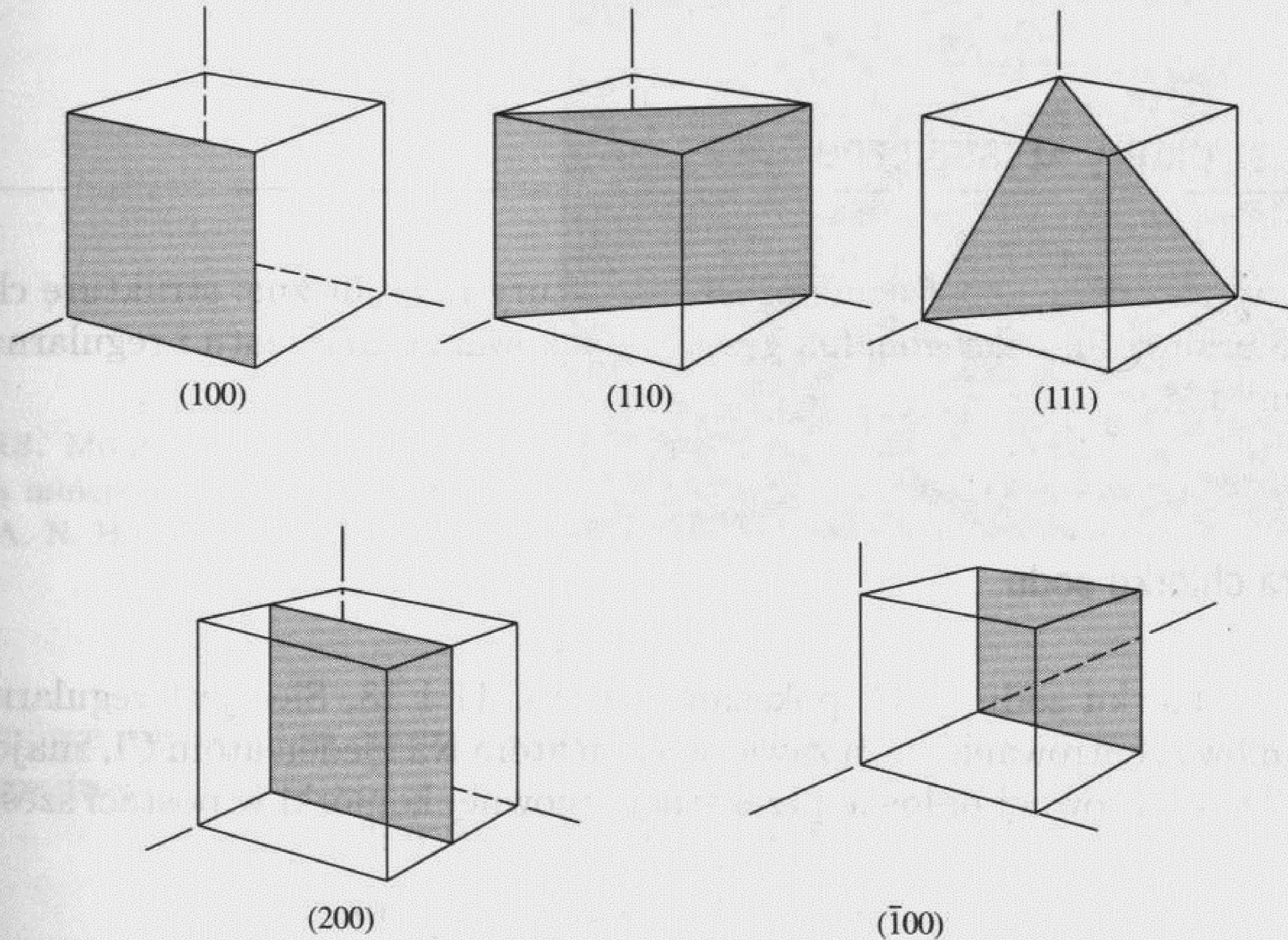

Rys. 16. Wskaźniki ważniejszych płaszczyzn kryształu o strukturze regularnej. Płaszczyzna (200) jest równoległa do płaszczyzn (100) i ($\bar{1}00$)

(100)
(010)
(001)
(110)
(1,-1,0)
(-1,1,0)
(111)
{111}

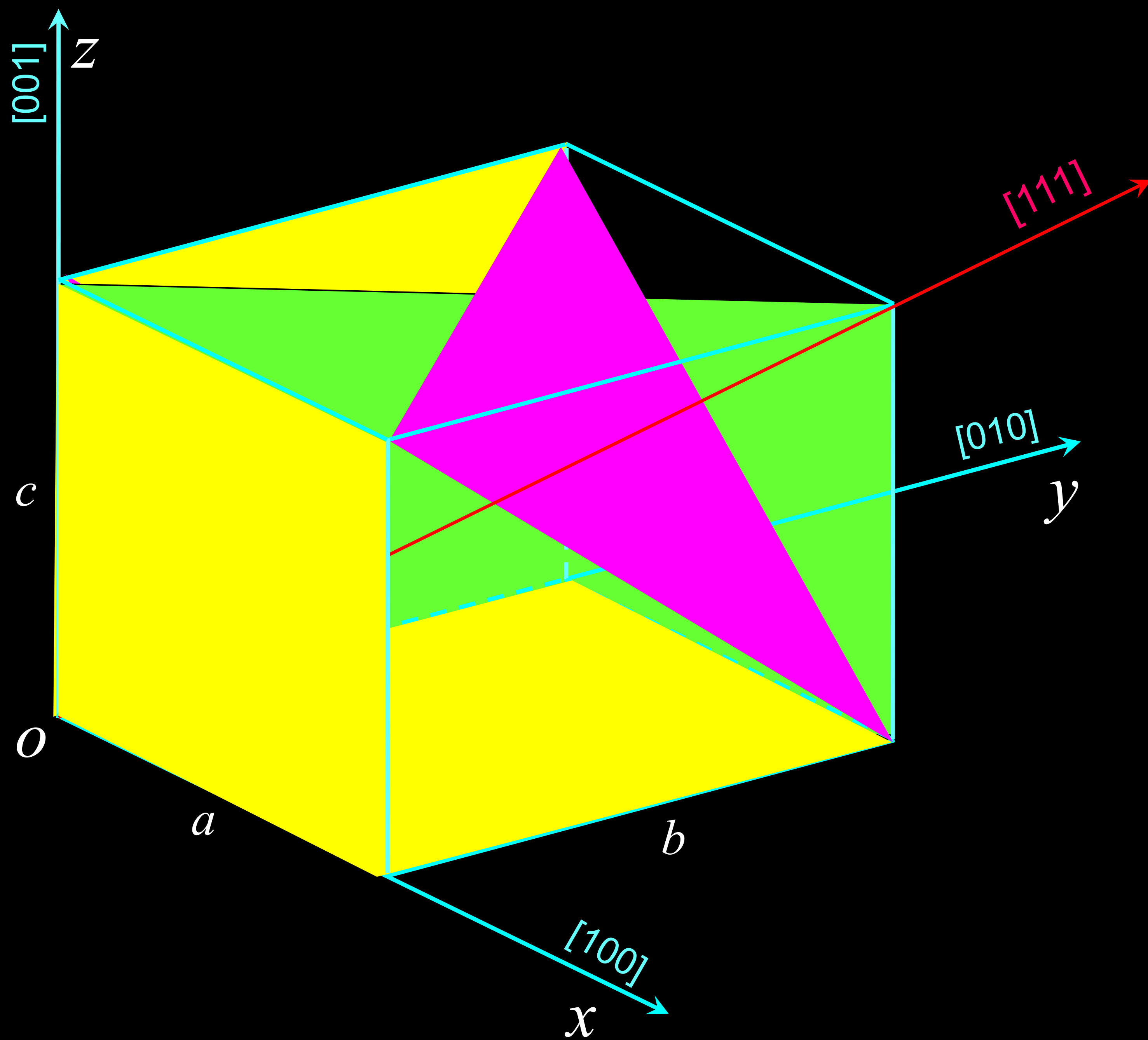

(112)

[112]

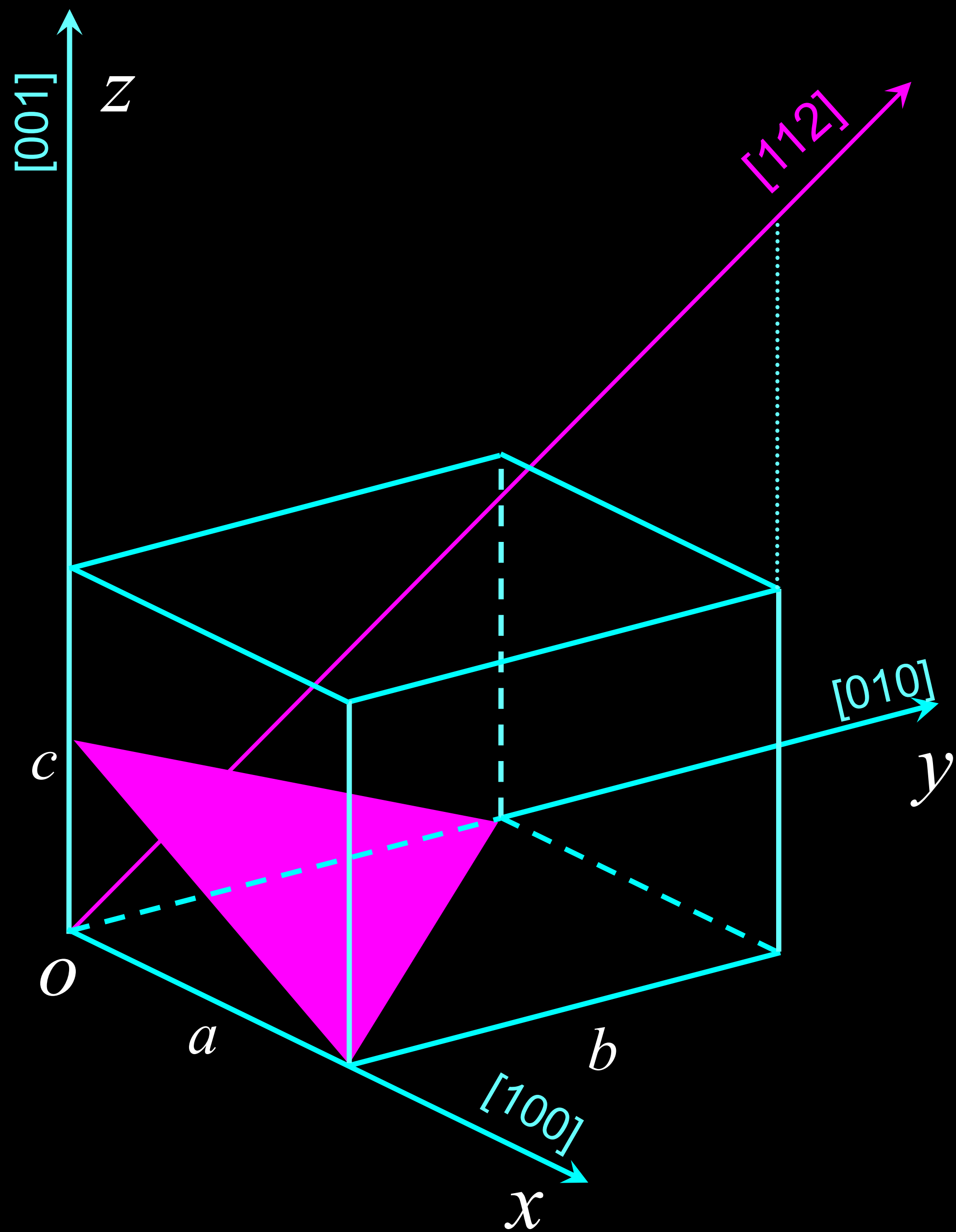

X-ray diffraction phenomenon. Part II

Jan T. Bonarski

Instytut Metalurgii i Inżynierii Materiałowej
im. Aleksandra Krupkowskiego
POLSKIEJ AKADEMII NAUK w Krakowie

Indexing the crystallographic planes and directions

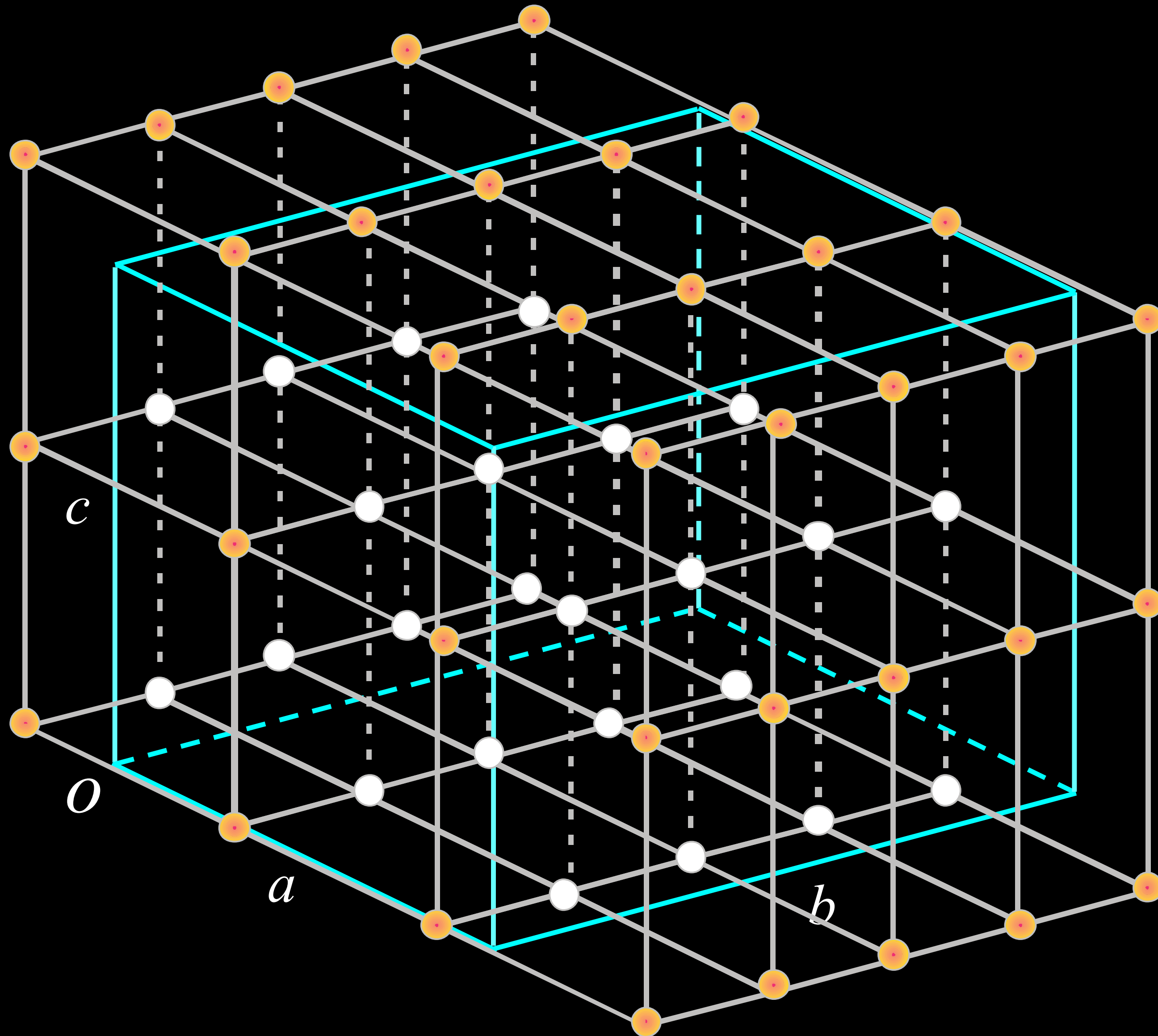

Miller indicies – notation of the planes and directions defined in crystallographic lattice based on the elementary lattice cell.

Crystallographic **direction** – fractions of the basal vectors of the lattice cell [uvw], where u, v and w are complete numbers.
The family of directions crystallographically equivalent <uvw>.

Crystallographic directions in 2-D orthogonal lattice

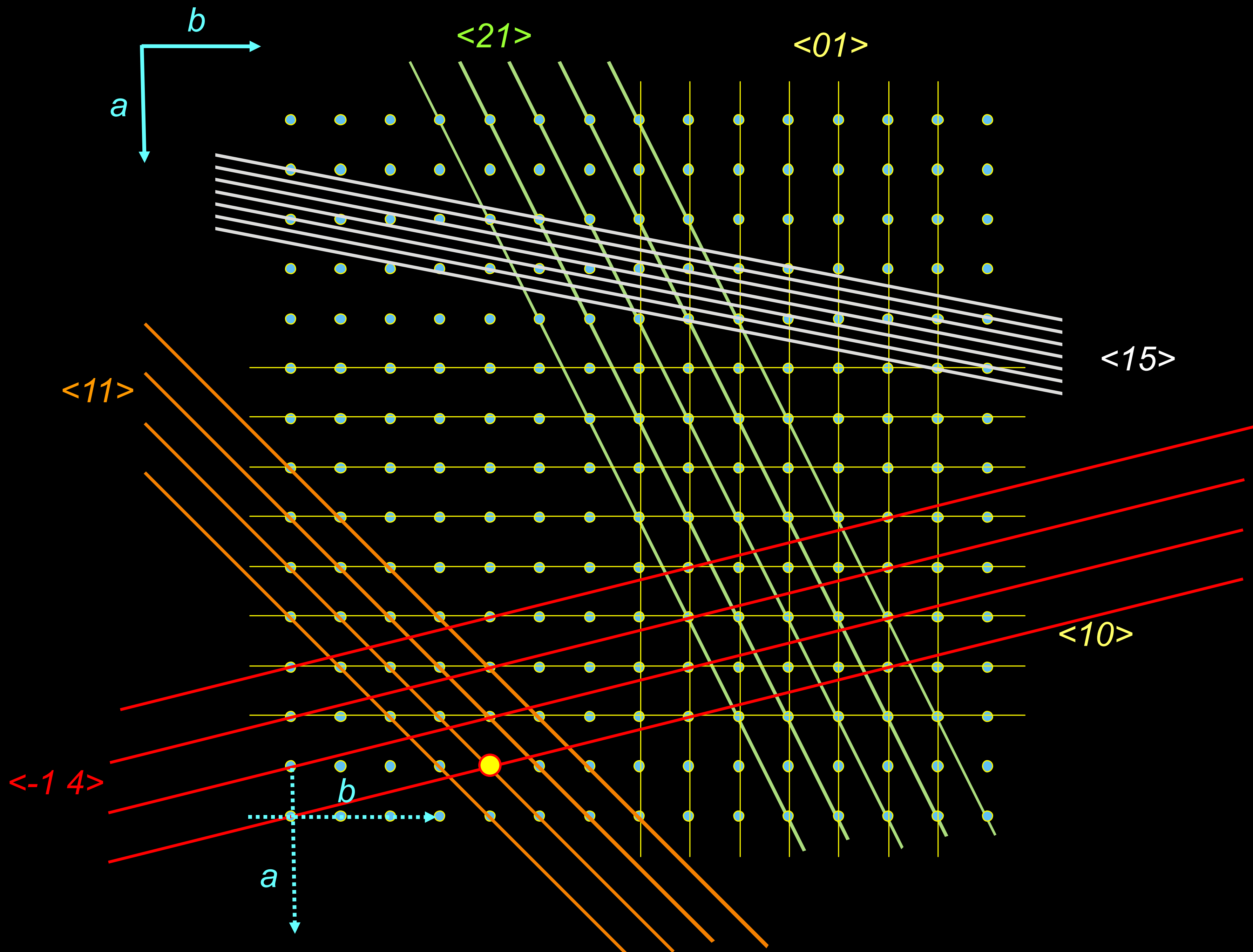

Miller indicies for **lattice planes** are expressed in form (hkl), where h, k, l are complete numbers indicate to how many parts of the basal periods a, b, c are divided by the plane

(na ile części dana płaszczyzna (najbliższa początku układu) dzieli podstawowe periody na osiach układu współrzędnych).

Family of crystallographically equivalent planes: {hkl}.

Crystalline body *– condensed matter with 3D ordered structure.*

Properties od crystals: electrical, magnetical, optical and mechanical, contrary to amorphous bodies.

Single (mono)- or Polycrystals

Single crystals: *mono-phase, non-defected crystalline body, eg.:*

- ***sapphire*** *(Al_2O_3 + small amount TiO_2 and Fe_3O_4)*
- ***ruby*** *(Al_2O_3 + small amount Cr_2O_3)*

Polycrystal*: conglomeration of single crystals (micro-meter dimension)*

Elementary cell

Ideal- and real crystals

Spatial lattice *– infinit conglomeration of ideal elementary cells*

Lattice nods *– points of intersection of edges of the elementary lattice.*

Lattice lines *– lines indicated by selected lattice nodes.*

Lattice planes *– planes indicated by the selected lattice nodes.*

Crystal structure *– way of distribution of atoms (ions, particles) in elementary cell.*

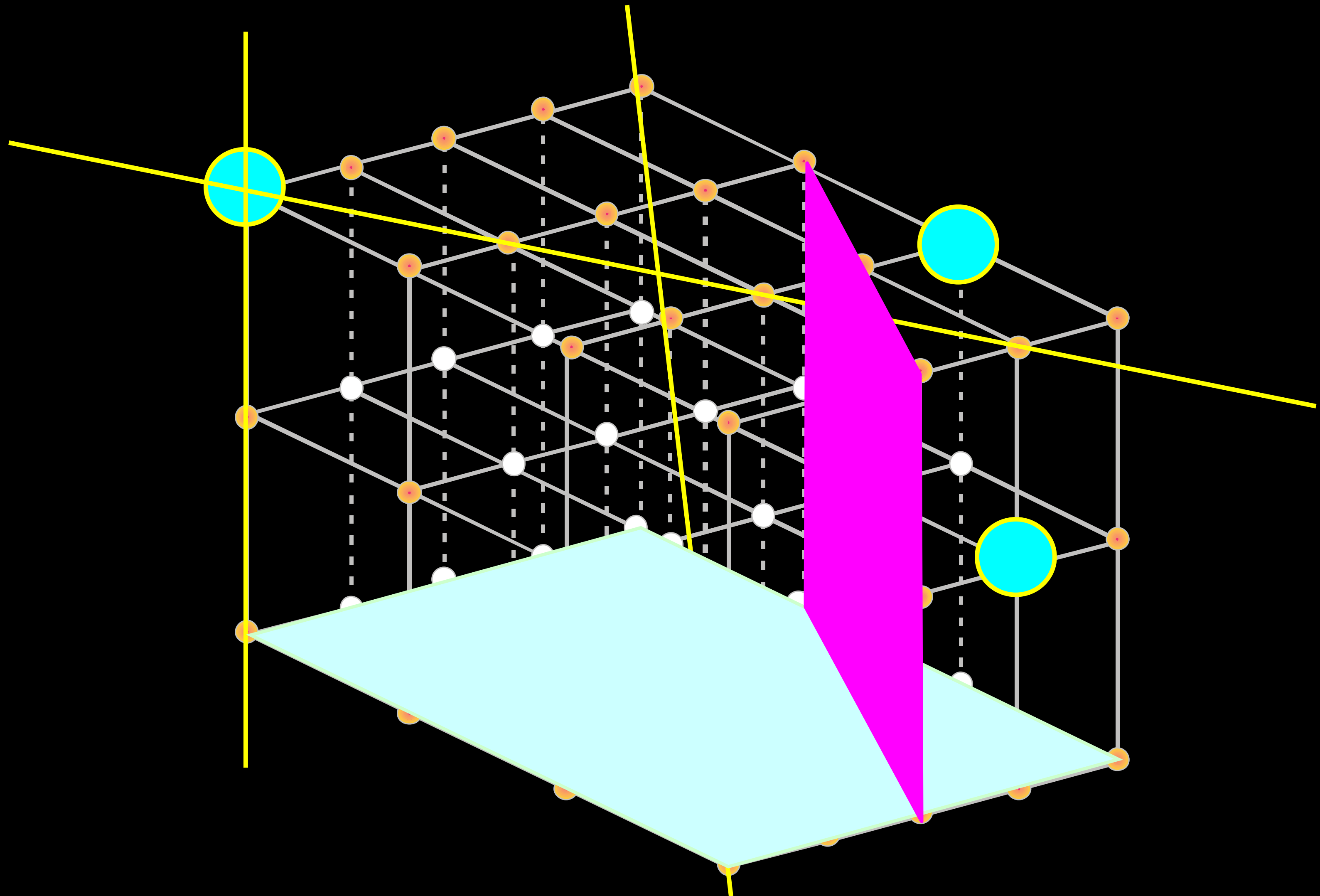

Regarding the values of lattice constants of the crystals and symmetry of spatial lattice ***6(7)*** various ***crystallographic systems*** have been defined. Lattice periods ***a, b, c*** and angles α, β and γ.

An elementary cell which translation along X, Y, Z reconstruct whole spatial lattice can be distinguished in each of the crystallographic system.

Cells: *primitive* **P**, *centered:* **C** (on basal planes), **F** (face-centered), **I** (spatial-centered)
Each of the ***6(7)*** crystallographic system, dependig on its symmetry, have a strictly defined number of the elementary cells. As it was prooved, there are ***14*** various cells – ***Bravais cells***

TRICLINIC

MONOCLINIC

RHOMBOHEDRAL ≡ *ORTHORHOMBIC*

TRIGONAL
(describing analogically to hexagonal)

TETRAGONAL

HEXAGONAL ≡ *RHOMBOHEDRAL*

REGULAR

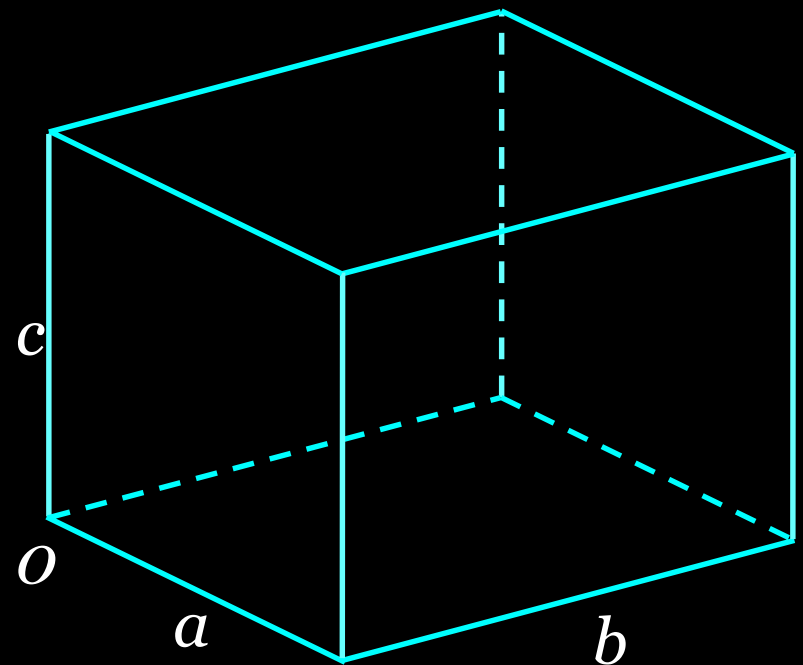

Crystallographic system: **REGULAR** $a_0 = b_0 = c_0$ $\alpha = \beta = \chi = 90°$

Bravais cells: **P** (primitive) **I** (body centered, *bcc*, A2) **F** (face centered, *fcc*, A1)

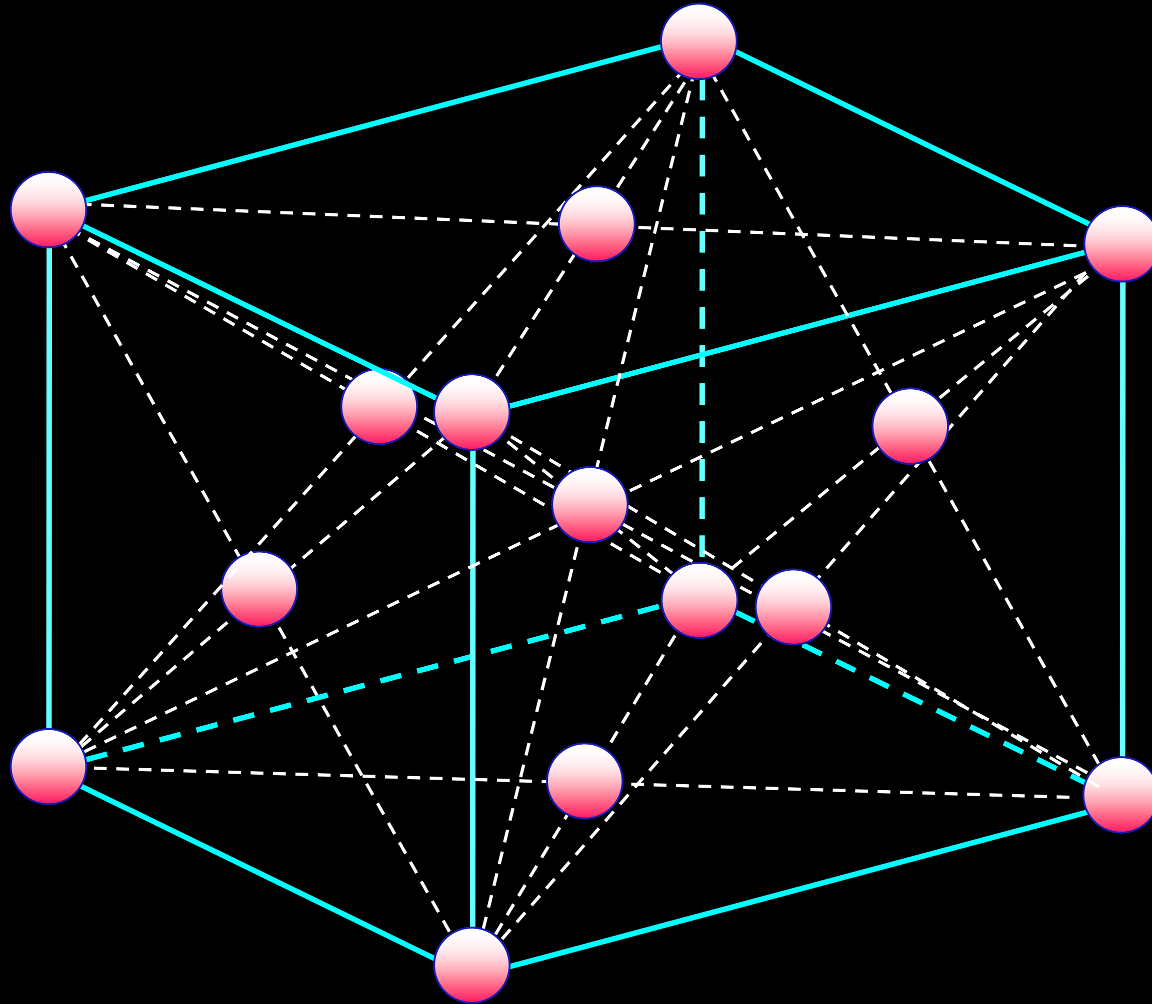

Table 19. Periodic Table of the Face Centered Cubic Elements

1 IA	2	3	4	5	6	7	8	9	10	11	12	13	14	15	16	17	18 VIIA
	IIA											IIIA	IVA	VA	VIA	VIIA	
																	10 Ne
		IIIB	IVB	VB	VIB	VIIB	-----	VIII	-----	IB	IIB	13 Al	14 Si				18 Ar
	20 Ca								28 Ni	29 Cu			32 Ge				36 Kr
	38 Sr							45 Rh	46 Pd	47 Ag							54 Xe
								77 Ir	78 Pt	79 Au			82 Pb				86 Rn

57 La														
89 Ac														

Table 18. PERIODIC TABLE OF THE BODY CENTERED CUBIC ELEMENTS

	1	2	3	4	5	6	7	8	9	10	11	12	13	14	15	16	17	18
	IA	IIA	IIIB	IVB	VB	VIB	VIIB	-----	VIII	-----	IB	IIB	IIIA	IVA	VA	VIA	VIIA	VIIA
	3 Li																	
	11 Na																	
	19 K				23 V	24 Cr	25 Mn	26 Fe										
	37 Rb				41 Nb	42 Mo												
	55 Cs	56 Ba			73 Ta	74 W												
	87 Fr	88 Ra																
								63 Eu										

Crystallographic system: **TETRAGONAL** $a_0 = b_0 \neq c_0$ $\alpha = \beta = \chi = 90°$

Bravais cells: **P** (primitive) **I** (body centered)

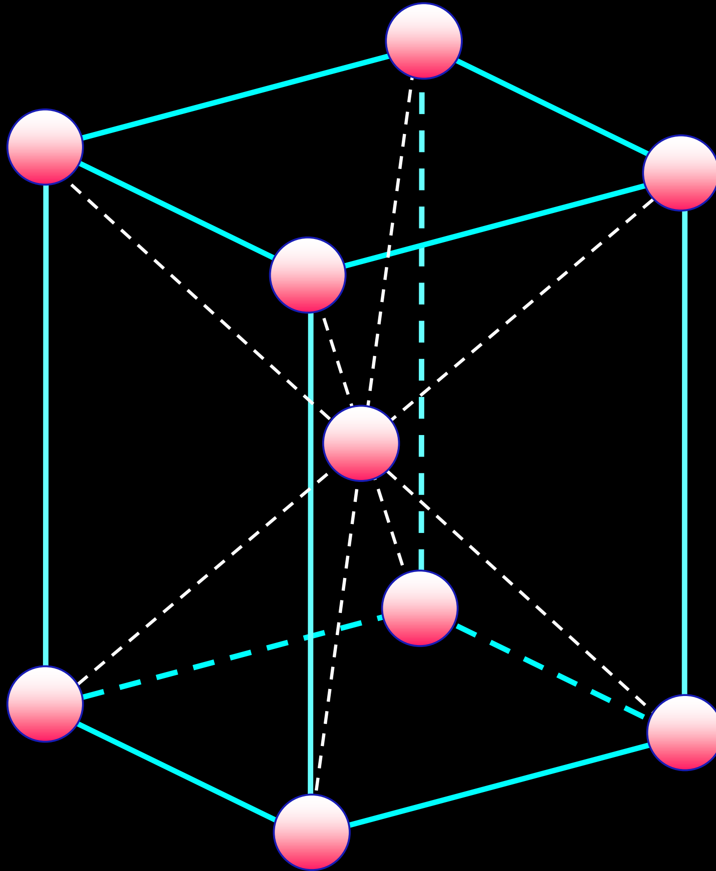

Tetragonal: eg. corundum, *quartz, turmalinum, α-Fe_martensite*

Crystallographic system: **RHOMBOHEDRAL** $a_0 \neq b_0 \neq c_0$ $\alpha = \beta = \chi = 90°$

Bravais cells: **P** (primitive) **I** (body centered) **C** (basal-planes centered) **F** (face centered)

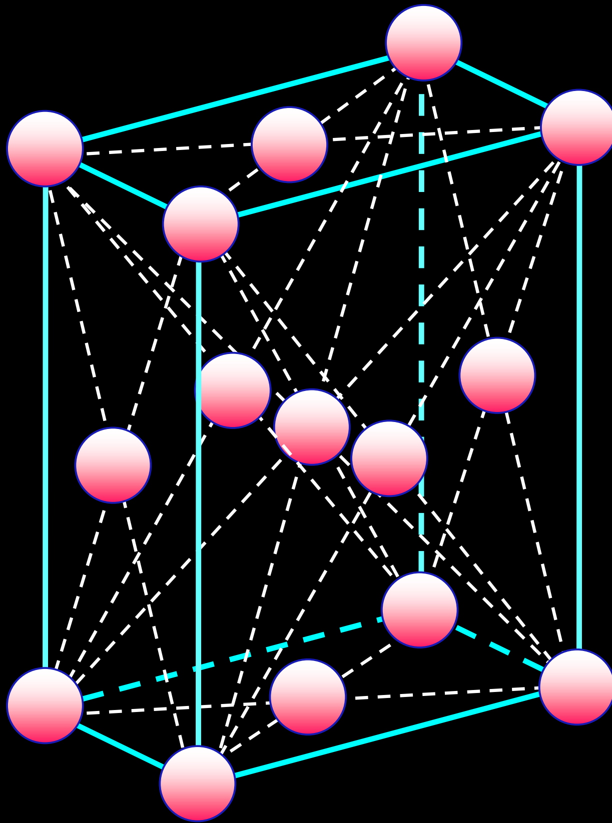

Rhombohedral: eg. *topaz, aragonite (variant of $CaCO_3$, eg. Conus Marmoreus)*

Crystallographic system: **MONOCLINIC** $a_0 \neq b_0 \neq c_0$ $\alpha = \gamma = 90°$, $\beta \neq 90°$

Bravais cells: **P** (primitive) **C** (basal-planes centered)

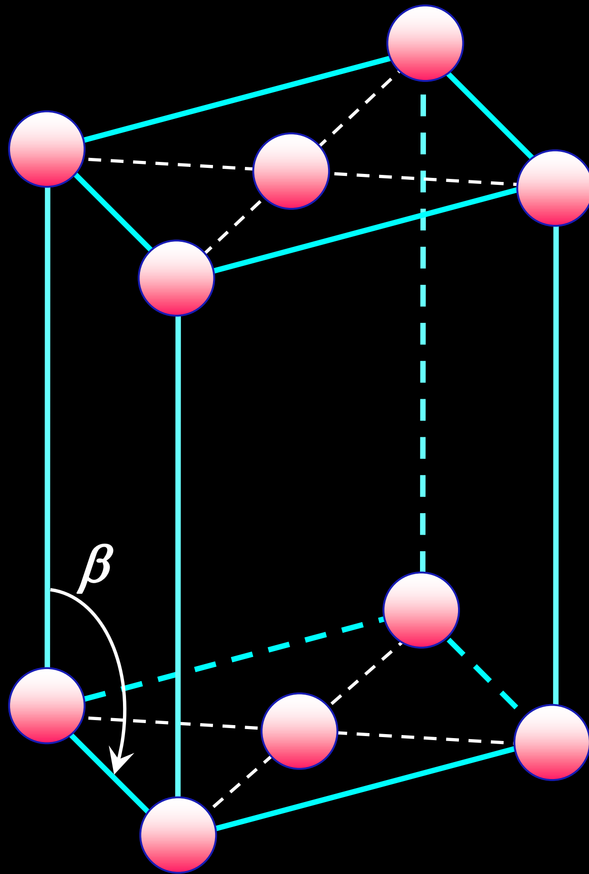

Monoclinic: eg. *cellulose (crystalline part), jade (nefryt)*

Crystallographic system: **TRICLINIC** $a_0 \neq b_0 \neq c_0$ $\alpha \neq \beta \neq \gamma \neq 90°$

Bravais cells: **P** (primitive)

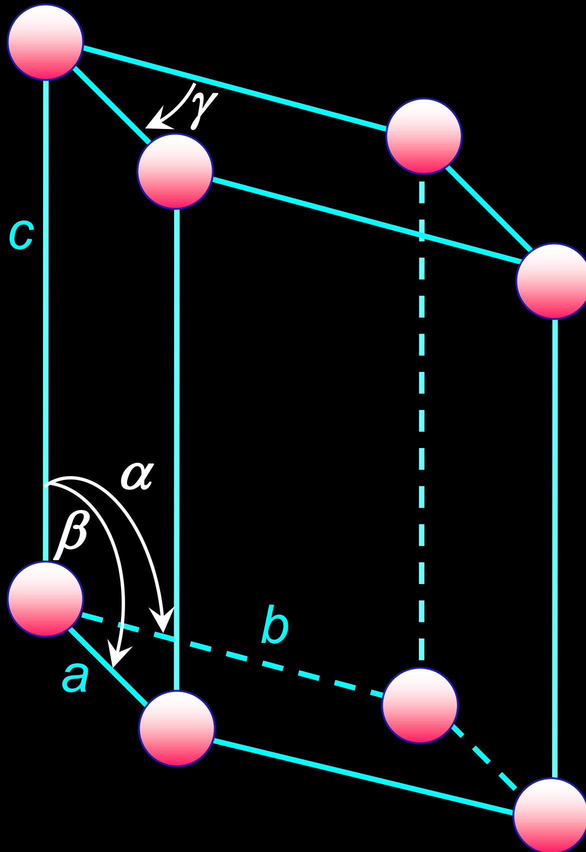

Triclinic: eg. *turquoises (turkus), amazonite*

Crystallographic system: **HEXAGONAL** $a_0 = b_0 \neq c_0$ $\alpha = \beta = 90°$, $\gamma = 120°$

Bravais cells: **P** (primitive)

hcp (hexagonal close packed)

$c_0 / a_0 = 1.633$

Ti ($c_0 / a_0 = 1.588$)

Mg ($c_0 / a_0 = 1.624$)

Co ($c_0 / a_0 = 1.623$)

Zn ($c_0 / a_0 = 1.856$)

Cd ($c_0 / a_0 = 1.886$)

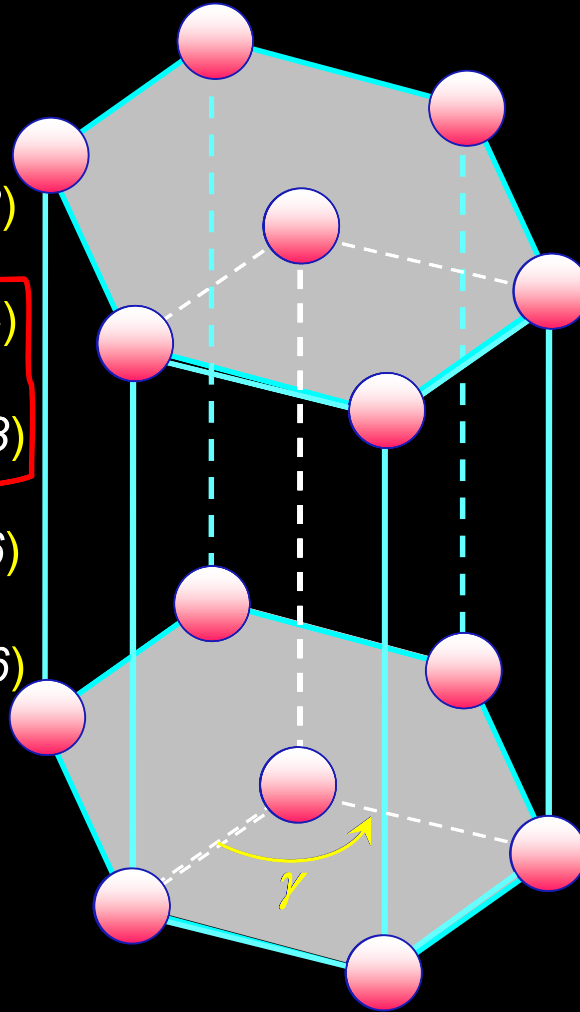

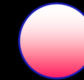

Table 21. PERIODIC TABLE OF THE HEXAGONAL ELEMENTS

1	2	3	4	5	6	7	8	9	10	11	12	13	14	15	16	17	18
IA	IIA	IIIB	IVB	VB	VIB	VIIB	-----	VIII	-----	IB	IIB	IIIA	IVA	VA	VIA	VIIA	VIIA
													6 C				
															34 Se		
															52 Te		

57 La		59 Pr	60 Nd	61 Pm										
						95 Am	96 Cm	97 Bk						

Table 20. PERIODIC TABLE OF THE HEXAGONAL CLOSE PACKED ELEMENTS

1	2	3	4	5	6	7	8	9	10	11	12	13	14	15	16	17	18
IA																	VIIA
	IIA											IIIA	IVA	VA	VIA	VIIA	
	4 Be																
	12 Mg	IIIB	IVB	VB	VIB	VIIB	-----	VIII	-----	IB	IIB						
			22 Ti					27 Co			30 Zn						
		39 Y	40 Zr			43 Tc	44 Ru				48 Cd						
			72 Hf			75 Re	76 Os					81 Tl					

							64 Gd	65 Tb	66 Dy	67 Ho	68 Er	69 Tm		71 Lu

Crystallographic system: **HEXAGONAL**

A9 (graphite type structure)

typical layered structure

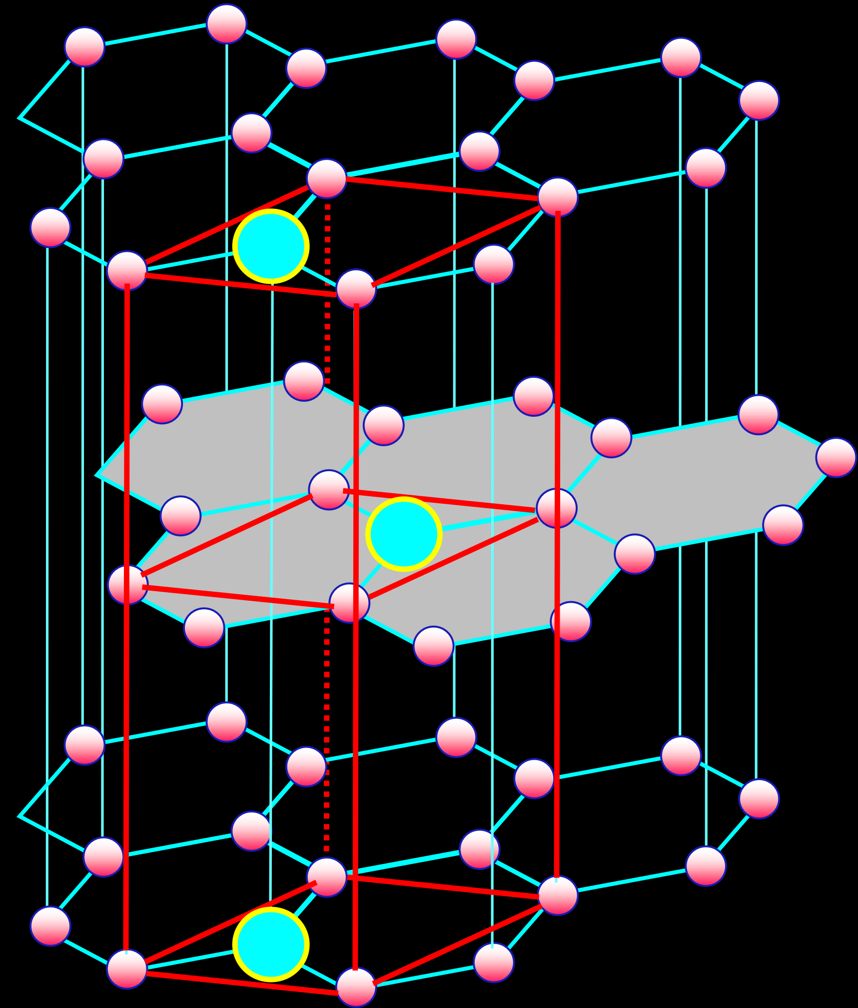

$c_0 / a_0 = 2.76$

Allotropic variety of carbon:

- **Diament** (regular + hexagonal)
- **Graphite *β*** (rhombohedric ≡ hexagonal)
- **Fulerens C_{60}** (since 1985r)
- **Graphene** (since 2010r)

Graphite-type structures – strong anizotropy of properties: cleavage (łupliwość), thermal expansion, electric conductivity

Crystallographic system: **TRIGONAL** $a_0 = b_0 \neq c_0 \quad \alpha = \beta = 90°, \gamma = 120°$

RHOMBOHEDRAL $a_0 = b_0 = c_0 \quad \alpha = \beta = \gamma \neq 90°$

Bravais cells: **P** (primitive)

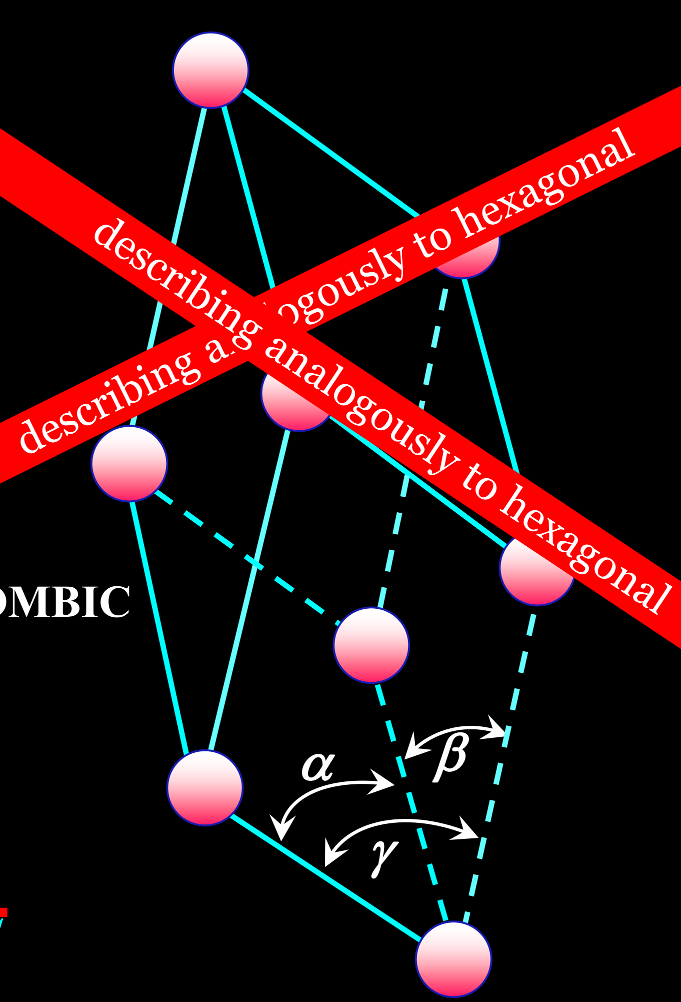

Rhombohedral: eg. *graphite β*

TRICLINIC

MONOCLINIC

~~**RHOMBOHEDRAL**~~ ≡ **ORTHORHOMBIC**

~~**TRIGONAL**~~

(describing analogically to hexagonal)

TETRAGONAL

HEXAGONAL ≡ ~~***RHOMBOHEDRAL***~~

REGULAR

by. Int. Tabl. Cryst., ***6*** *crystallographic families and* ***7*** *crystallographic systems*

α-corundum α-Al_2O_3

~~Rhombohedral~~ Hexagonal lattice (R-3c):

a_0 = 4.7580 Å, c_0 = 12.9910 Å, $\alpha = \beta = 90°$, $\gamma = 120°$

$50 \times 50 \times 8$ mm^3

silicon carbide SiC

Hexagonal lattice (P63mc):

a_0 = 3.0810 Å, c_0 = 10.0610 Å, $\alpha = \beta = 90°$, $\gamma = 120°$

$50 \times 50 \times 10$ mm^3

Miller-Bravais Indicies

In 3-digit Miller's notation (planes and directions) for ***hexagonal system*** the crystallographicaly equivalent planes have various indicies. The inconvenience is not exists in 4-digit Miller-Bravais notation.

Plane (HKiL), where *H*, *K*, *i* and *L* are complete numbers, where $i = -(H + K)$

$H = h$

$K = k$

$i = -(h + k)$

$L = l$

Direction expressed as [UVTW] where *U*, *V*, *T* and *W* are complete numbers, additionally $\mathbf{T} = -(\mathbf{U} + \mathbf{V})$, …but indicies of directions *can not be derived directly* from the equivalent Miller indicies

$U = (2u - v)/3$

$V = (2v - u)/3$

$T = -(u + v)/3$

$W = w$

Crystallographic system: **HEXAGONAL** $a_0 = b_0 \neq c_0 \quad \alpha = \beta = 90°, \gamma = 120°$

Bravais cells: **P** (primitive)

$c_0 / a_0 = 1.633$

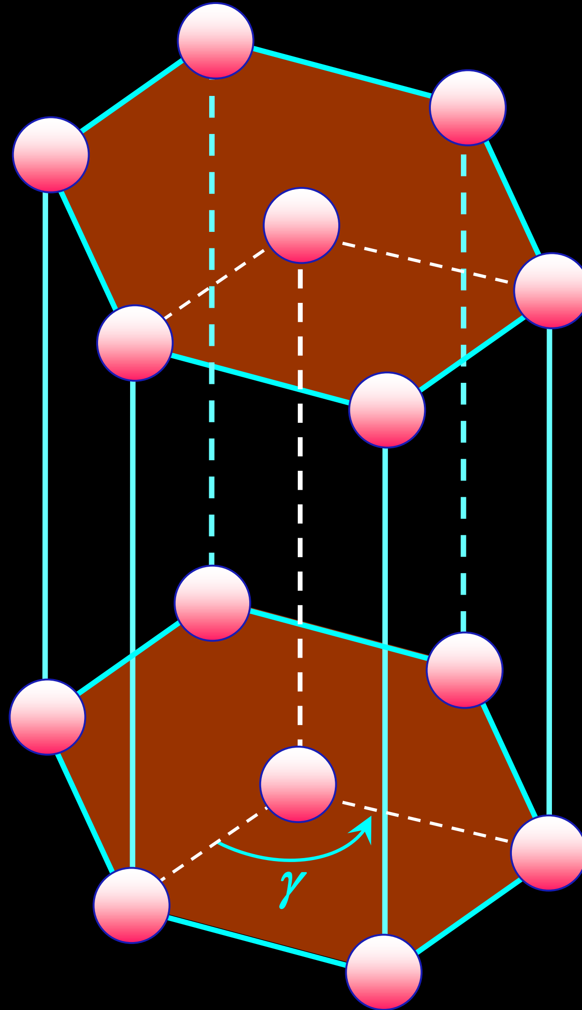

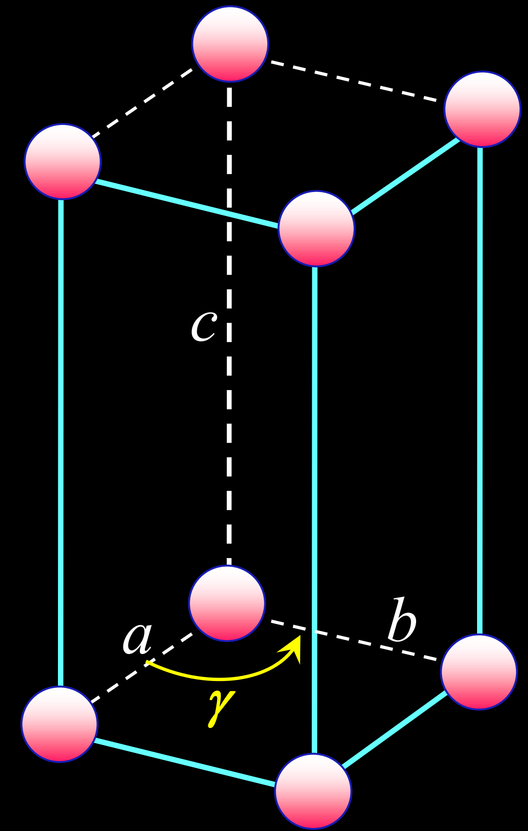

Crystallographic system: **HEXAGONAL** $a_0 = b_0 \neq c_0 \quad \alpha = \beta = 90°,\ \gamma = 120°$

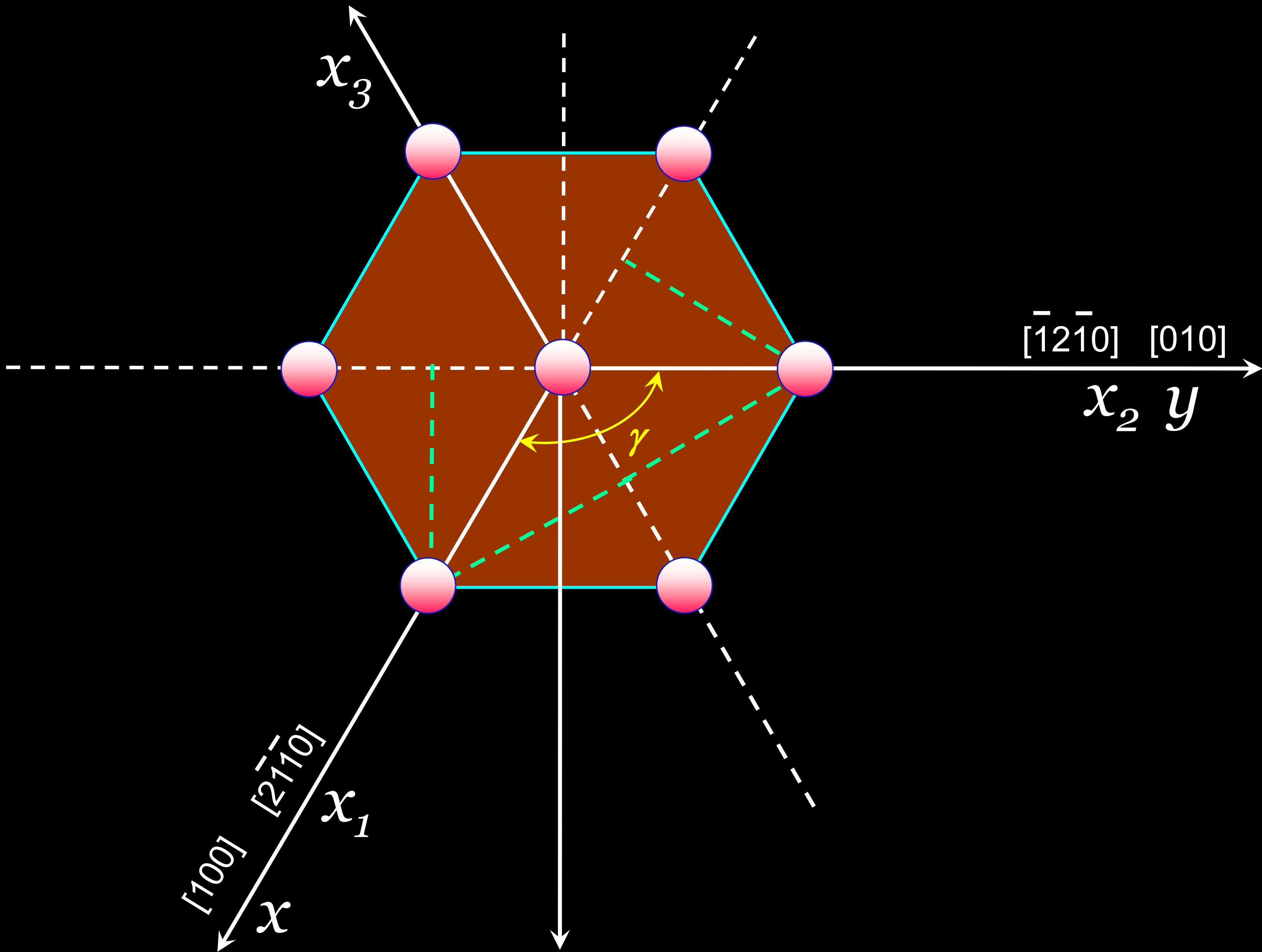

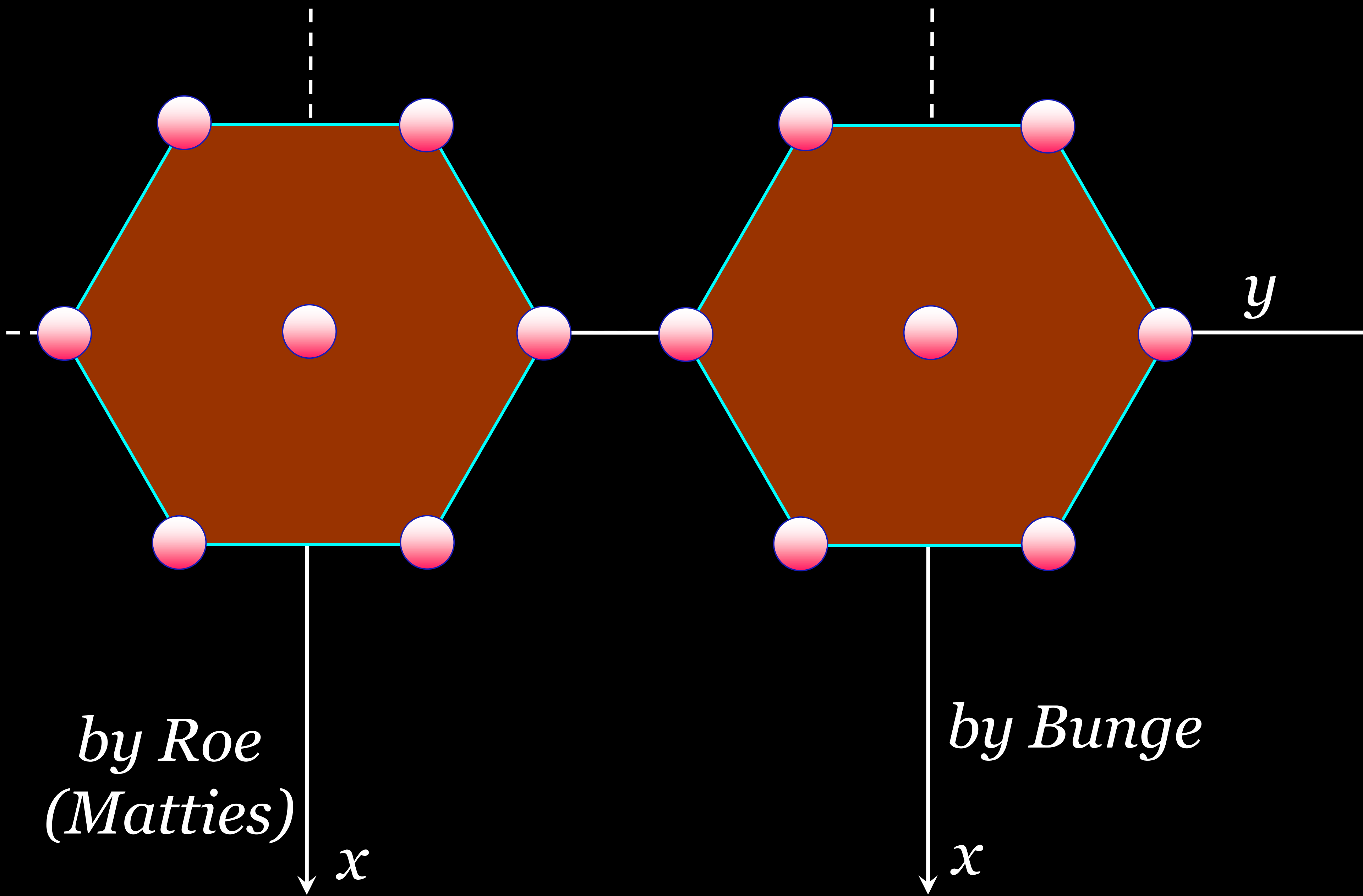

y
by Roe
(Matties)
x
by Bunge
x

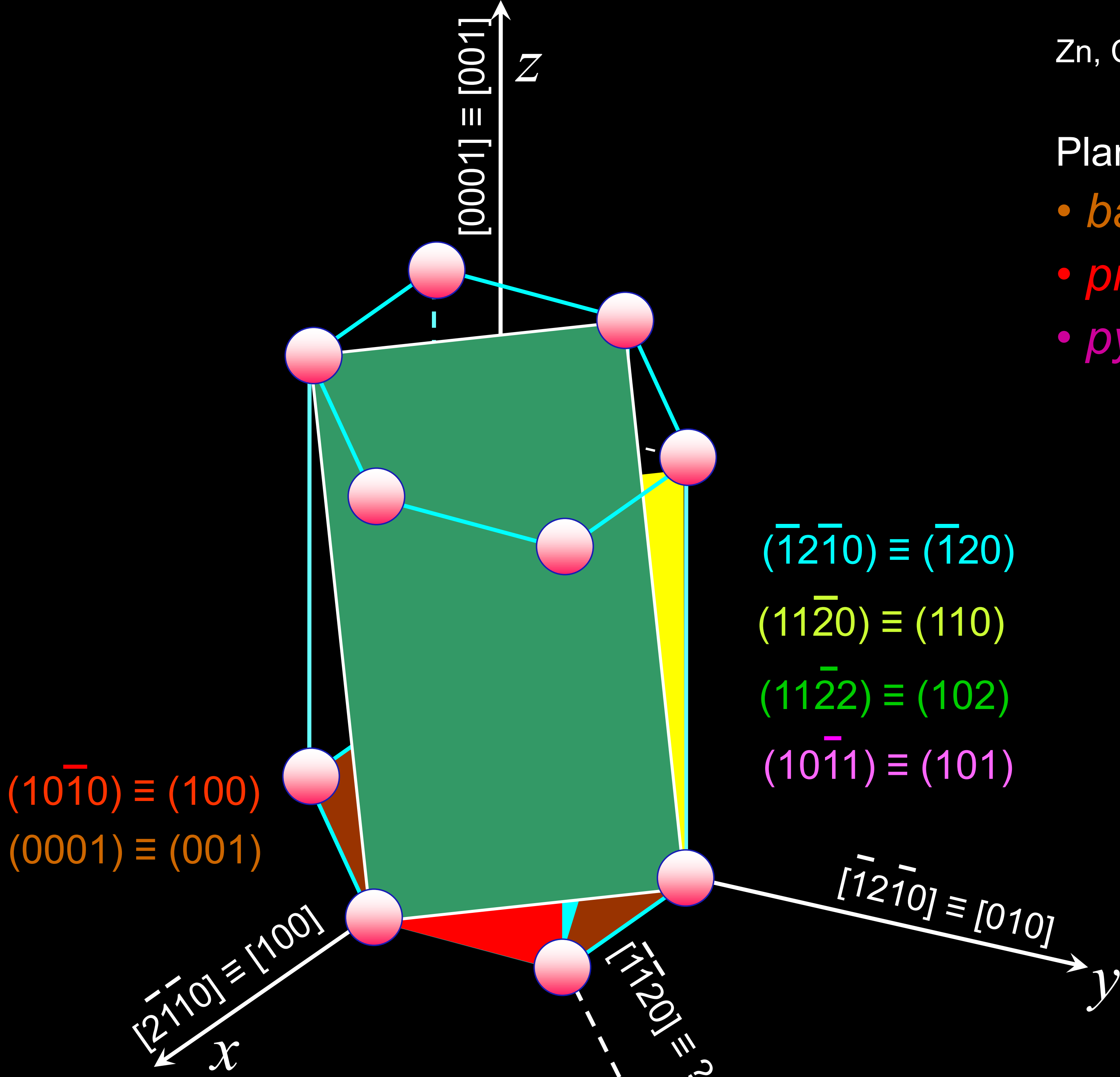

Zn, Cd, Mg, Co, Ti, Zr
Planes:
• basal,
• prismatic,
• pyramidal
$(\bar{1}2\bar{1}0) \equiv (\bar{1}20)$
$(11\bar{2}0) \equiv (110)$
$(11\bar{2}2) \equiv (102)$
$(10\bar{1}1) \equiv (101)$
$(10\bar{1}0) \equiv (100)$
$(0001) \equiv (001)$
$[0001] \equiv [001]$
z
$[2\bar{1}\bar{1}0] \equiv [100]$
x
$[\bar{1}2\bar{1}0] \equiv [010]$
y
$[\bar{1}\bar{1}20] \equiv$

…thus, what for we use the 4-digit (Millera-Bravais) indicies instaed of the 3-digit (Miller) one if the both describe the same (hexagonal) system?

…because the 4-digit (Millera-Bravais) indicies better express the lattice symmetry, eg. Lattice planes (110) and (-1 2 0)

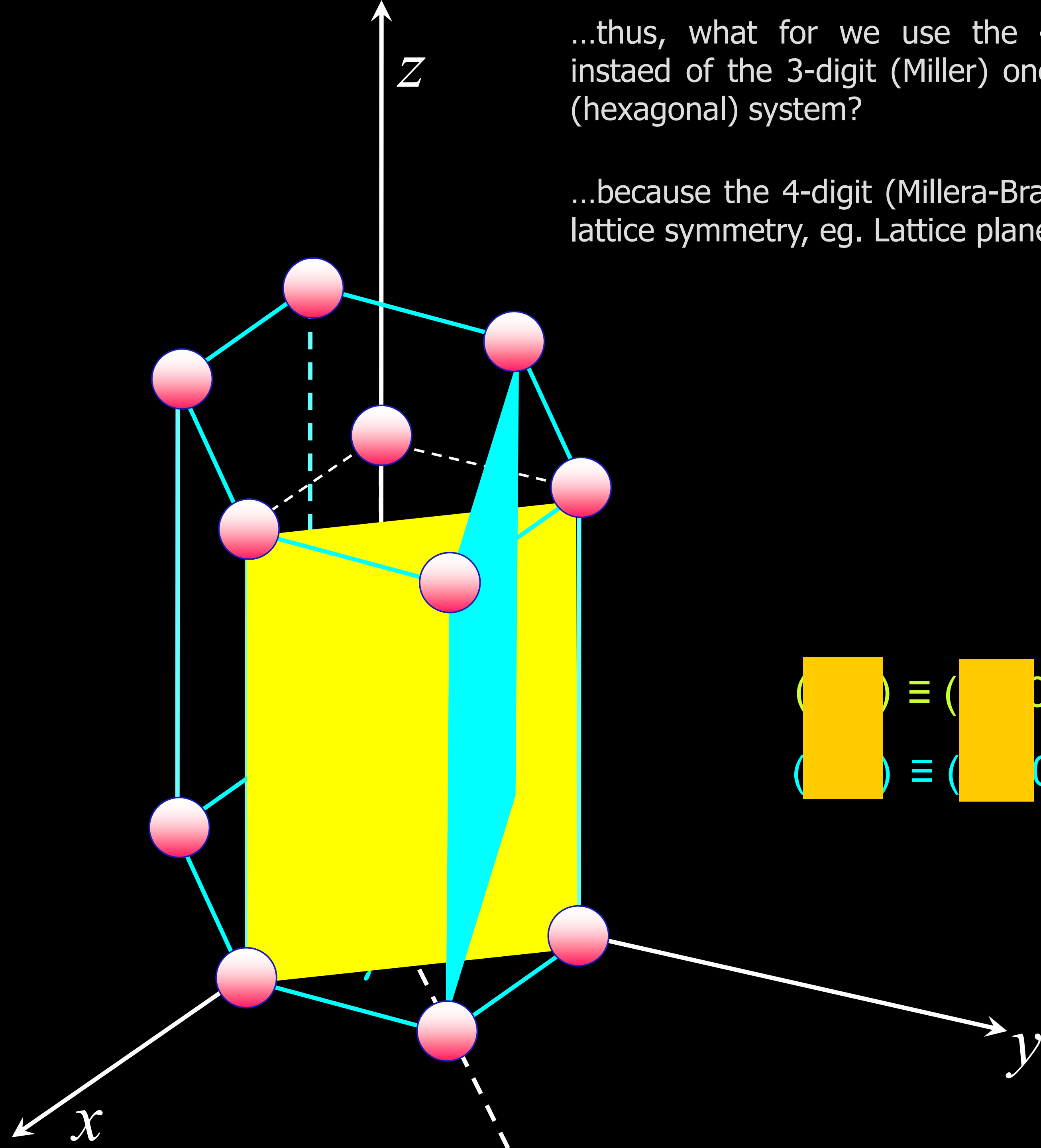

( ) ≡ (0)

( ) ≡ (0)

Crystal zone (pas krystalograficzny)

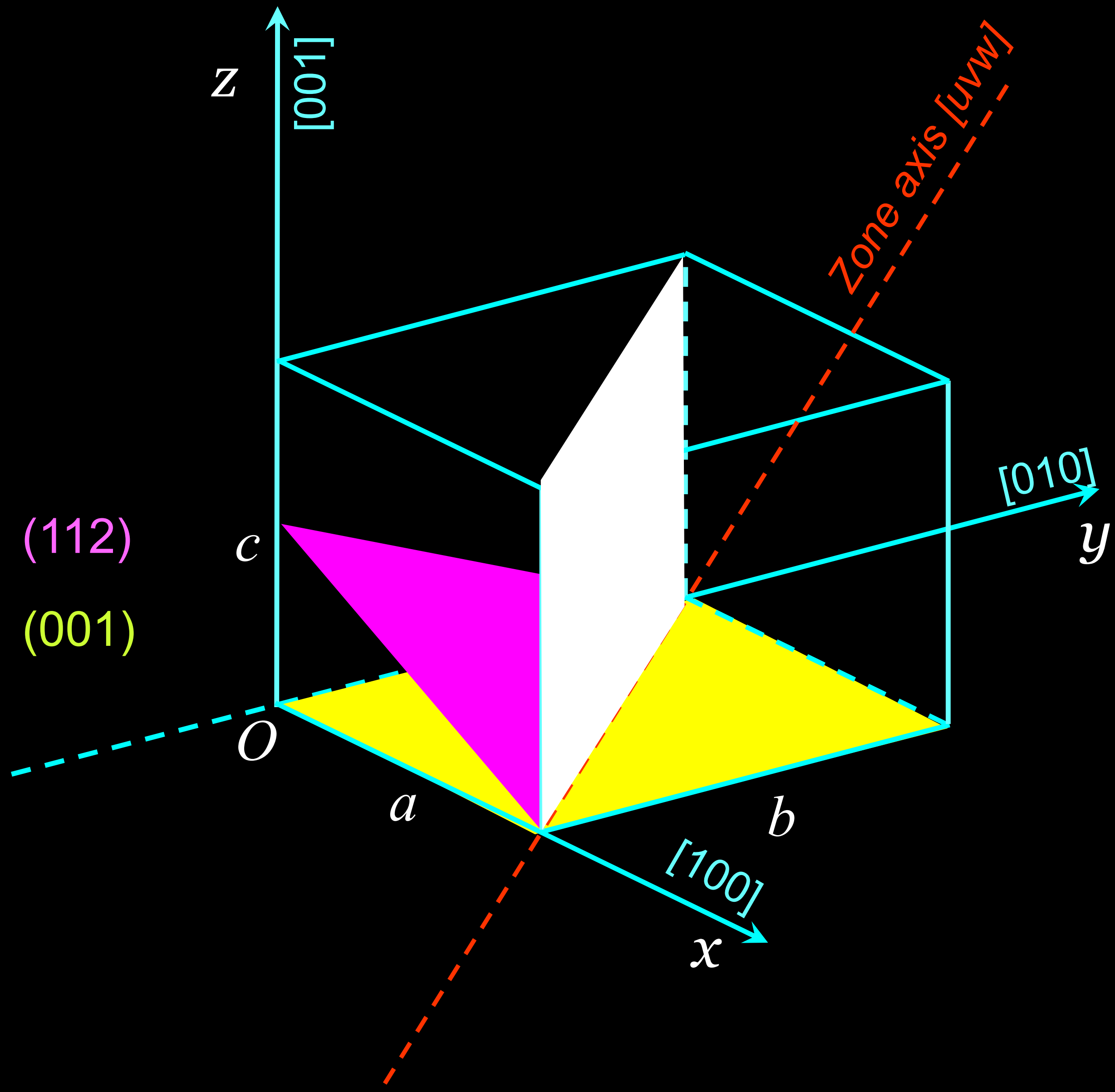

$h_1 k_1 l_1$ $h_2 k_2 l_2$

zone axis [uvw]:

$u = k_1 l_2 - k_2 l_1$

$v = l_1 h_2 - l_2 h_1$

$w = h_1 k_2 - h_2 k_1$

Crystal zone law:

gdy dwa wektory są ⊥ to ich iloczyn skalarny musi = 0

[hkl] · [uvw] = 0

hu + kv + lw = 0

(112) (001)

1 1 2 1 1 2
0 0 1 0 0 1

1-0, 0-1, 0-0

$[1\bar{1}0]$

W układzie heksagonalnym → analogicznie, ale użyć 3-wskaźnikowego zapisu

Idea of reciprocal lattice

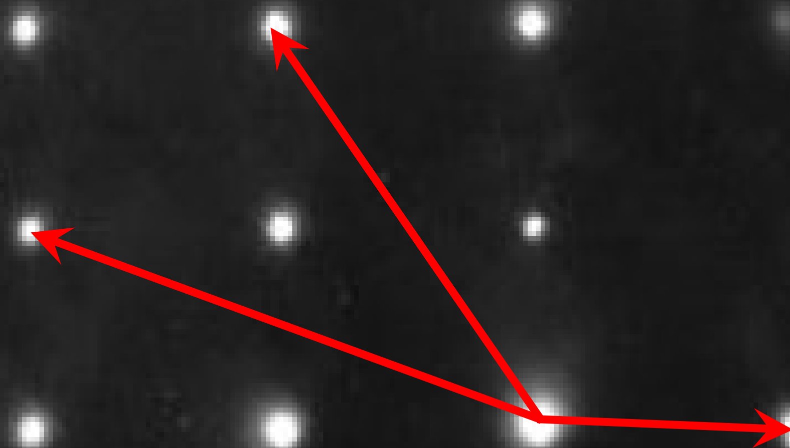

Reciprocal lattice is defined by **6** *parametrs, and given equations – using parameters of the real space – allow to calculate the* ***length of vectors***:

$$\bar{a}^* = \frac{\bar{b} \times \bar{c}}{\bar{a}(\bar{b} \times \bar{c})}$$

a* *is perpendicular to* **b** *and to* **c** → **a* · b = a* · c = 0**

$$\bar{b}^* = \frac{\bar{c} \times \bar{a}}{\bar{a}(\bar{b} \times \bar{c})}$$

b* *is perpendicular to* **c** *and to* **a** → **b* · a = b* · c = 0**

$$\bar{c}^* = \frac{\bar{a} \times \bar{b}}{\bar{a}(\bar{b} \times \bar{c})}$$

c* *is perpendicular to* **a** *and to* **b** → **c* · a = c* · b = 0**

$$\bar{a}(\bar{b} \times \bar{c}) = V$$

V *– volume of elementary cell of the real lattice, defined by vectors*

$$\cos\alpha^* = \frac{\cos\beta\cos\gamma - \cos\alpha}{\sin\beta\sin\gamma}$$

$$\cos\beta^* = \frac{\cos\alpha\cos\gamma - \cos\beta}{\sin\alpha\sin\gamma}$$

$$\cos\gamma^* = \frac{\cos\alpha\cos\beta - \cos\gamma}{\sin\alpha\sin\beta}$$

Properties of reciprocal lattice

EWALD's construction

Peter **Ewald** publication (in 1913) of geometrical construction for interpretation of diffraction patterns.

---

równanie W.L. ***Bragga*****:**

$$n\lambda = 2d_{hkl} \sin\theta_B$$

[Proceedings of the Royal Society, 1913, 88, 428]

Nagroda Nobla 1915 (wraz z ojcem W.H. Braggiem) za badania struktur kryształów.

równanie ***G.V. Wulfa*****:**

$$\frac{\lambda}{2} = \frac{\delta\varepsilon}{m}$$

„Ueber die Kristallroentgenogramme" [Physikalishe Zeitschtrift, 1913, z. 6, s. 217]

gdzie $\delta = d_{hkl}$, *zaś* $\varepsilon = \cos\psi$ *(*ψ *– kąt pomiędzy wiązką padającą a normalną do płaszczyzny uginającej), m – rząd refleksu)*

Odkrycie dyfrakcji promieni rentgenowskich (M. von LAUE), Nagroda Nobla 1914r.

Początek I-wszej Wojny Światowej 1914r

$S_1 - S_0 = S$ – scattering vector

Diffraction condition:

$S_1/\lambda - S_0/\lambda = H$ – diffraction vector

$|H^*_{hk0}| = n/d_{hk0}$ – reciprocal lattice vector for (hk0) planes

By the chart:

$\frac{1}{2}|H^*_{hk0}| = |S_1/\lambda| \sin(\theta_B)$

$n\lambda = |S_1| 2d$ ...

When the beam is fallig down on crystal, the *Ewald's sphere* indicates exactly the lattice planes (families) which fulfill *Bragg's diffraction condition*. For a 2D-lattice, the Ewald's sphere is a circle.

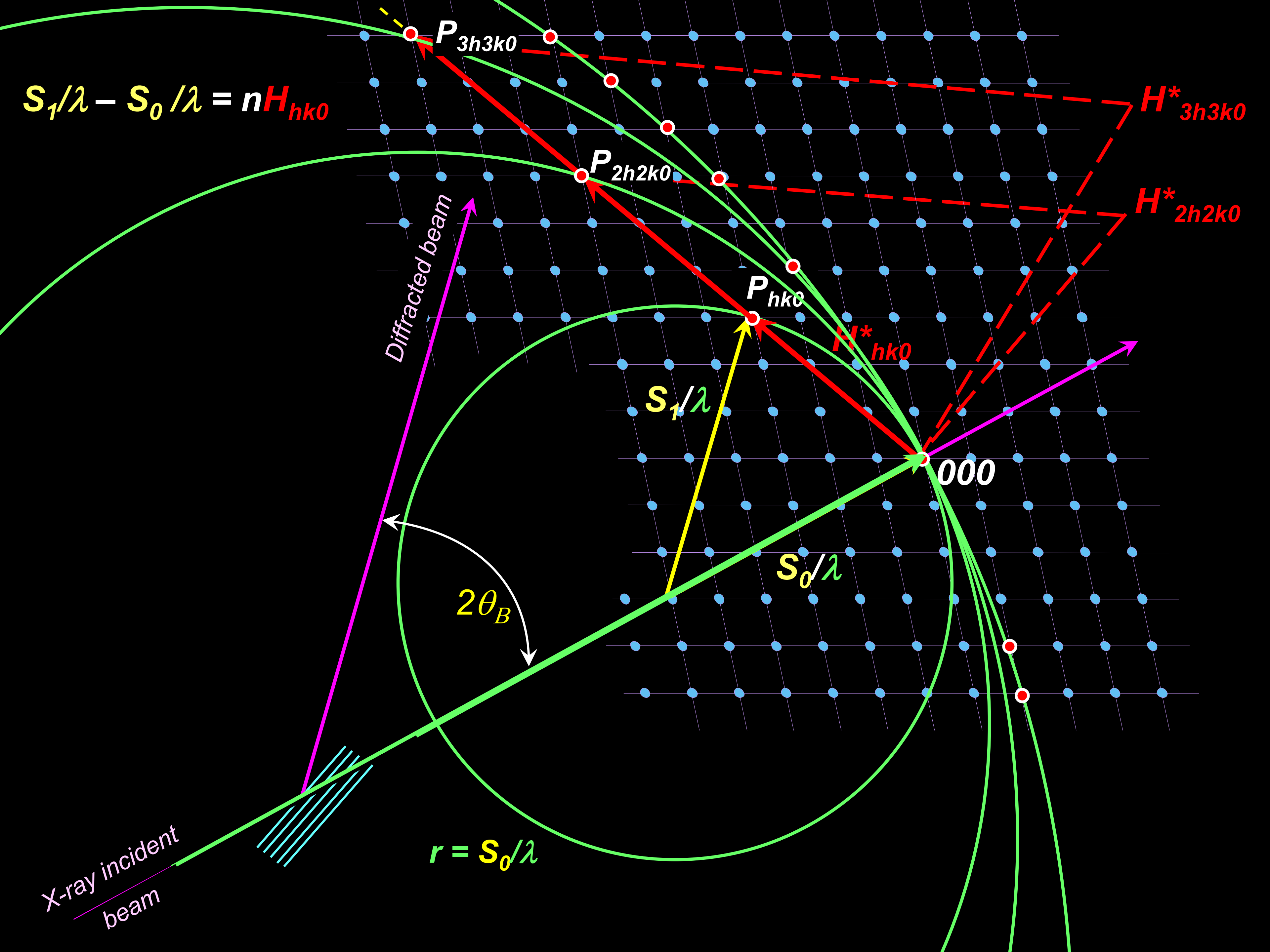

$S_1/\lambda - S_0/\lambda = nH_{hk0}$
P_{3h3k0}
H^*_{3h3k0}
P_{2h2k0}
H^*_{2h2k0}
P_{hk0}
H^*_{hk0}
Diffracted beam
S_1/λ
000
$2\theta_B$
S_0/λ
X-ray incident
beam
$r = S_0/\lambda$

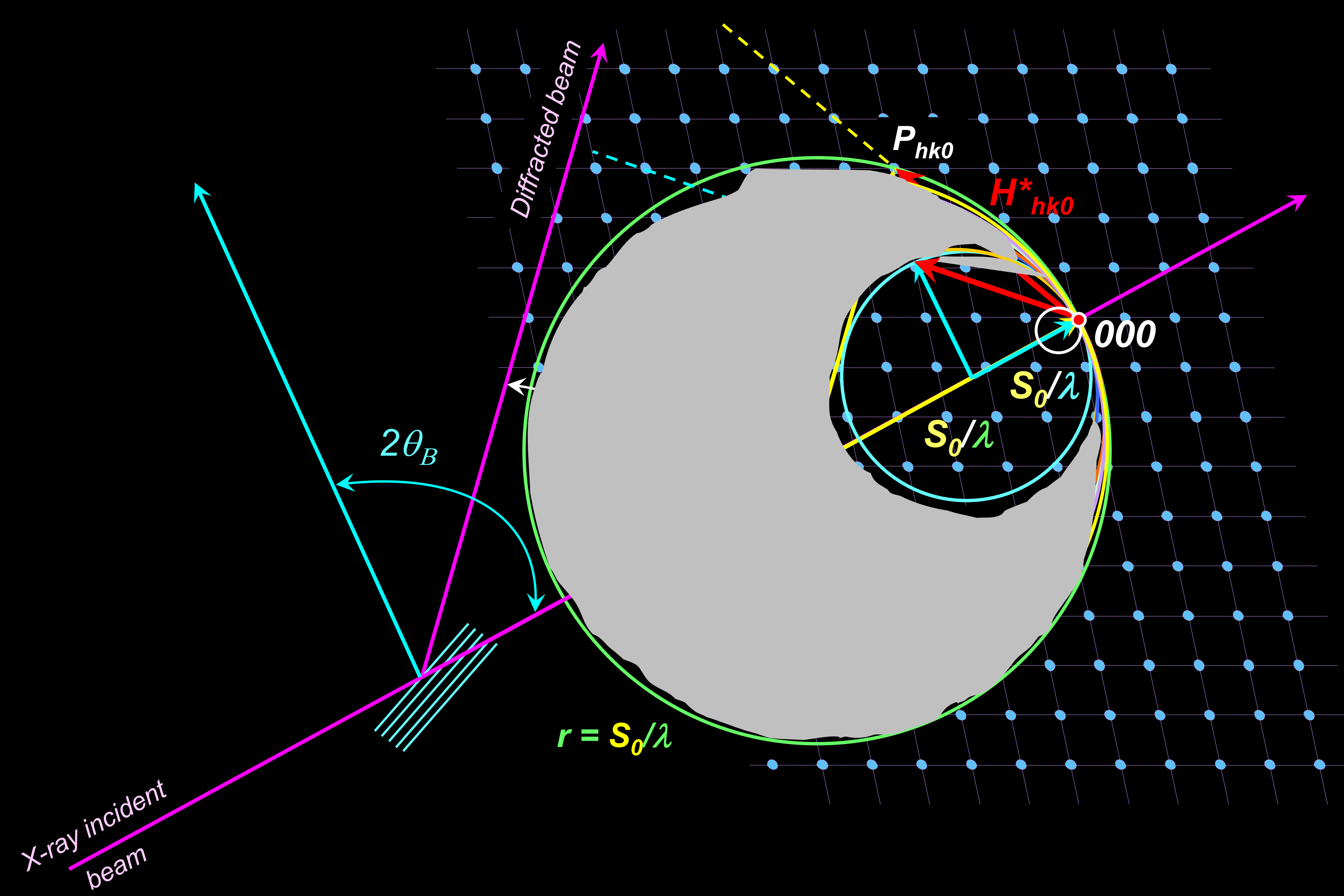

Diffracted beam
P_{hk0}
H^*_{hk0}
000
S_0/λ
S_0/λ
$2\theta_B$
$r = S_0/\lambda$
X-ray incident beam

Diffraction on 3D-lattice

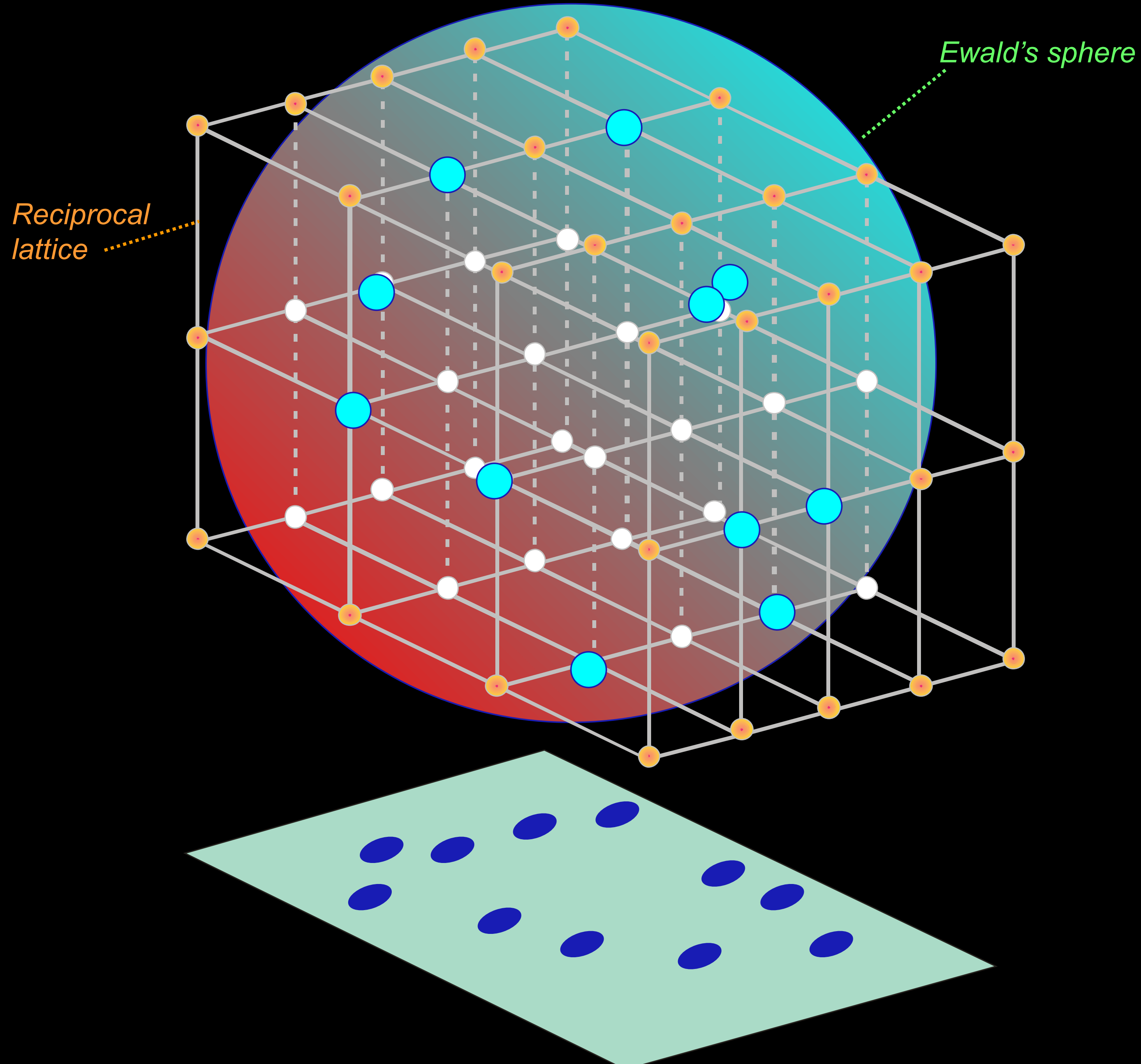

SADP electron diffractions from melt spun NiTiZr ribbons

Anomalous X-ray scattering

→ Application in identification of early stage of precipitation (ASAXS)

Miara intensywności rozpraszania

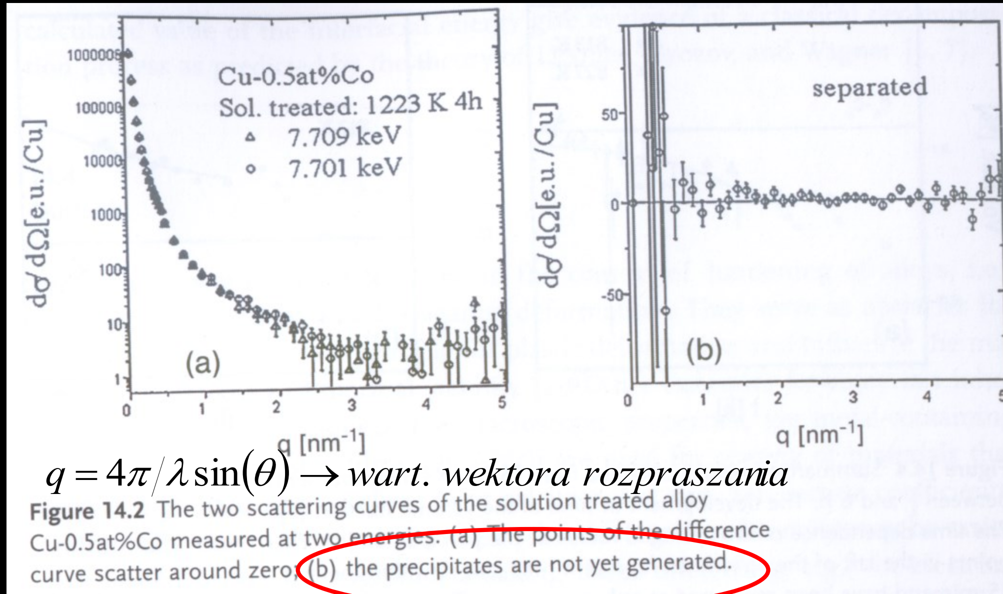

$q = 4\pi/\lambda \sin(\theta) \rightarrow$ *wart. wektora rozpraszania*

Figure 14.2 The two scattering curves of the solution treated alloy Cu-0.5at%Co measured at two energies. (a) The points of the difference curve scatter around zero (b) the precipitates are not yet generated.

Miara intensywności rozpraszania

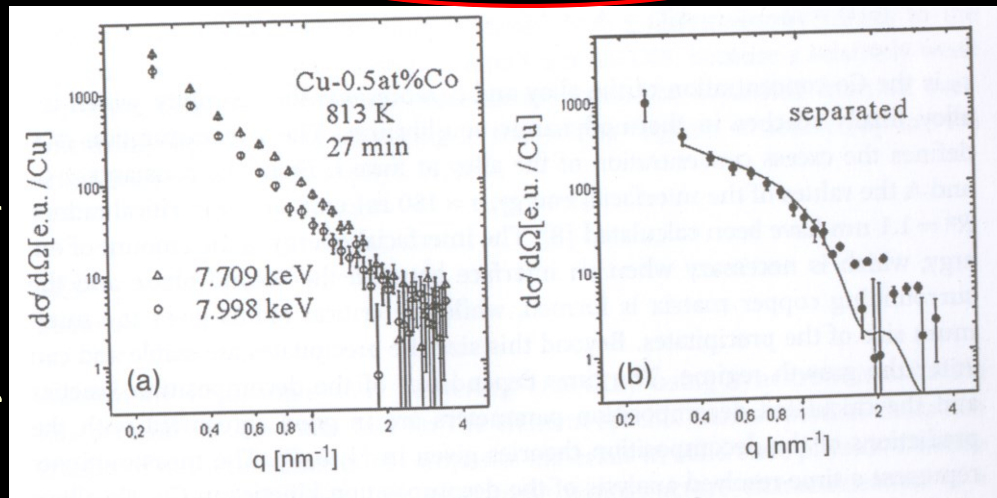

Figure 14.3 After heating the alloy to a temperature of 813 K significant differences are observed after 1/2 hour in the scattering curves measured at different energies. The differences can be attributed to small Co precipitates. From the two scattering curves (a) the scattering curve related to the Co precipitates can be separated (b).

X-Ray Texture Tomography

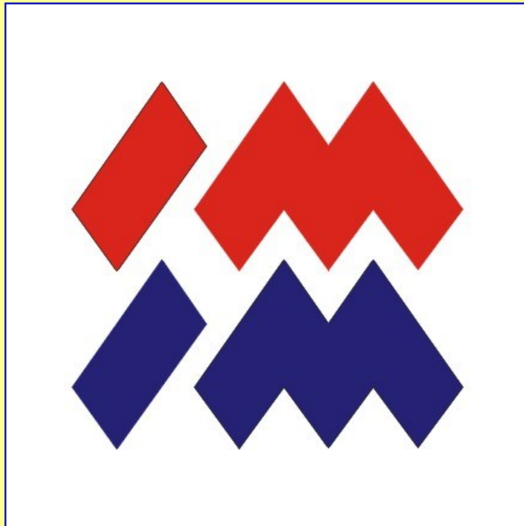

Jan Bonarski

Polish Academy of Sciences

***Aleksander Krupkowski* Institute**

of Metallurgy and Materials Science

Kraków, POLAND

http\\www.al.imim-pan.krakow.pl

X-ray texture tomography is a new, non-destructive method of th
investigation of the near-the-surface layers of the sample.

The method is based on single-layer pole figures, which are two
dimensional density distribution of poles of the lattice planes, referred t
the near-the-surface layer of precisely defined thickness.
Because some of the elements of this procedure are similar to the know
techniques of spatial imaging of objects localised inside some definit
volume, such as magnetic-resonance tomography, seismic tomography, c
positron emission tomography, the introduced described investigatio
method has been called X-ray texture tomography.
In this newly introduced concept the meaning of the commonly use
expression "**tomography**" becomes extended, as it refers to the imaging c
a material feature, as represented by texture, and not to material object
(e.g. accumulation of tissues).

Texture tomography represents a research tool, which may be applied i
the analysis of texture inhomogeneity, its heredity, the control of th

Investigation of crystallographic texture:

How ?

Electron, x-ray and neutron diffraction techniques (SEM, TEM, EBSD, OIM, XRD, ND),
Optical observations,

What for?

• For controlling of technological processes,
• For understanding the "natural construction" of materials and it application in technology
• For knowing of geological history of the Earth,
• For archeological/medical expertises (texture of animal/human bones)

Crystallographic texture:

What is it?

a statistical feature of polycrystalline materials, manifests by preferred crystallographic orientation of grains, particles or distinguished sub-areas.

Sources of texture

- natural anisotropy of crystals (determined crystal symmetry),
- technological processing of materials (crystallization, deformation)
- Nature (seismic vibration of Earth, “architecture” of plants, selective synthesis of proteins)

Is the texture advantage or disadvantage of materials?

Yes

deep drawing steel <111>
electromagnets
transformators (Fe + 3%Si)
photovoltaics (Si-multicrystalline solar cells)
superconductivity
....

No

structure inhomogeneity
diffraction phase identification/analysis
Problems of samples standardization
electrodepositing (inheritance effect)
....

From application point of view, the properties (structure and texture) of a relative thin, near-the-surface layers of constructing elements play a very important role.

Examples:

- Elements working in friction and fatique conditions (bearings),
- Deposited coatings,
- Solar cells.

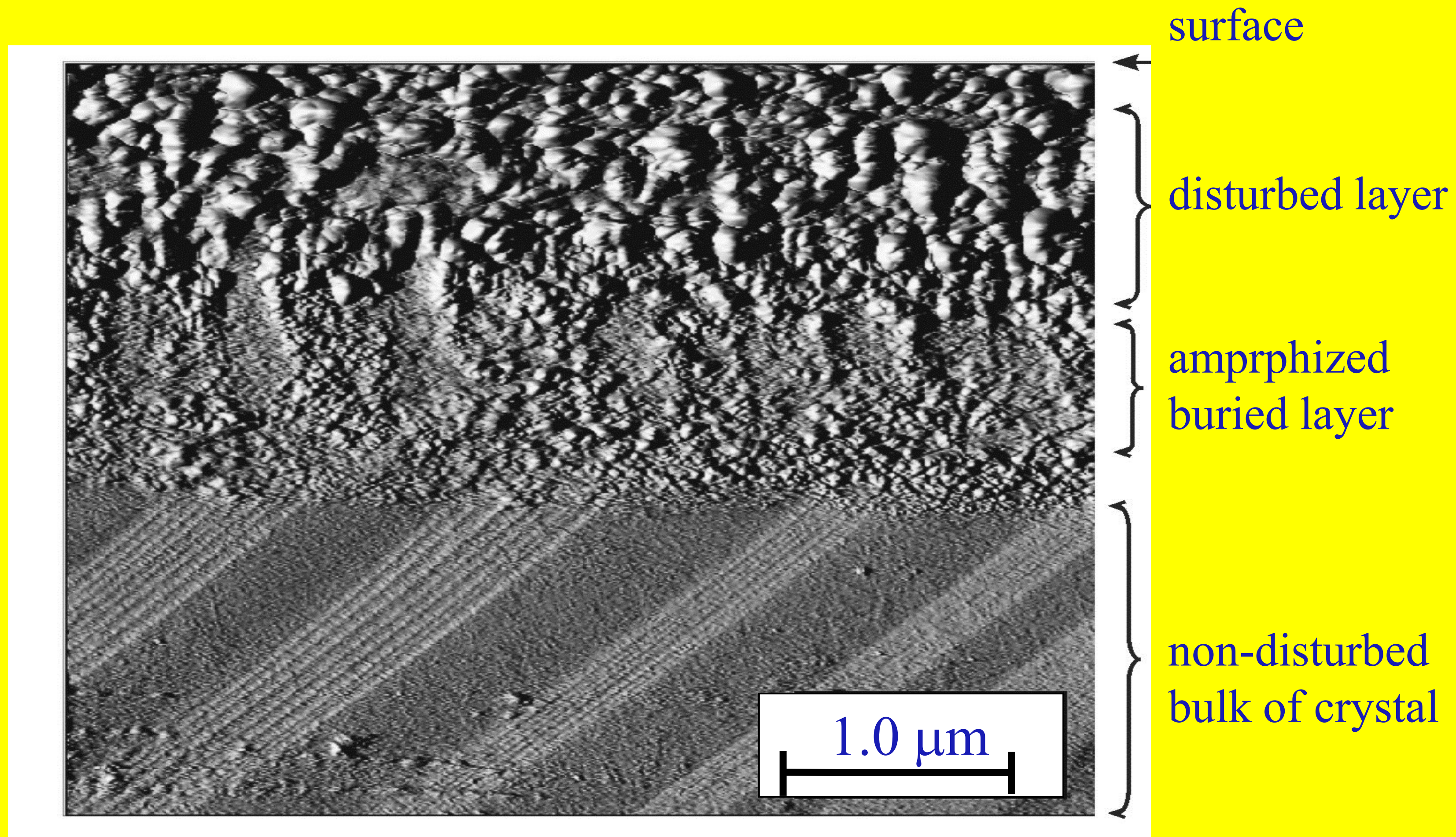

Microstructure of the broken cross-section of (001)-oriented Si single crystal after implantation (P^+ ions) and subsequent thermal treatment, registered by means of contact AFM technique.

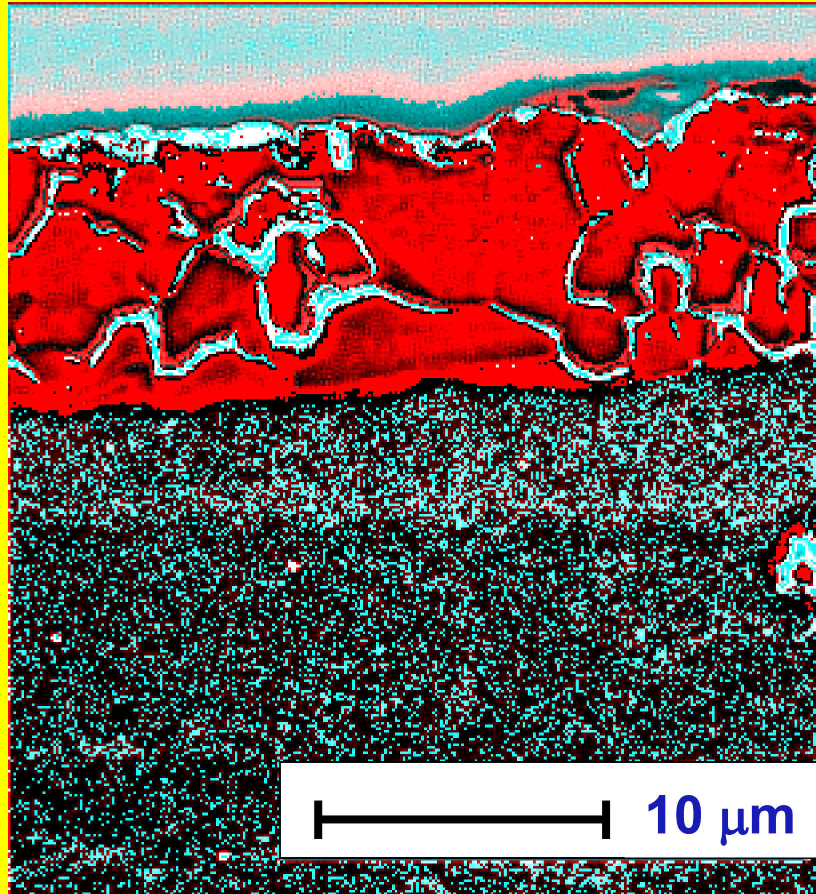

Microstructure of the cross section of deep drawing steel sheet with deposited Zn-protective layer (thickness of 7.5 μm) observed in SEM [IMIM PAN, Kraków]

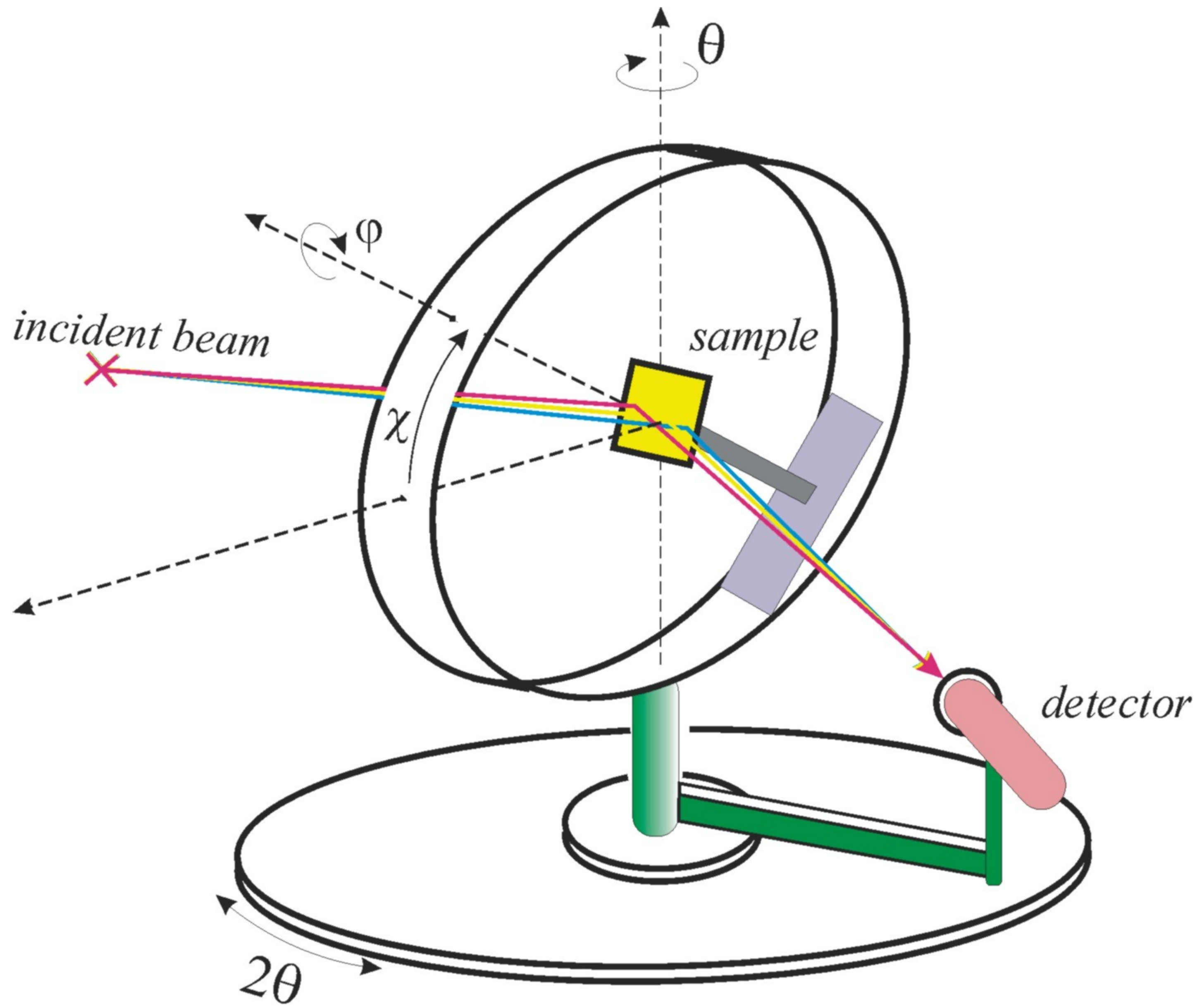
θ
φ
incident beam
sample
χ
detector
2θ

Effective information depth $X_{99\%}$

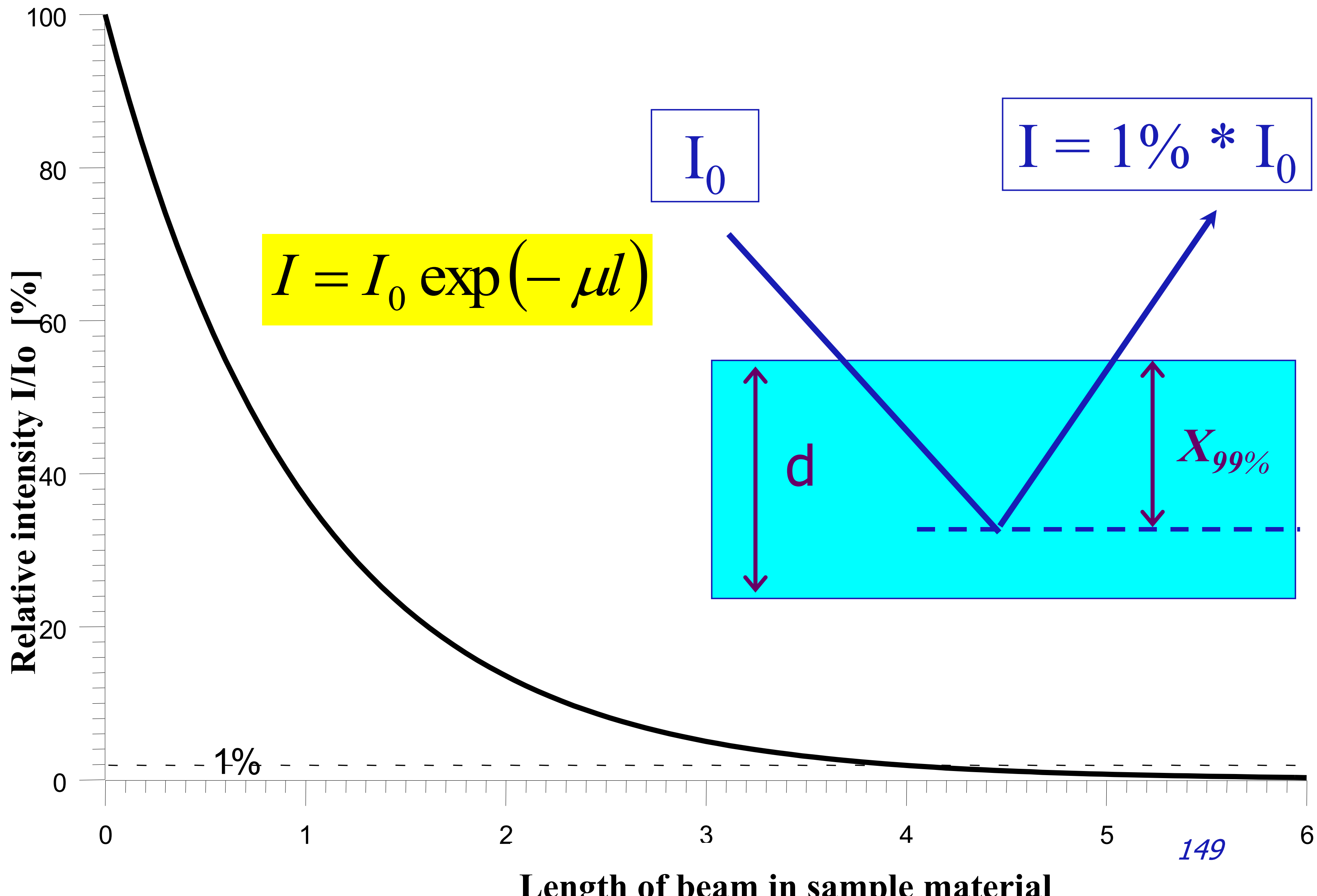

Changes of information depth

During texture analysis based on the back-reflection pole figures registered by means of x-ray diffraction, information depth {$\mathbf{X_{0.01}}$} changes with the sample position in goniometer, determined by the θ, χ angles.

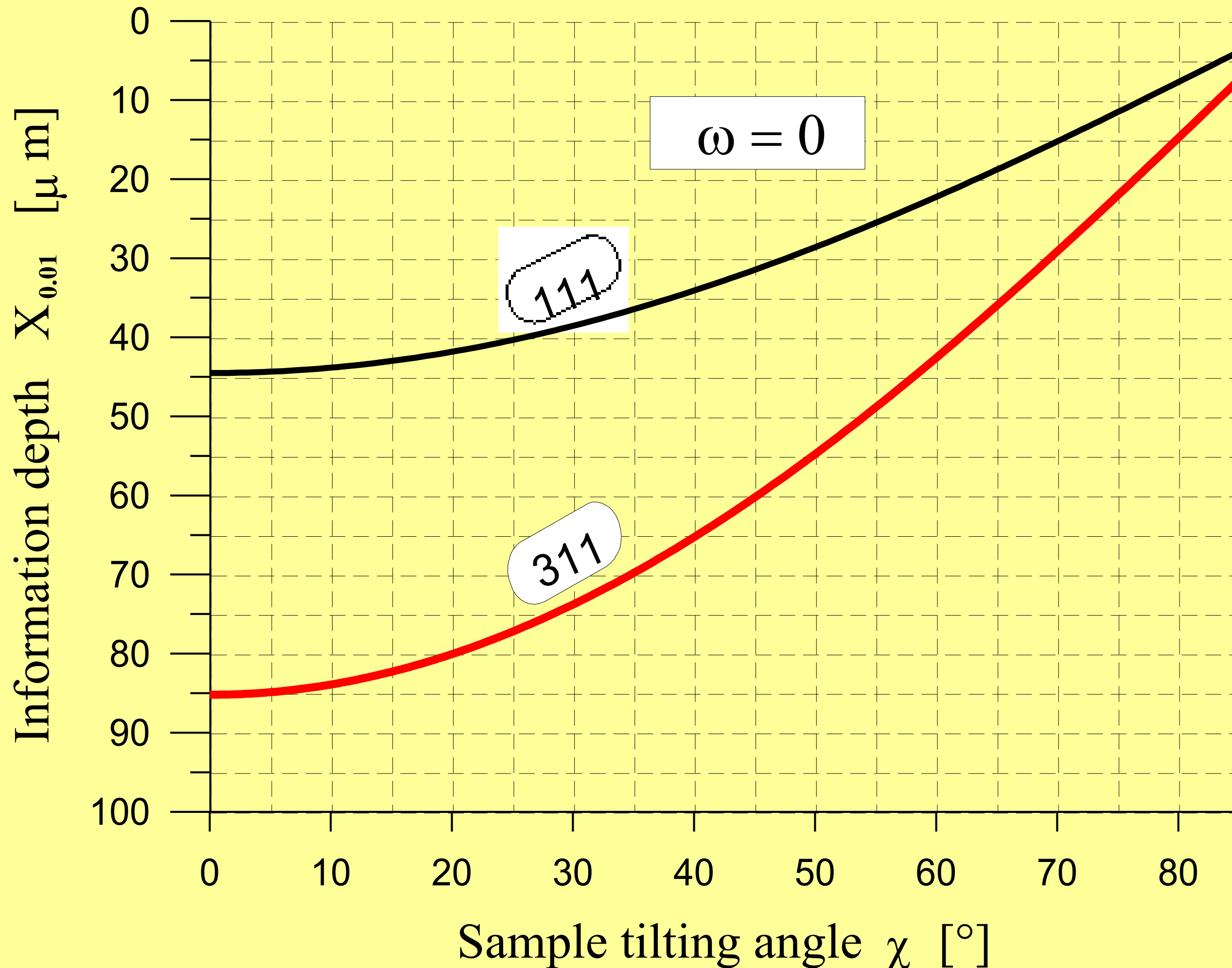

<u>Consequence:</u>
internal contradiction of pole figure in case of inhomogenous texture.

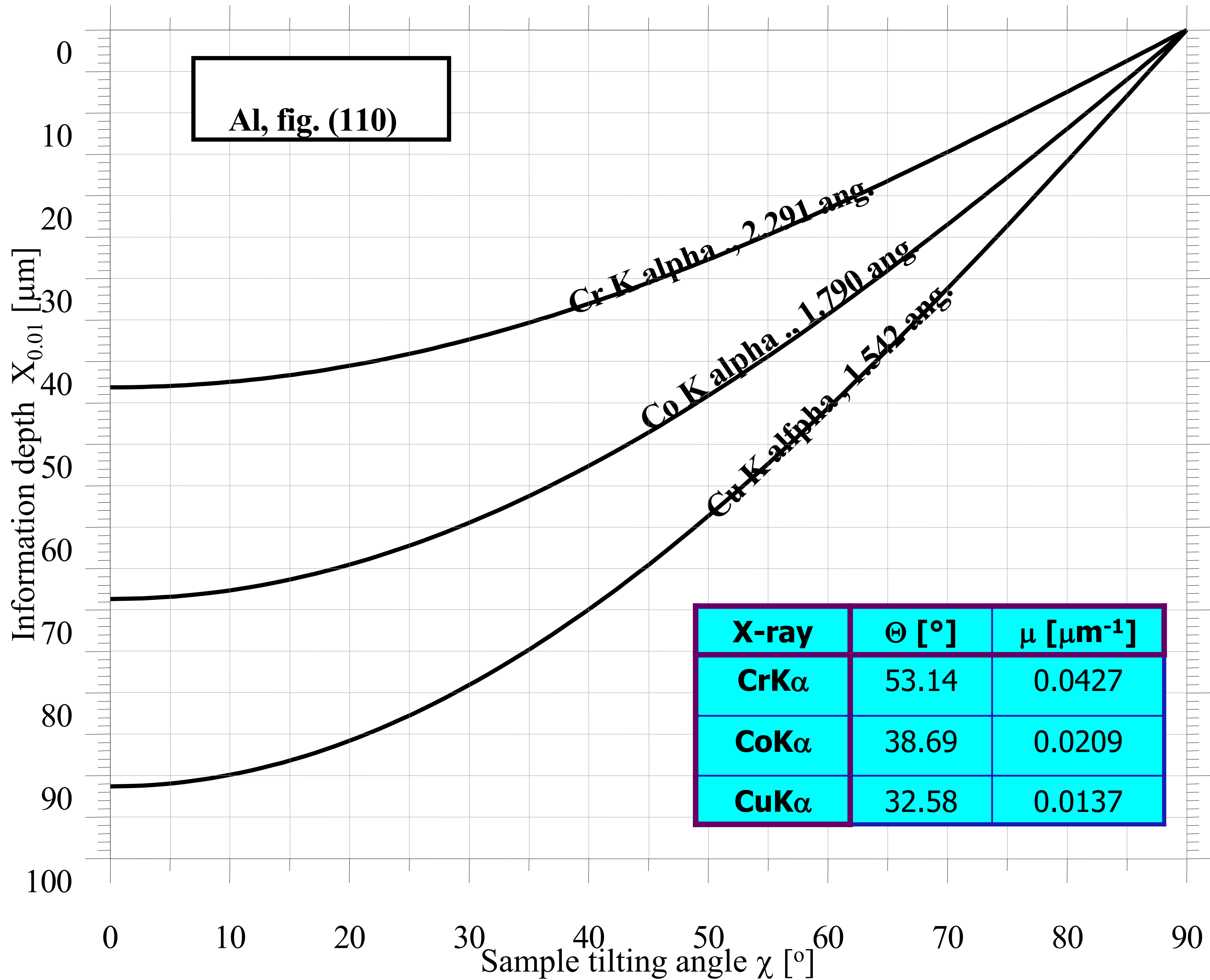
Al, fig. (110)
Cr K alpha , 2.291 ang.
Co K alpha , 1.790 ang.
Cu K alfpha , 1.542 ang.
Information depth $X_{0.01}$ [μm]
Sample tilting angle χ [°]
0
10
20
30
40
50
60
70
80
90
100
X-ray | Θ [°] | μ [μm^{-1}]
CrKα | 53.14 | 0.0427
CoKα | 38.69 | 0.0209
CuKα | 32.58 | 0.0137

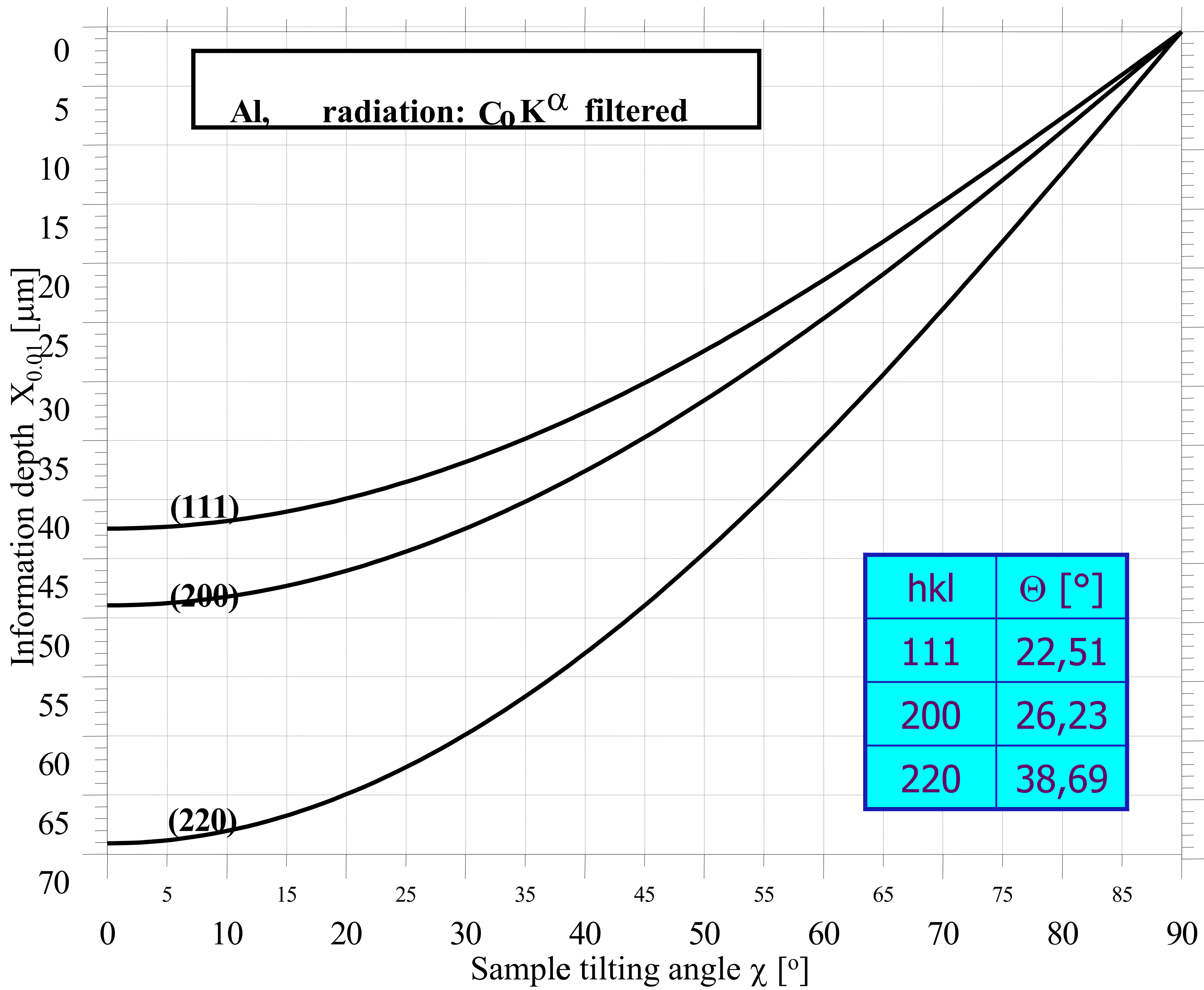

Al, radiation: CoKα filtered
Information depth X0.01 [µm]
0
5
10
15
20
25
30
35
40
45
50
55
60
65
70
(111)
(200)
(220)
hkl
Θ [°]
111
22,51
200
26,23
220
38,69
5
15
25
35
45
55
65
75
85
0
10
20
30
40
50
60
70
80
90
Sample tilting angle χ [°]

Geometrical conditions of measurement at constant information depth (CID)

The information depth $\{\mathbf{X_{0.01}}\}$ can be controlled and kept at the constant level by:

- changes of wavelength,
- introducing an additional goniometer angle ω:

$$X_{0.01} = -\frac{\ln(0.01)}{\mu} \cdot \frac{\sin(\theta+\omega)\cdot\sin(\theta-\omega)}{\sin(\theta+\omega)+\sin(\theta-\omega)} \cdot \cos\chi$$

where, the geometrical factor $\xi(\theta,\omega,\chi)$

$$\xi = \frac{\sin(\theta-\omega)+\sin(\theta+\omega)}{\sin(\theta+\omega)\cdot\sin(\theta-\omega)} \cdot \frac{1}{\cos\chi}$$

determines the condition of registration of the pole figure with constant information depth, termed here as a single-layer pole figure.

Information valley of X-ray CoKα radiation in *Al* sample for the ***311*** Bragg reflection.

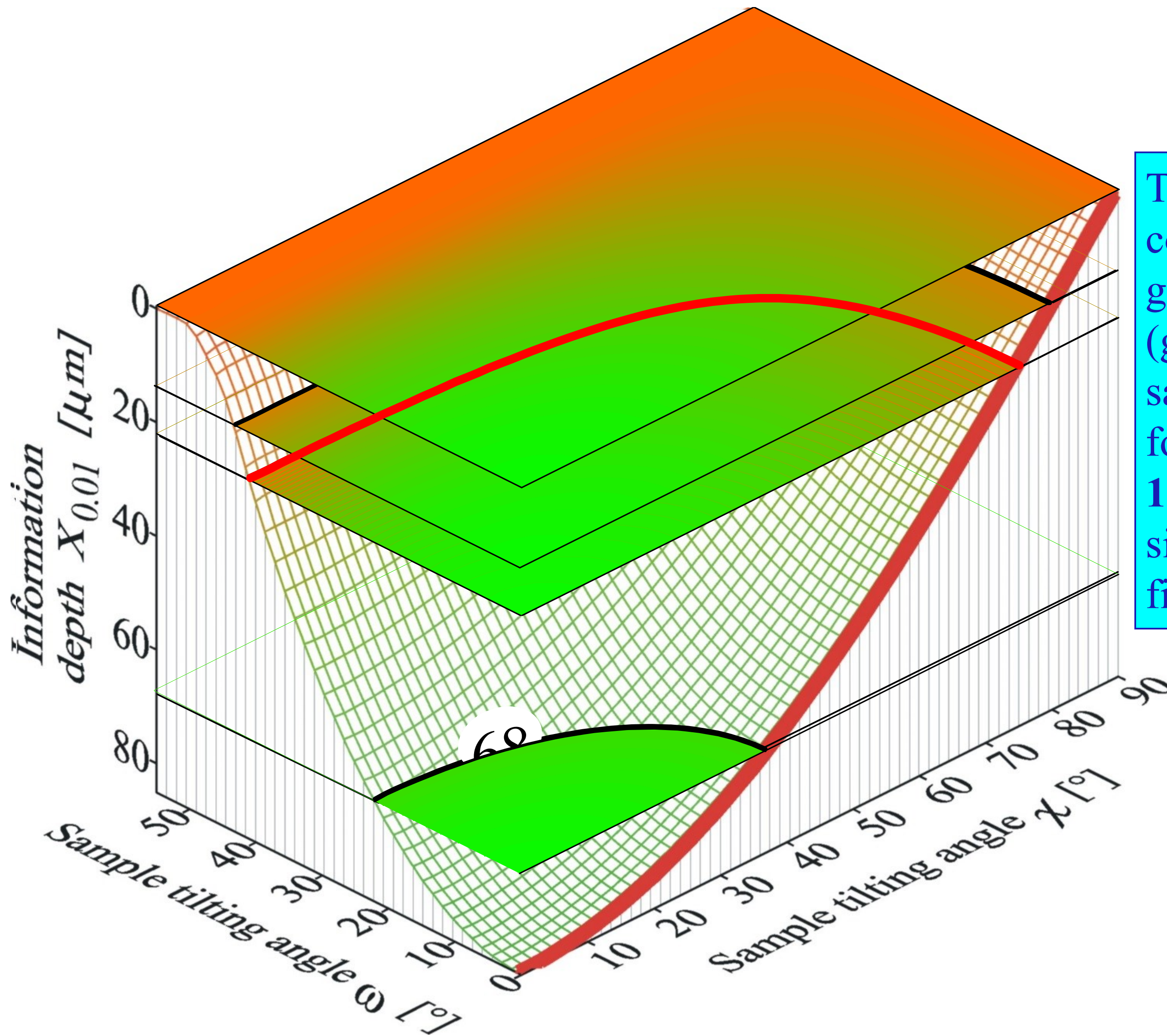

The izo-depth lines correspond to the geometrical conditions (goniometer angles of sample tilting **ω** and **χ**) for registration of **15μm, 22μm** and **68μm** single-layer (311) pole figures.

Consequences of introducing the additional sample tilting angle ω

- desymmetrization of focalization conditions (offset from Bragg-Brentano geometry),
- deformation of the peak profile and the pole figure coordinates,
- necessity of mathematical transformation to the symmetrical system,
- arising of blind areas in experimental data,
- necessity of additional geometrical correction of the registered pole figures.

Transformation of the coordinates

$$(\omega, \chi, \varphi) \Rightarrow (\alpha, \beta)$$

ω > 0

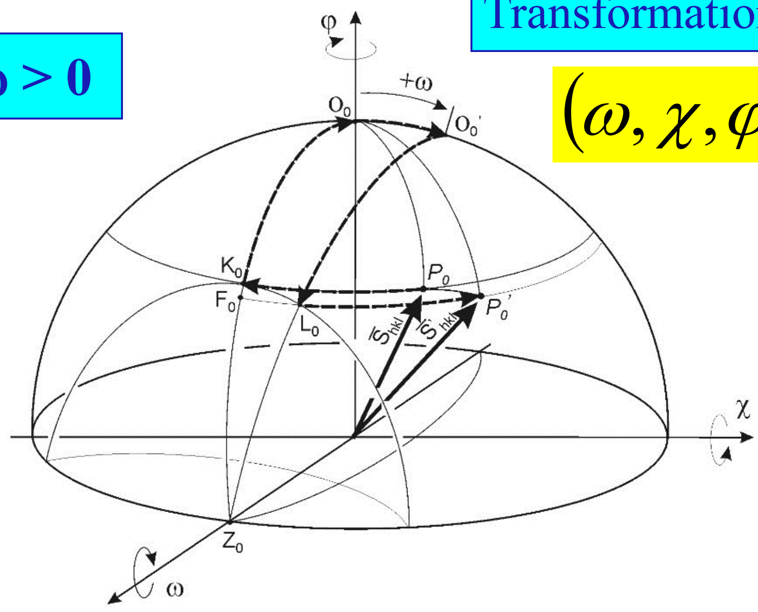

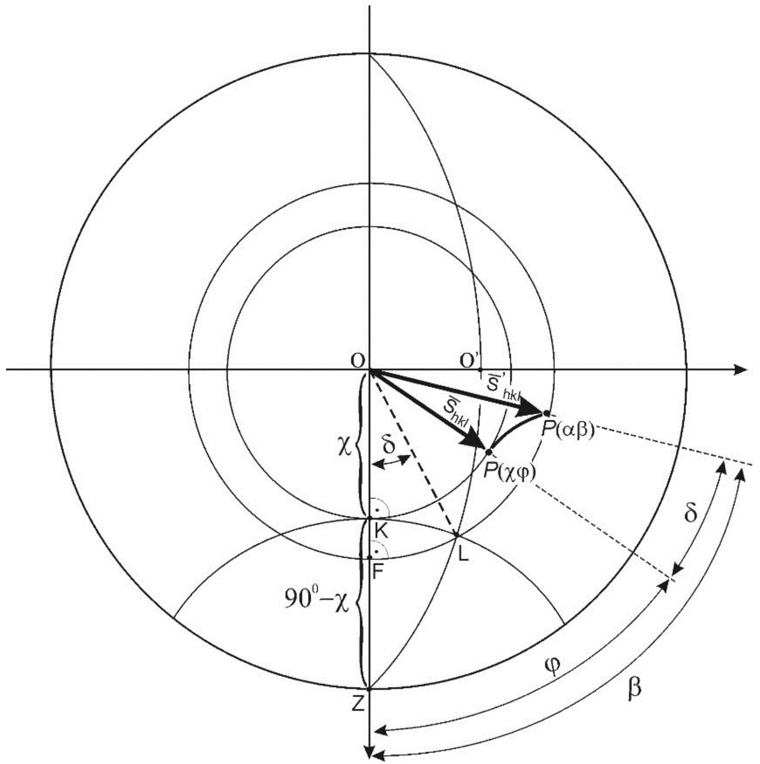

ω < 0

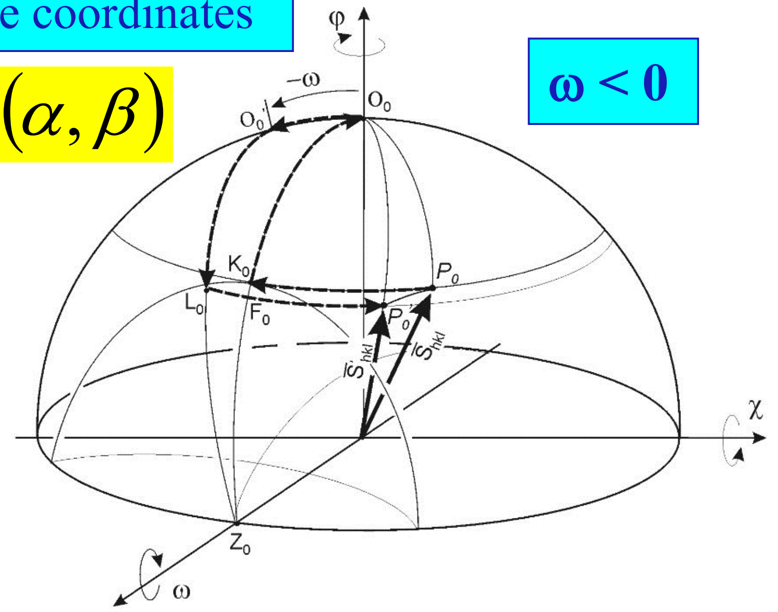

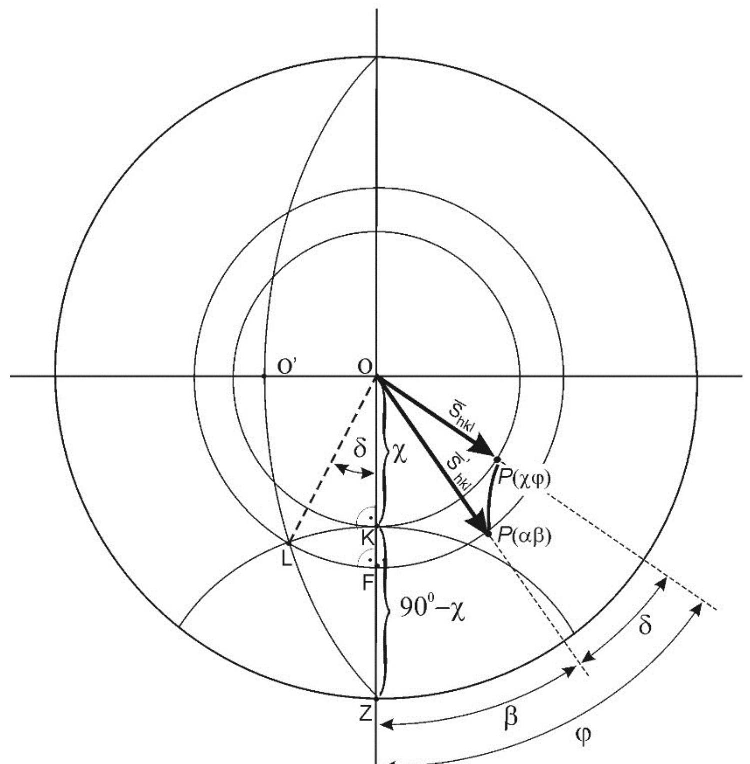

$\omega = 0$

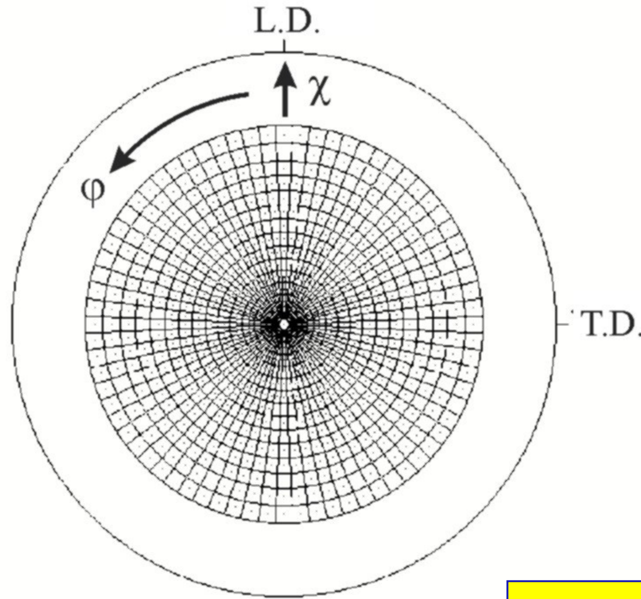

$$(\omega, \chi, \varphi) \Rightarrow (\alpha, \beta)$$

$$\alpha = \arccos\left(\cos\chi \cdot \cos\left(\arcsin\left(\sin\omega \cdot \cos\chi\right)\right)\right)$$

$$\beta = \varphi + \arcsin\left(\sin\omega \cdot \frac{\sin\chi}{\sin\alpha}\right)$$

$\omega < 0$

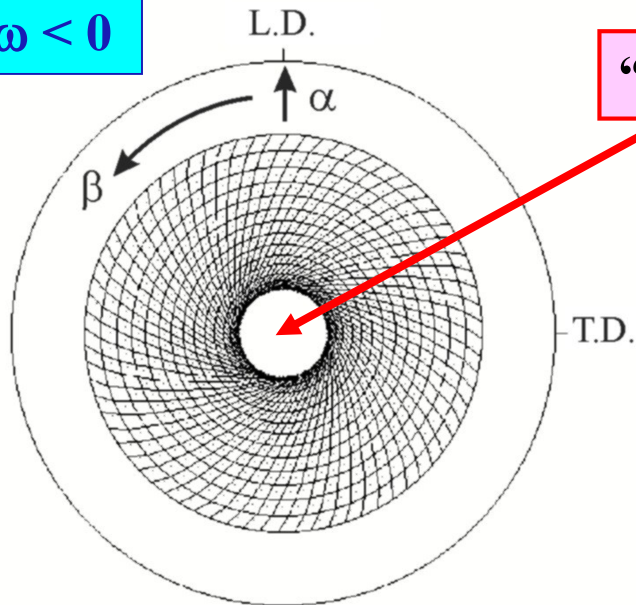

"blind" areas

$$-\frac{\pi}{2} < \omega < \frac{\pi}{2}$$

$$0 \leq \chi < \frac{\pi}{2}$$

$\omega > 0$

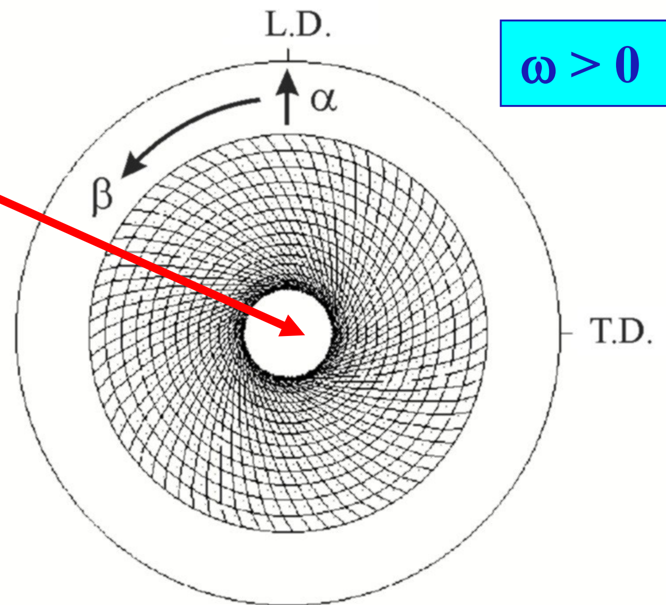

Experimental verification of the X-Ray Texture Tomography (XTT)

has been performed on a model sample of layered structure with accurately defined and known texture inhomogenity.

standard Al sample

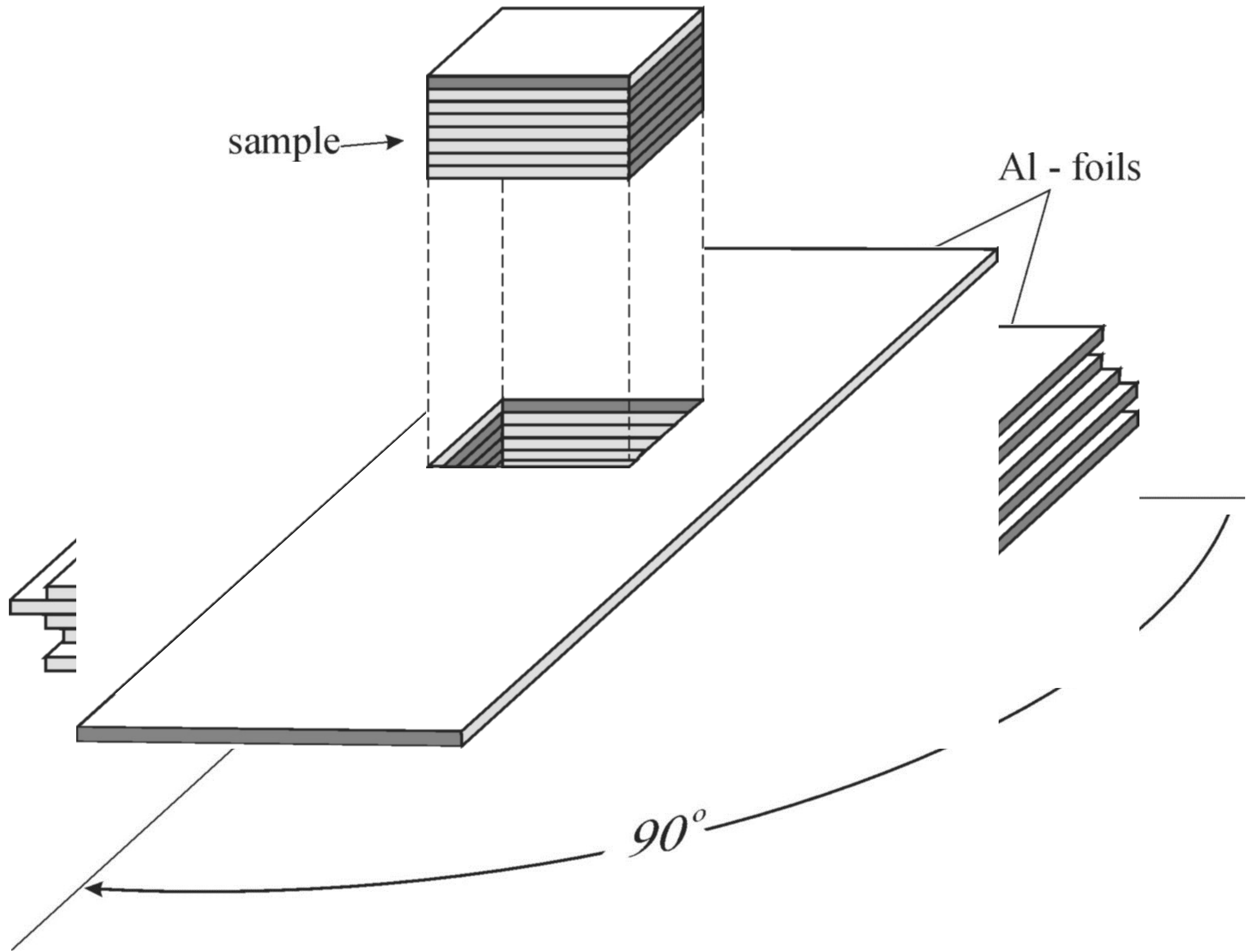

standard Al sample

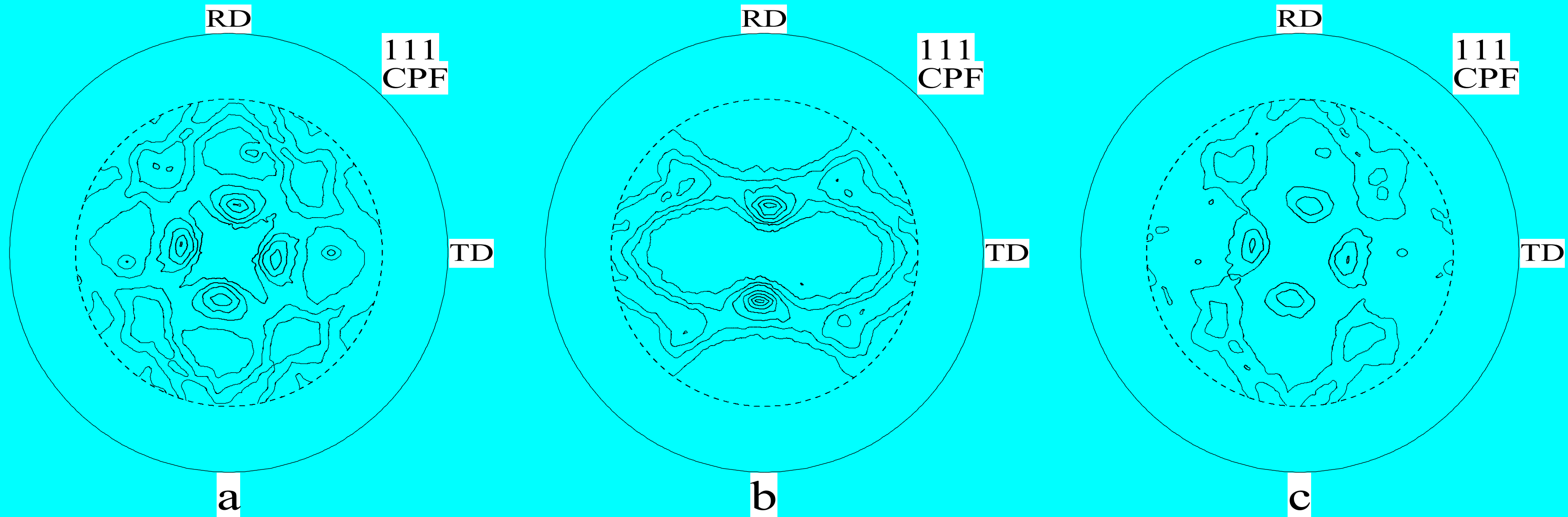

Set of (111) back-reflection pole figures for the standard sample Al with inhomogeneous texture (CoKα radiation used):

a) registered traditionally (information depth: 44.5 μm – 11.5 μm),

b) figure of top layer only (constant information depth, ca. 15.0 μm),

c) diference between the (a) and (b) case.

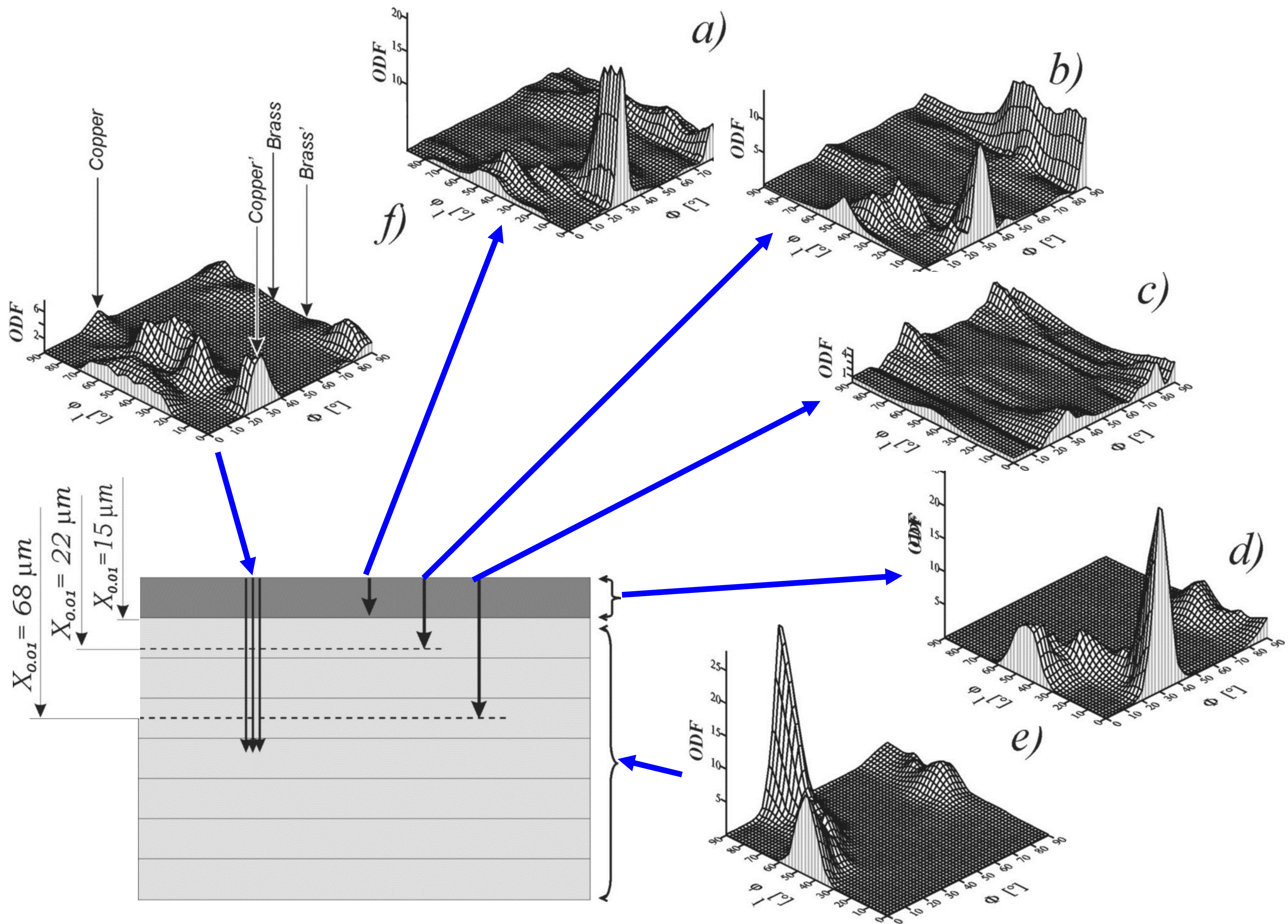
Copper
Copper'
Brass
Brass'
ODF
Φ [°]
a)
b)
c)
d)
e)
f)
$X_{0.01}$= 68 μm
$X_{0.01}$= 22 μm
$X_{0.01}$=15 μm

Identified texture components, volume fractions and inhomogeneity degrees for the standard Al sample, based on diffraction of CoKα and CoKβ x-ray beams.

No of component	Euler angles of component			Volume fractions of the components [% obj.] and they degree of inhomogeneity ***DI***						Miller indices of texture component
				Sample areas subjected to diffraction of CoKα & CoKβ			Separated layers *T* = top layer *B* = Bulk			
	φ_1 [°]	Φ [°]	φ_2 [°]	CoKα [%vol]	CoKβ [%vol]	*DI*	*T* [%vol]	*B* [%vol]	*DI*	*(hkl)[uvw]*
1	31.12	36.70	26.57	42.2	45.1	0.1	52.7	0.0	2.0	~ (122)[21] *S'*
2	0.00	35.26	45.00	23.7	26.9	0.1	18.4	0.0	2.0	(112)[10] *Copper'*
3	58.98	36.70	63.43	9.7	11.0	0.0	0.0	34.2	2.0	(132)[63] *S*
4	90.00	35.36	45.00	7.5	8.5	0.1	0.0	18.4	2.0	(112)[11] *Copper*
5	35.26	90.00	45.00	5.4	5.2	0.1	5.2	0.7	1.5	(110)[11] *Brass'*
6	54.74	90.00	45.00	2.6	2.7	0.0	0.8	5.3	1.5	(110)[12] *Brass*
7	0.00	0.00	0.00	1.4	1.1	0.2	4.9	4.9	0.0	(001)[100] *Cube*
The rest				~ 7	~ 0	----	~ 18	~ 35	----	-------------
Background				0	0	----	0	0	----	-------------

reference Al sample: ODF of **bulk (f_1)**	**top layer (f_2)**	**averaged texture ($f_1 + f_2$)**

$$f_2(\varphi_1, \Phi, \varphi_2) = f_1(90^o - \varphi_1,\ \Phi,\ 90^o - \varphi_2)$$

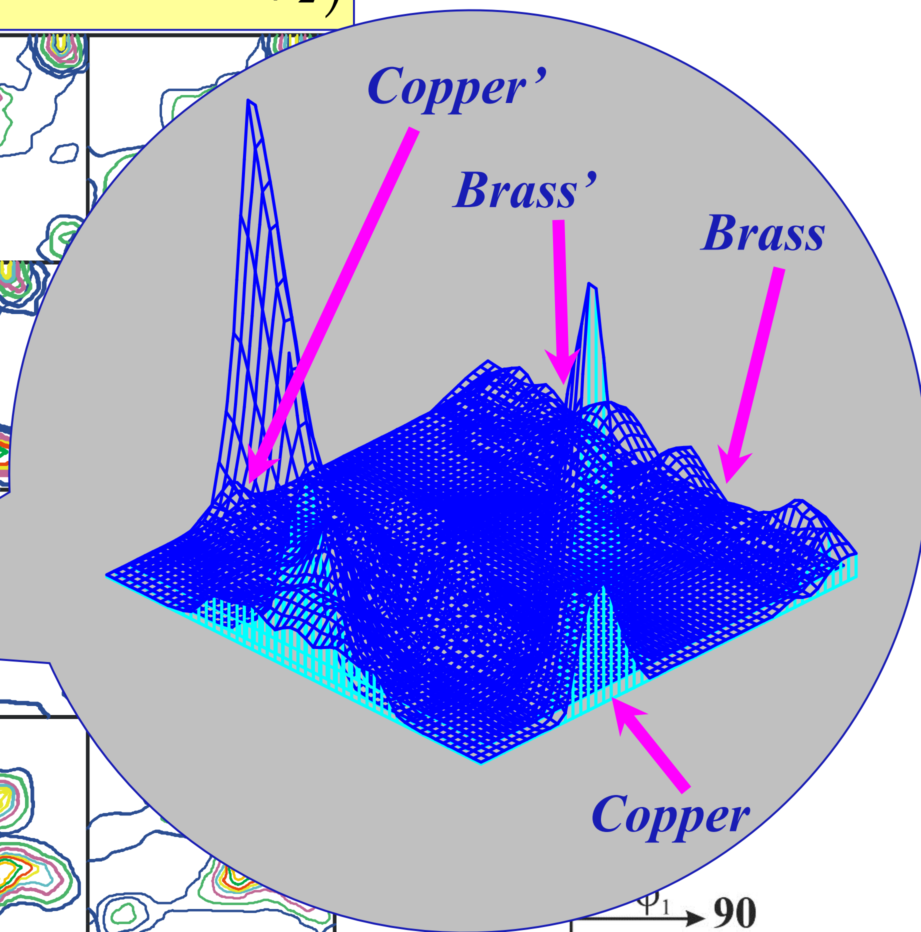

φ_1 → 90

Φ ↓ 90

φ_2 = 0–90

$\Delta\varphi_2$ = 5

Expected (simulated) texture:

$$\overline{f}(g) = (1 - A) \cdot f_1(g) + A \cdot f_2(g)$$

Weight factor:

$$A = e^{-\mu \cdot \xi \cdot X_w} = e^{\ln \varepsilon \cdot \frac{X_w}{X_\varepsilon}}$$

X_W – thickness ot top layer (ca. 15 µm)

X_ε – thickness of the chosen near-the-surface layer (15 µm, 22 µm, 68 µm,)

Verification of X-ray texture tomography

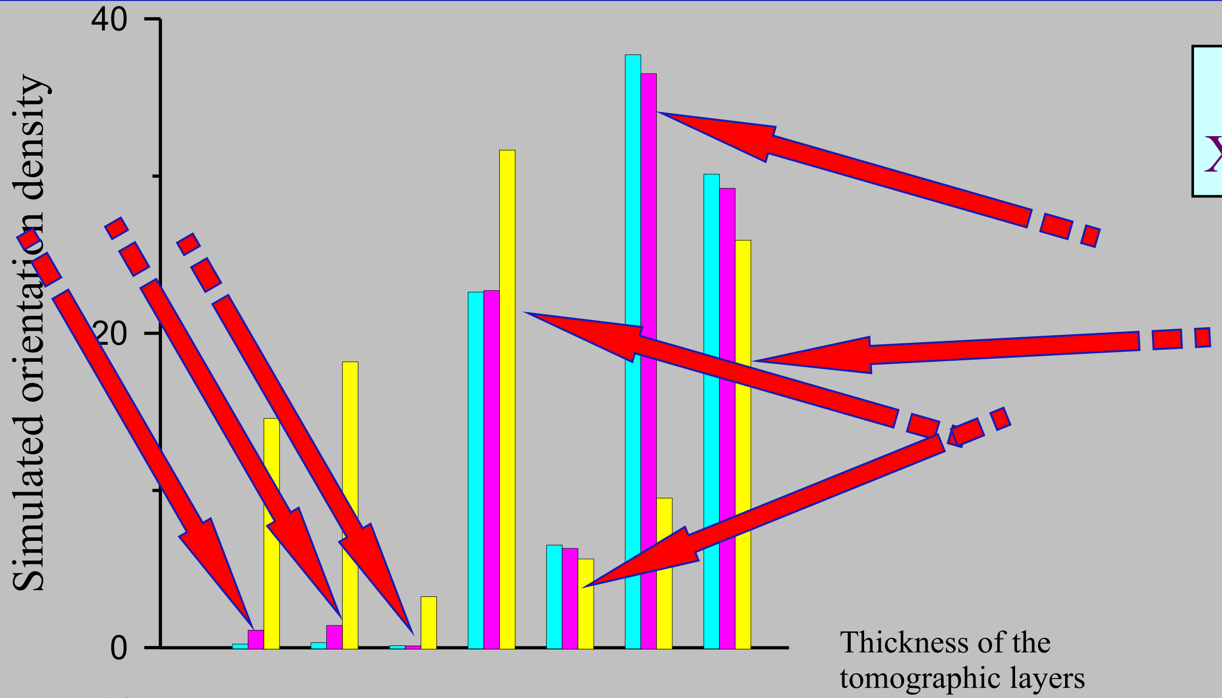

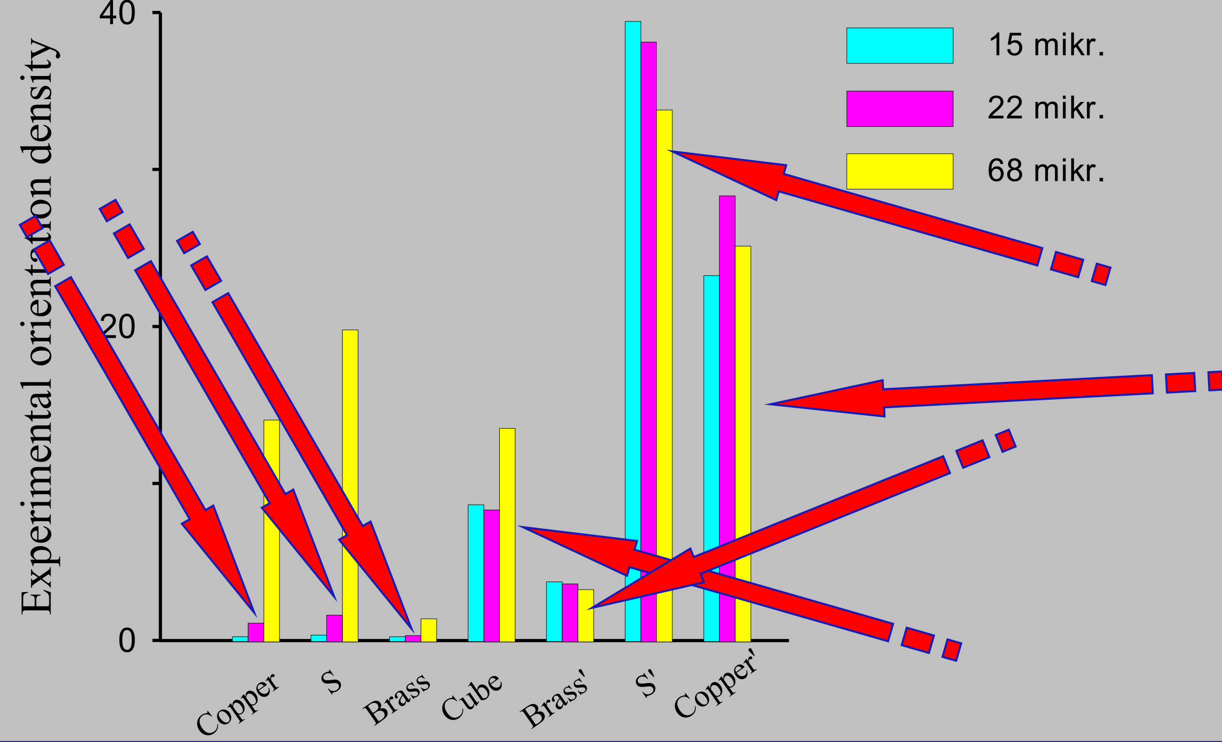

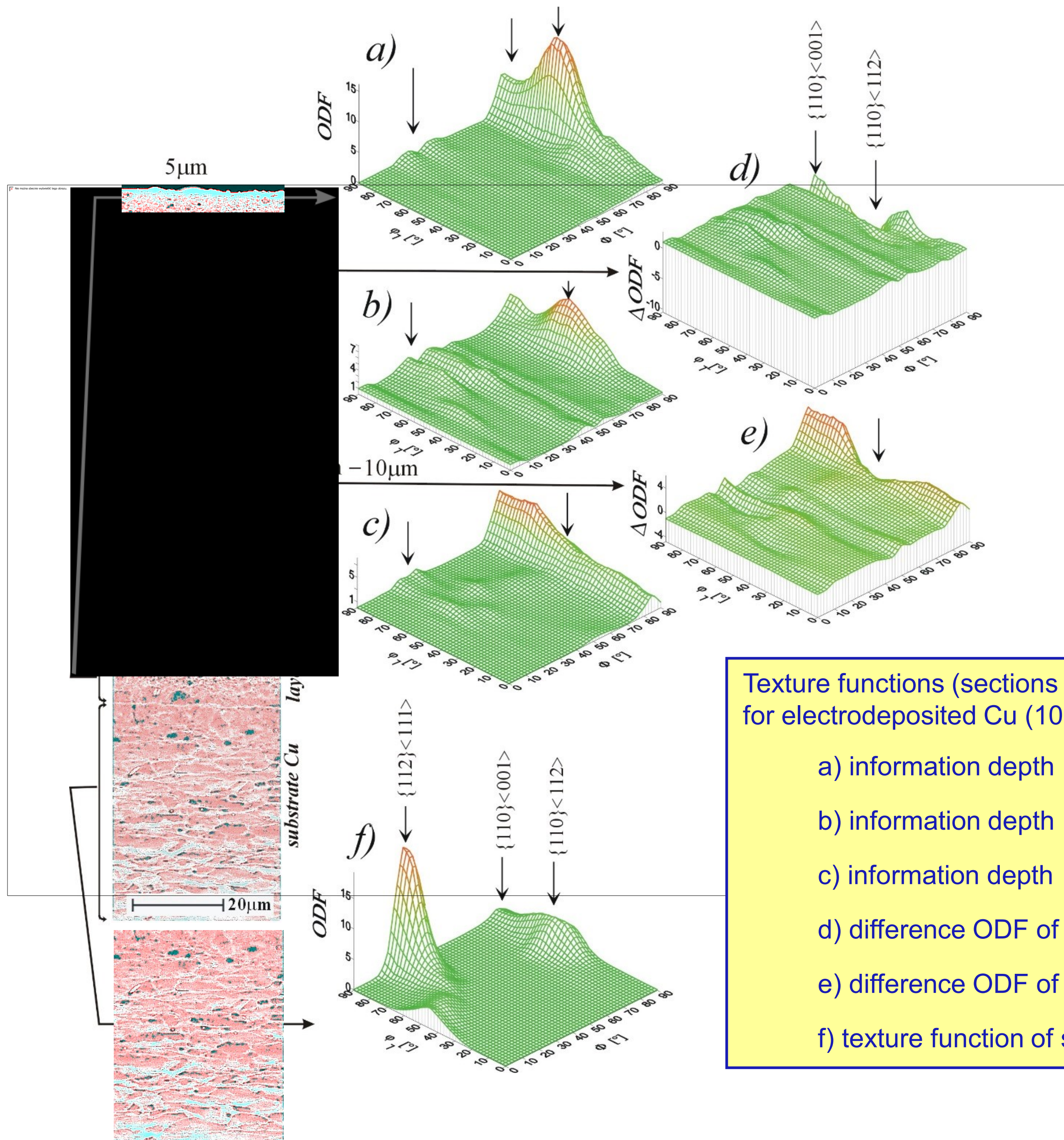

Texture functions (sections φ_2=45°) of X-ray tomographic layers for electrodeposited Cu (10μm thickness) on Cu substrate:

a) information depth $X_{0.01}$ = 5μm

b) information depth $X_{0.01}$ = 10μm

c) information depth $X_{0.01}$ = 12μm

d) difference ODF of 10μm - 5μm

e) difference ODF of 12μm - 10μm

f) texture function of substrate

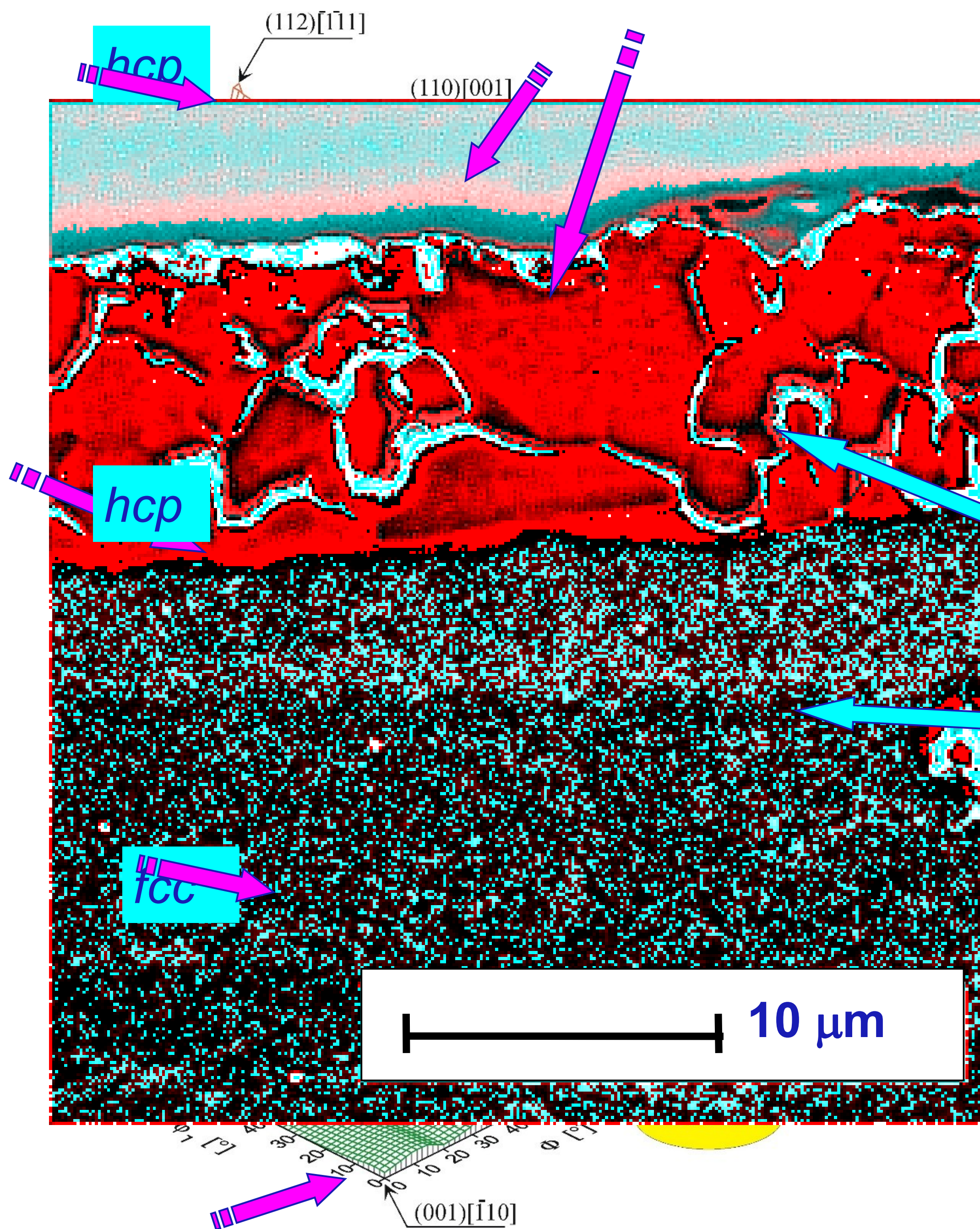

Texture tomography of Zn corrosion-protective layer (thickness of 7.5 μm), deposited on deep drawing steel by electrodeposition technique.

Presented texture functions (φ_2=45° sections) of Fe-Zn composition:

near-surface layer (5.0 μm) obtained by x-ray texture tomography,

averaged texture (7.5 μm) of Zn layer obtained by the back-reflection pole figures measured conventionally.

substrate (ferritic deep-drawing steel)

RD

111
CPF

TD

RD

200
CPF

TD

RD

111
CPF

TD

RD

200
CPF

TD

RD

111
RPF

TD

RD

200
RPF

TD

Experimental:
Max.= 8.4, Izolinie: 1, 2, 3, 4, 5, 6

Mathematically transformed:
Max.= 6.8, Izolinie: 1, 2, 3, 4, 5, 6

Calculated (complete):
Max.= 4.9, Izolinie: 1, 2, 3,

0 φ_1 90

Φ

90

$\varphi_2 = 0–90$

$\Delta\varphi_2 = 5$

Orientation distribution function (ODF) for the near-surface layer of **15µm** thickness, of reference Al sample, obtained by x-ray texture tomography. Calculated of the ODF was made by ADC method using LaboTex software.

Single-layer pole figures with co
procedure for reference Al sample
calculated from ODF by ADC method (bottom). The *hkl* indices corresponds to the measured reflections.

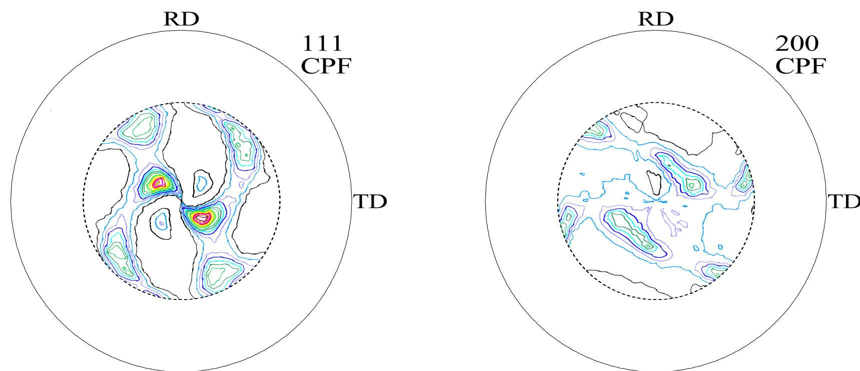

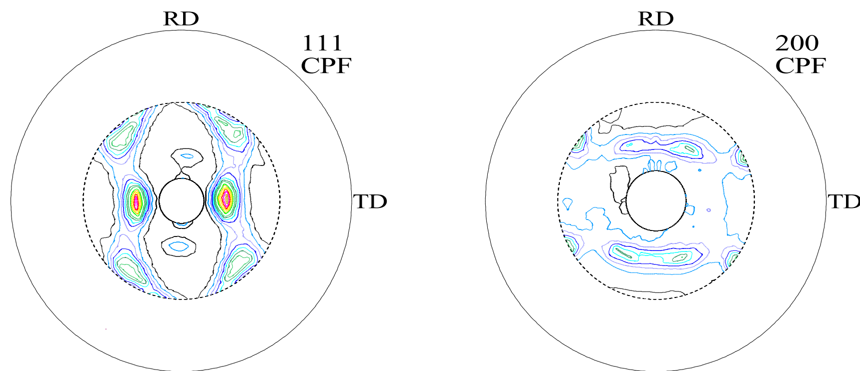

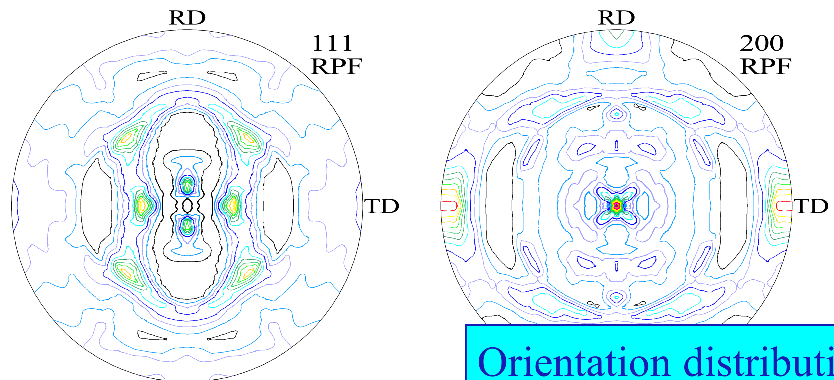

Experimental:
Max.= 8.4, Izolinie: 1, 2, 3, 4, 5, 6

Mathematically transformed:
Max.= 6.8, Izolinie: 1, 2, 3, 4, 5, 6

Calculated (complete):
Max.= 4.9, Izolinie: 1, 2, 3, 4

0 φ_1 90
Φ
90
φ_2 = 0–90
$\Delta\varphi_2$ = 5

Orientation distribution function (ODF) for the near-surface layer of **22µm** thickness, of reference Al sample, obtained by x-ray texture tomography. Calculated of the ODF was made by ADC method using LaboTex software.

Single-layer pole figures with cor[...] procedure for reference Al sample, registered by goniometer (top), mathematically transformed (middle), and calculated from ODF by ADC method (bottom). The *hkl* indices corresponds to the measured reflections.

Texture tomography of HfN layer (thickness of 0.5 μm), deposited on Si (111)-oriented single crystal by the reactive sputtering technique.

Presented texture functions

<u>Averaged texture</u> of HfN layer, obtained by means of the conventional back-reflection pole figures.

X-Ray texture tomography represents a new, non-destructive method of the investigation of the near-the-surface layers of the sample.

It is research tool, which may be applied in the analysis of texture inhomogeneity, its heredity, the control of the process of multi-layered structures etc.

Another possible applications the constant information depth (**CID**) measurement technique:

- deep-profile of phase volume fraction (phase volume tomography)

- deep profile of residual stresses (stress tomography)

Useful methods and the latest achievements in X-ray diffraction

Jan T. Bonarski

X-ray phase analysis

Identification of Fe structure -----> [4 phases: $\alpha, \beta, \gamma, \delta$?]

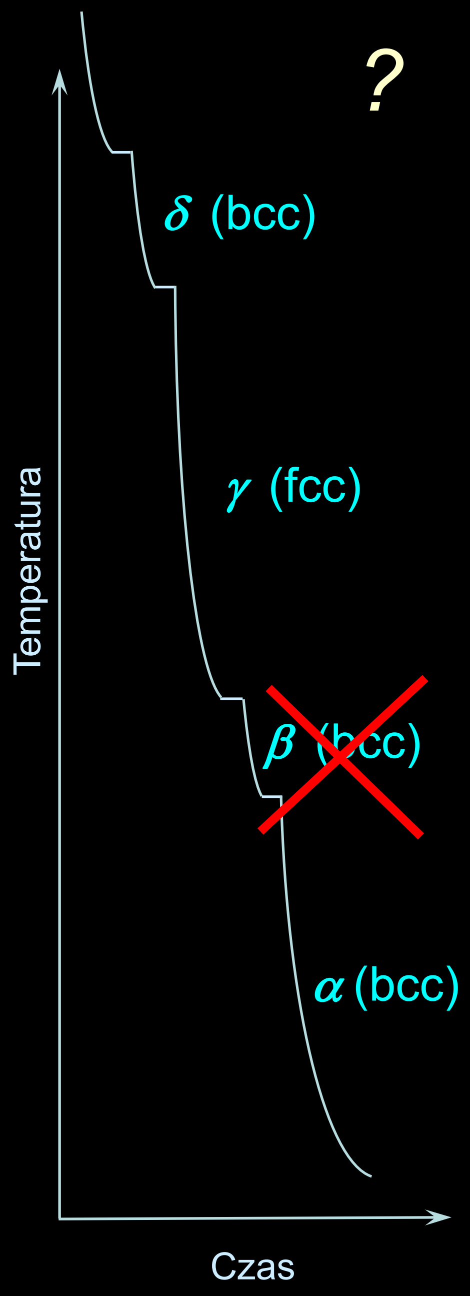

Temperature °F

Temperature °C

γ = Austenite
α = Ferrite
δ = Delta iron
CM = Cementite

A E B

3000, 2802, 2800, 2720, 2600, 2552, 2400, 2200, 2066, 2000, 1800, 1670, 1600, 1400, 1333, 1200, 1000, 410

1539, 1492, 1400, 1130, 910, 760, 723, 210

δ + L

δ

δ + γ

L

γ + L

CM begins to solidiffy

Primary austenite begins to solidify

Austenite in liquid

γ

L + Fe_3C

2066° F

Austenite solid solution of carbon in gamma iron

Austentite ledeburite and cementite

Fe_3C

Magnetic (1414° F) point A_2

A_{CM}

γ + Fe_3C

A_2 A_3

Austenite to pearlite

Cementite and ledeburite

α + γ

1333° F

$A_{1,2,3}$

α

A_1

0.025

Pearlite and ferrite

Pearlite and Cementite

Cementite, pearlite and transformed ledeburite

α + Fe_3C

A_0

Magnetic change of Fe_3C

0.008%

4.3

6.67

0.50, 0.83%, 1%, 2%, 3%, 4%, 5%, 6%, 6.5%

Hypo-eutectoid | Hyper-eutectoid

Steel | Cast Iron

Dwie techniki pomiarów dyfraktometrycznych stosowane szczególnie w badaniach materiałów o strukturze krystaliczno-amorficznej (polimery):

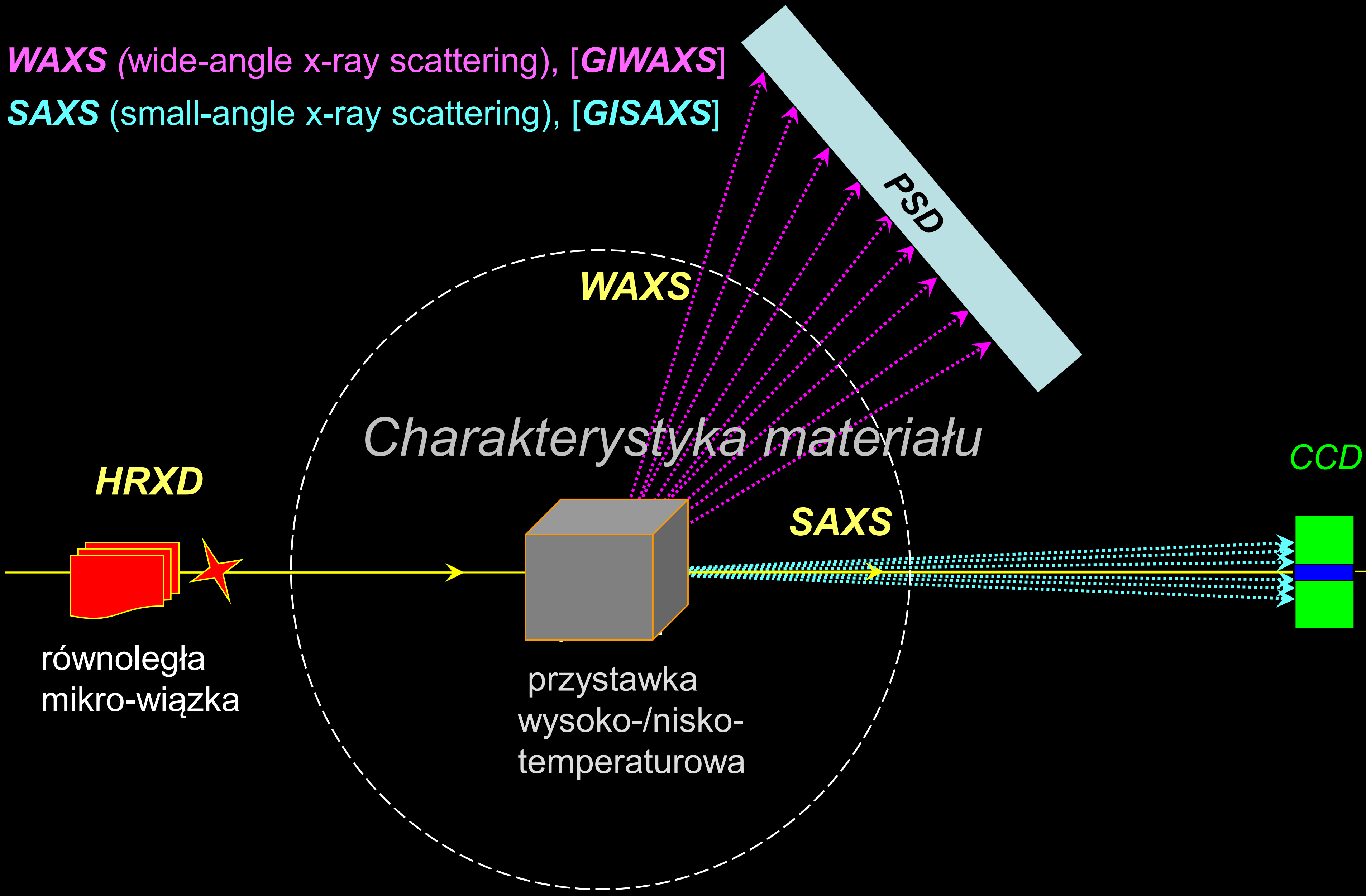

Refleks niesymetryczny **351 Si** w modzie θ-2θ

(udział obj. i rozkład obszarów zamorfizowanych)

(*płaszczyzny {351} nie są pł. symetrii komórki elementarnej*)

← surface

destructed layer

amorphized buried layer

non-destructed bulk of crystal

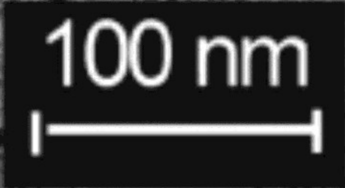

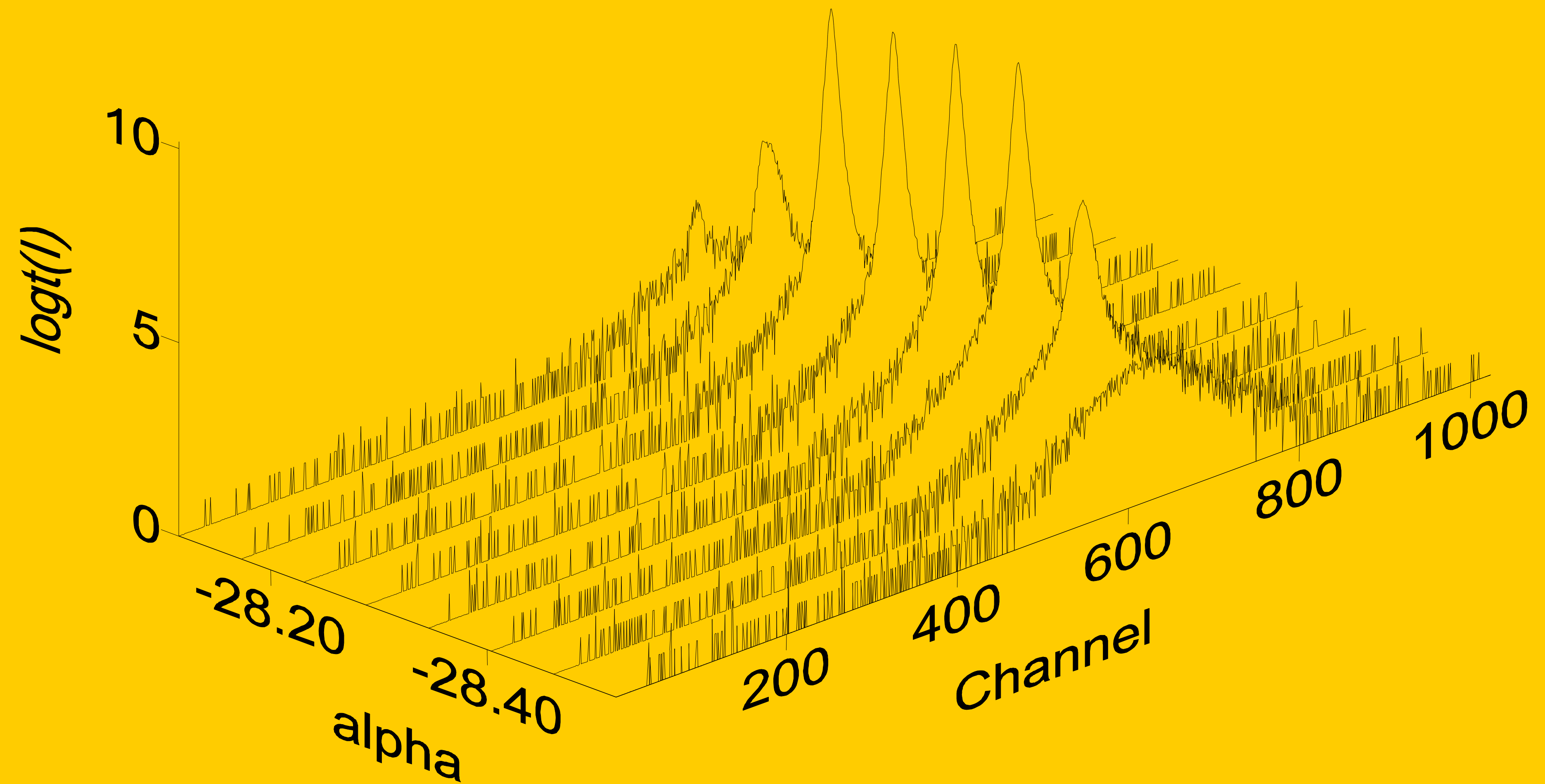

The 3-D distribution of the line profiles intensity (in logarithmic scale) for ***351*** reflection of the ⟨001⟩–oriented Si single crystal solar cell with the buried amorphized and porous silicon layers. Registration was performed for 8KeV synchrotron beam at constant azimuthal angle {*beta*}. [IMIM PAN, Kraków & Synchrotron Lab. *ELETRA*, Trieste, 1999]

mod ***2θ – scan***

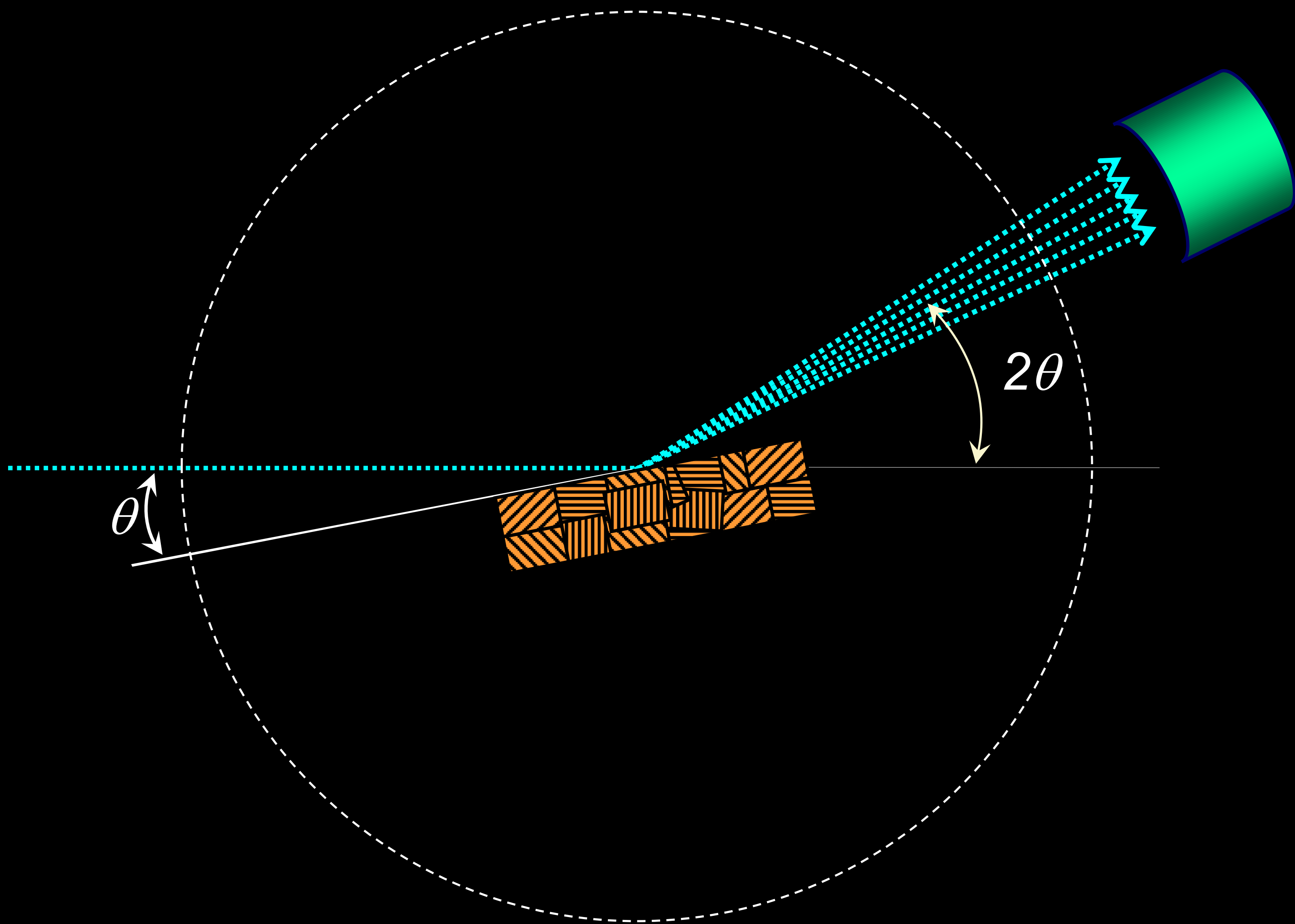

mod **2θ** *– scan*

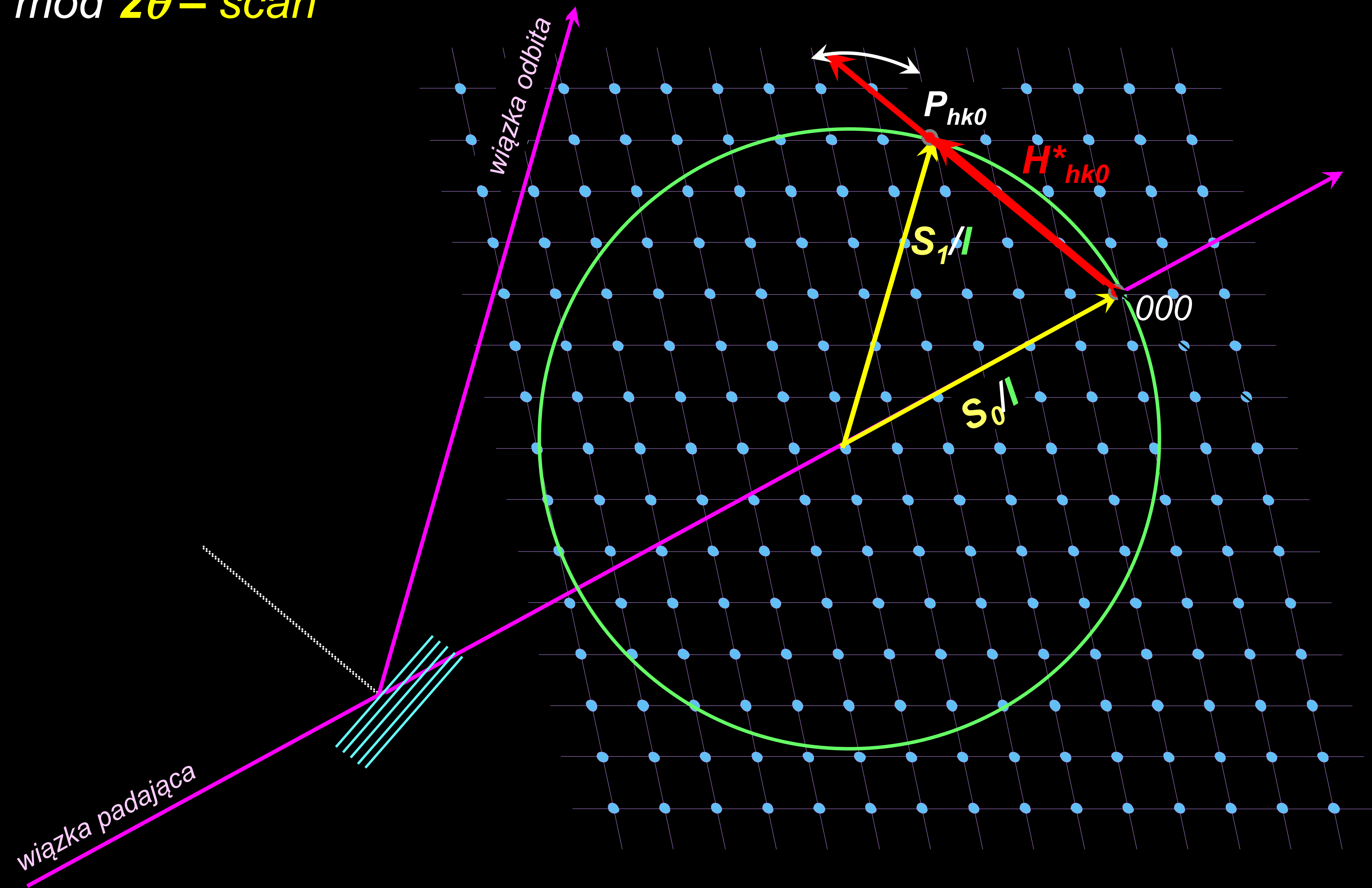

skanowanie sieci odwrotnej po sferze Ewalda

2θ – scan

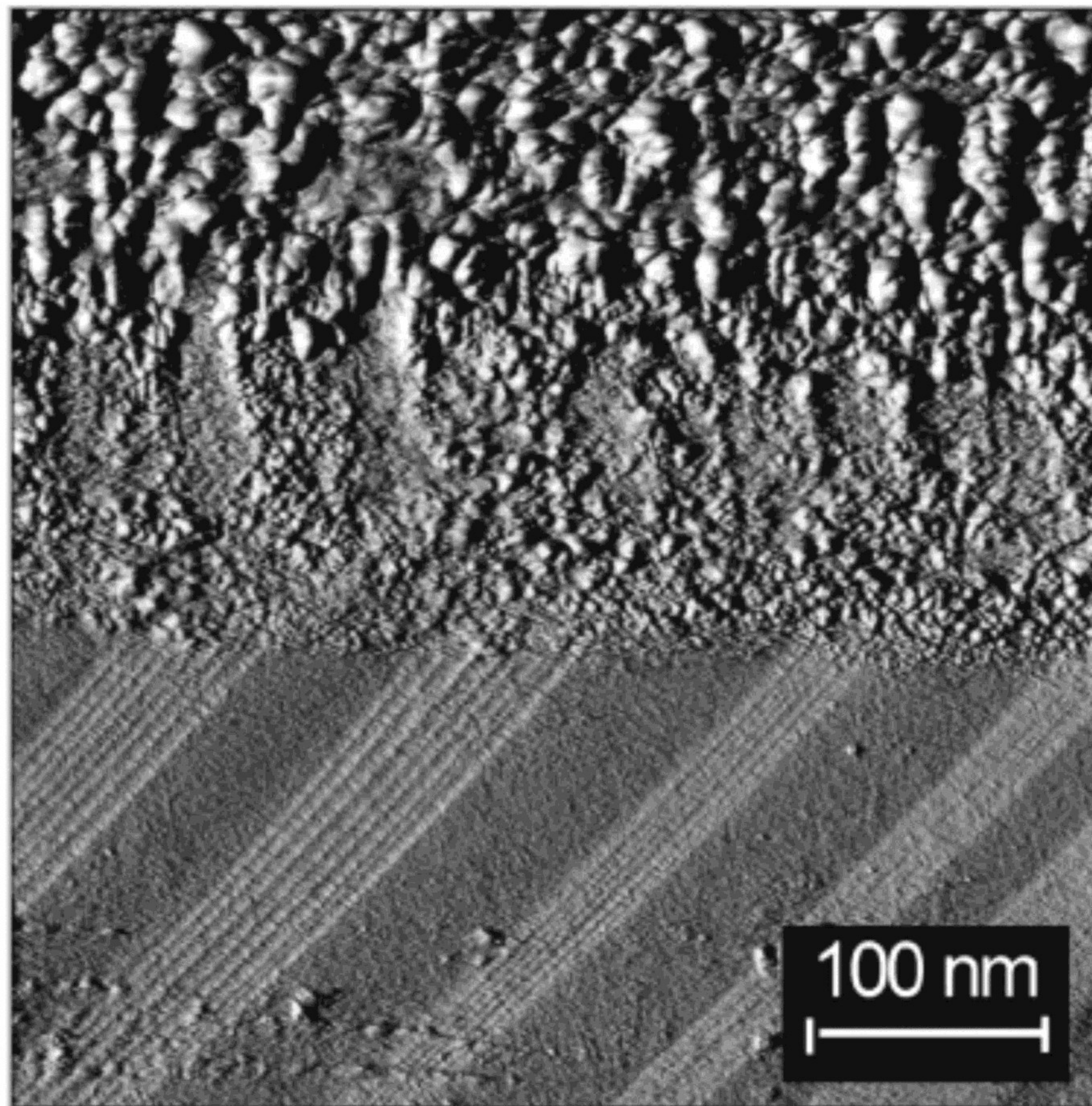

mod ω – scan („rocking curve")

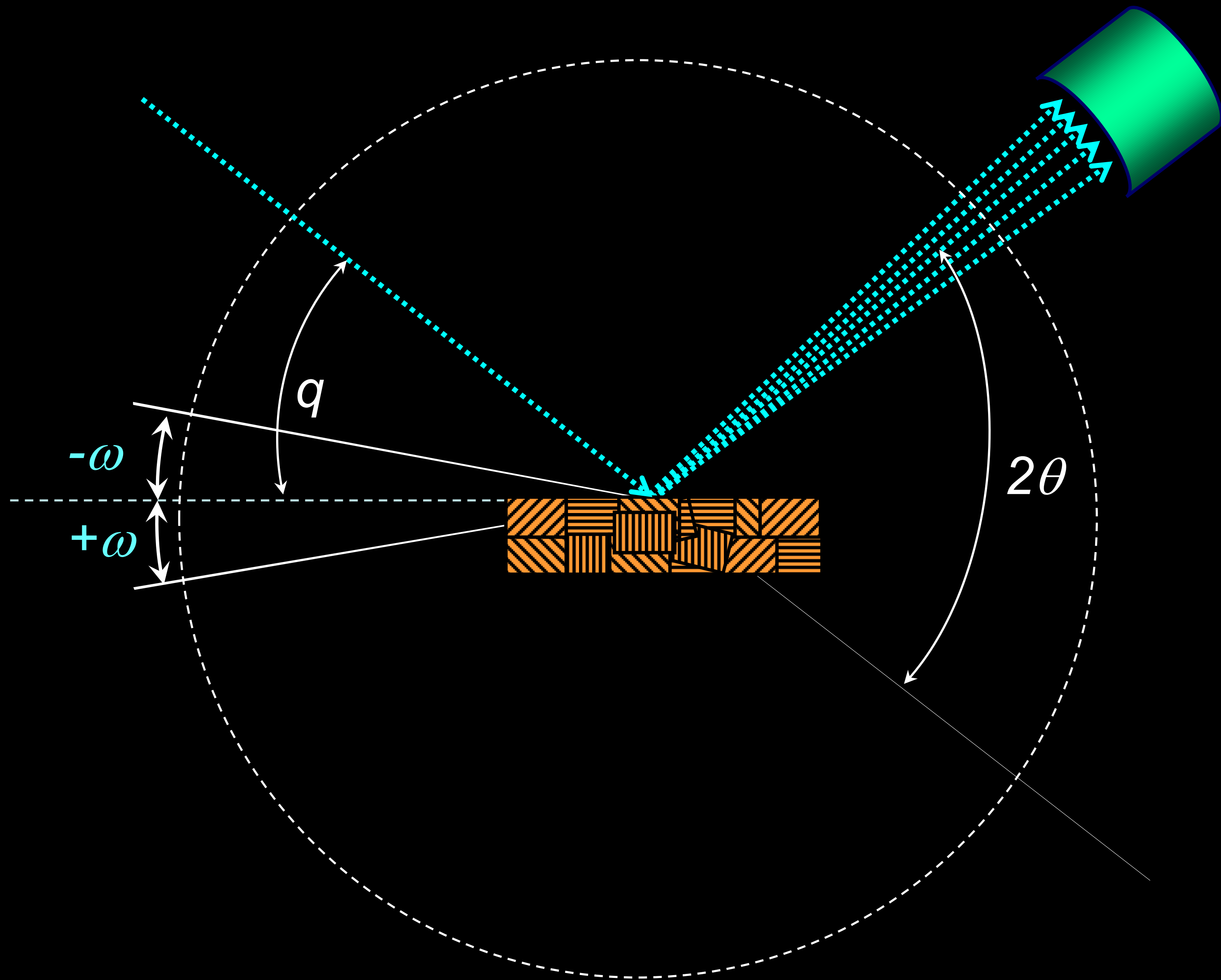

Rocking curve

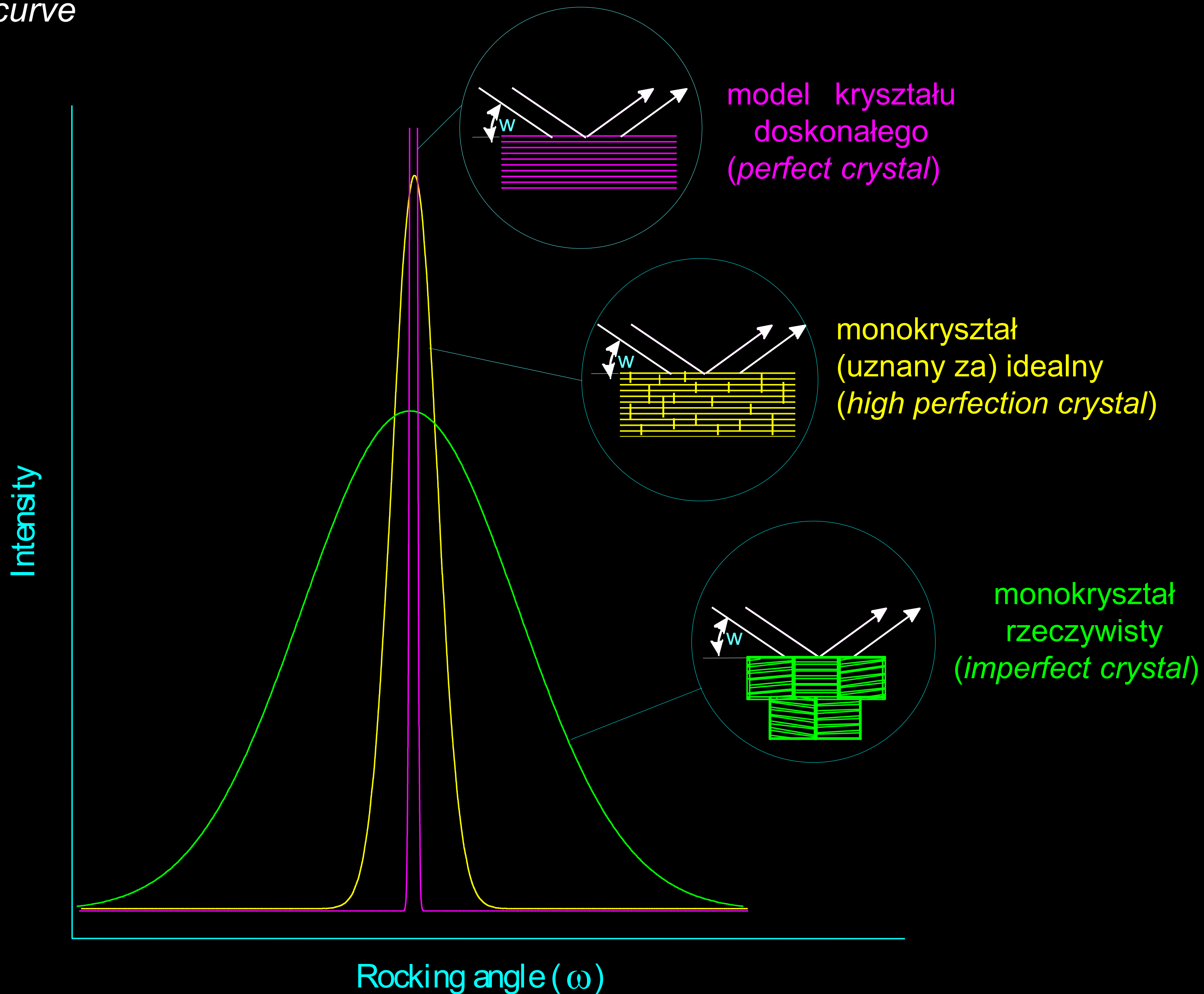

#

Size of crystallites

#

Lattice distortion

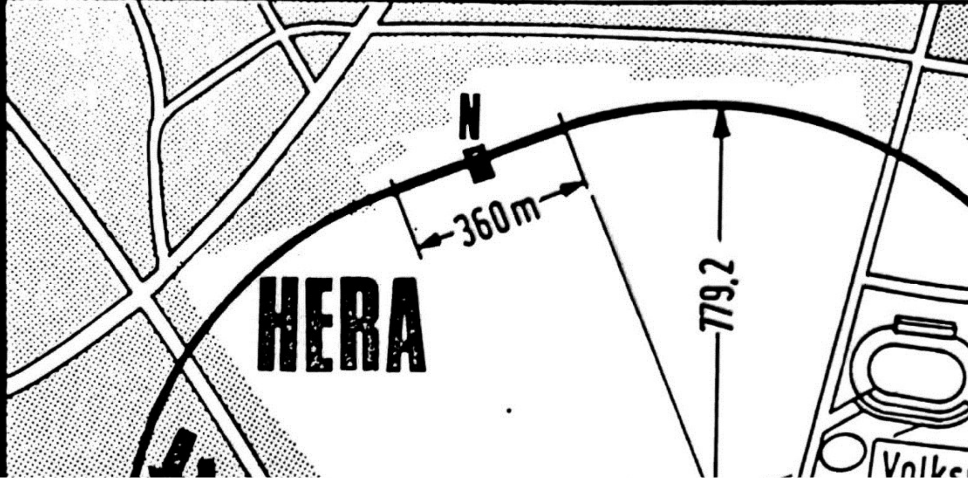

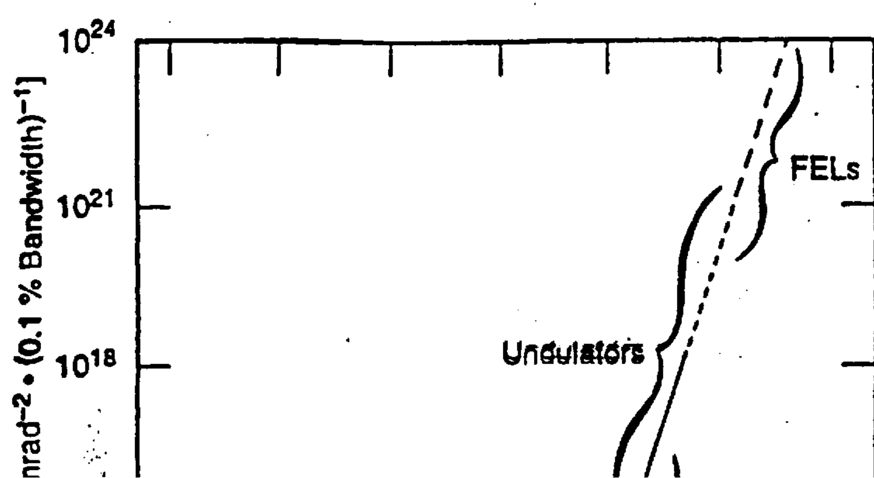

Długość fali [nm]
12,4
1,24
0,124
0,012
ESRF BM
SRS
ESRF wiggler
ADONE
DORIS
DCI
NSLS II
10^{14}
10^{13}
10^{12}
10^{11}
Gęstość strumienia fotonów [s^{-1} $mrad^{-1}$ na przedział energii szer. 0,1 %]
10^{-2}
10^{-1}
10^{0}
10^{1}
10^{2}
Energia fotonów [keV]

Rysunek 2.20
Widma promieniowania synchrotronowego dla następujących źródeł: ADONE (Frascati) – 1,5 GeV; DORIS (Hamburg) – 3,5 GeV; DCI (Orsay) – 1,8 GeV; NSLS II (Brookhaven) – 2,5 GeV; SRS (Daresbury) – 2 GeV; ESRF – 6 GeV. Oznaczenie: *BM* – promieniowanie z zakrzywiających tor elektromagnesów [16]

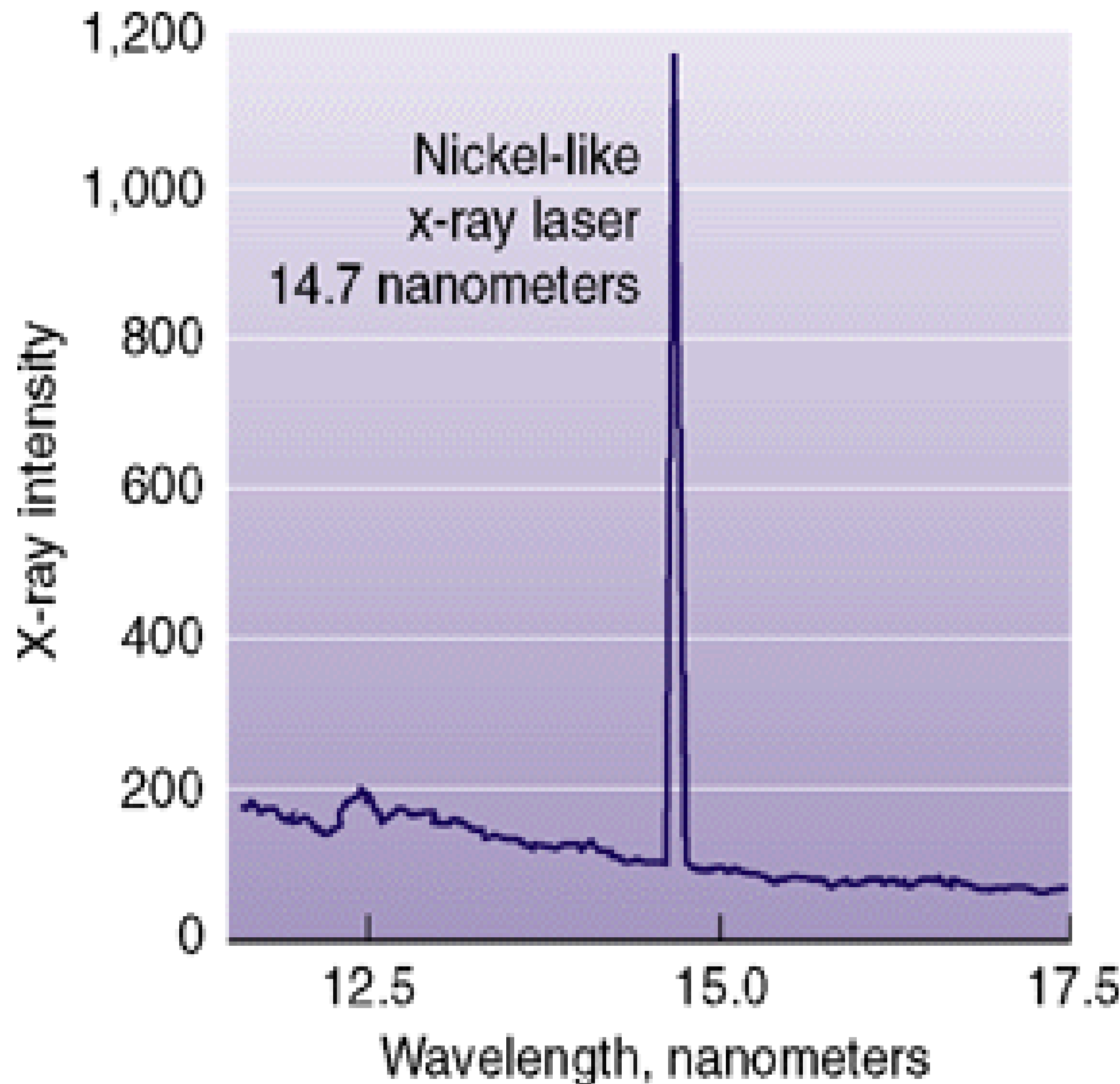

Figure 3. A line out of the emission spectrum from an x-ray laser experiment shows that the 14.7-nanometer x-ray laser line is orders of magnitude brighter than any other emission line.

Rtg. Laser

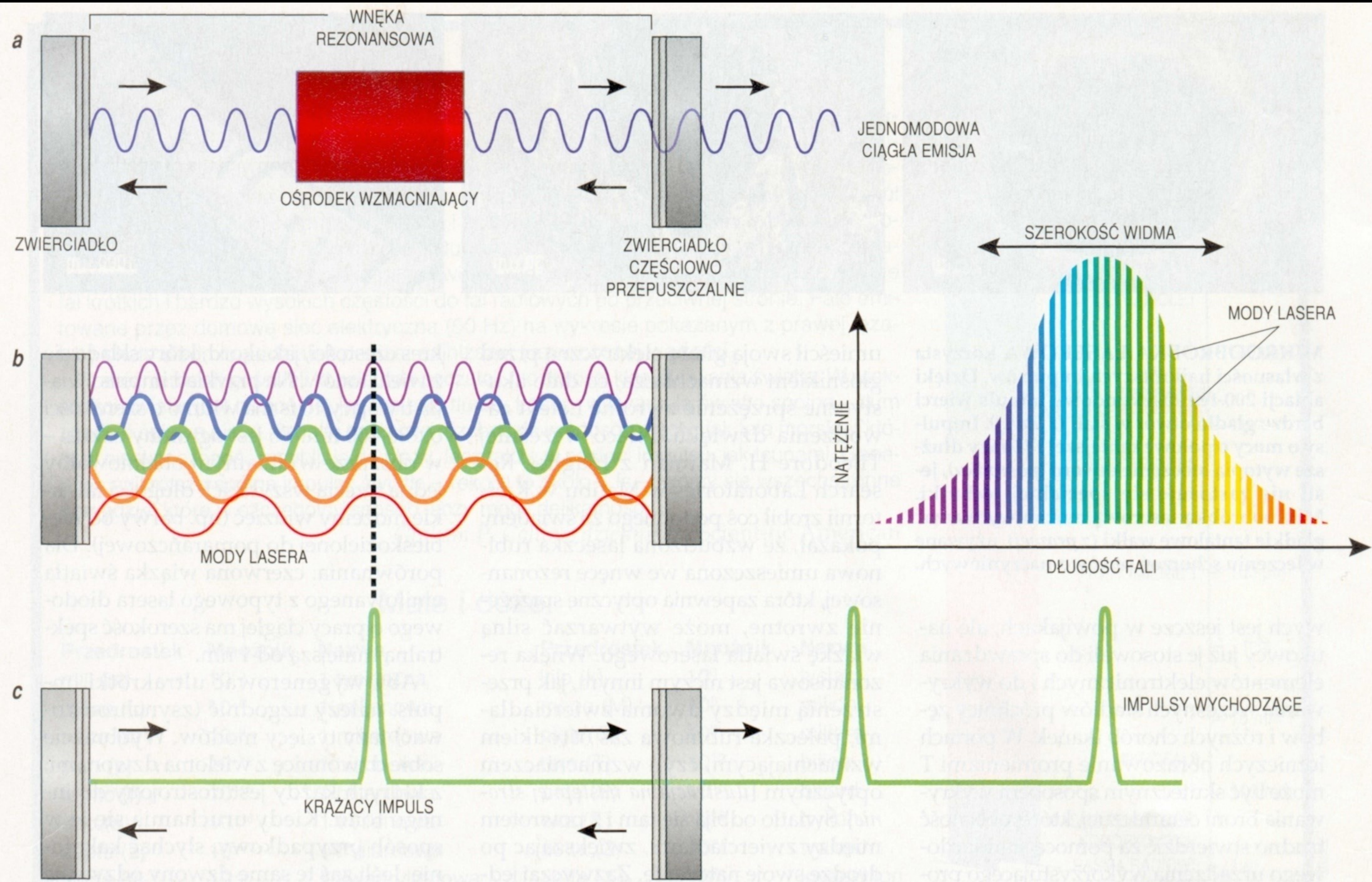

a
WNĘKA
REZONANSOWA
JEDNOMODOWA
CIĄGŁA EMISJA
OŚRODEK WZMACNIAJĄCY
ZWIERCIADŁO
ZWIERCIADŁO
CZĘŚCIOWO
PRZEPUSZCZALNE
SZEROKOŚĆ WIDMA
MODY LASERA
b
NATĘŻENIE
DŁUGOŚĆ FALI
MODY LASERA
c
IMPULSY WYCHODZĄCE
KRĄŻĄCY IMPULS

Wembley National Stadium
Wembley National Stadium
© GMJ 2001
WNSL

Free Electron Laser oznacza **laser na swobodnych elektronach**.

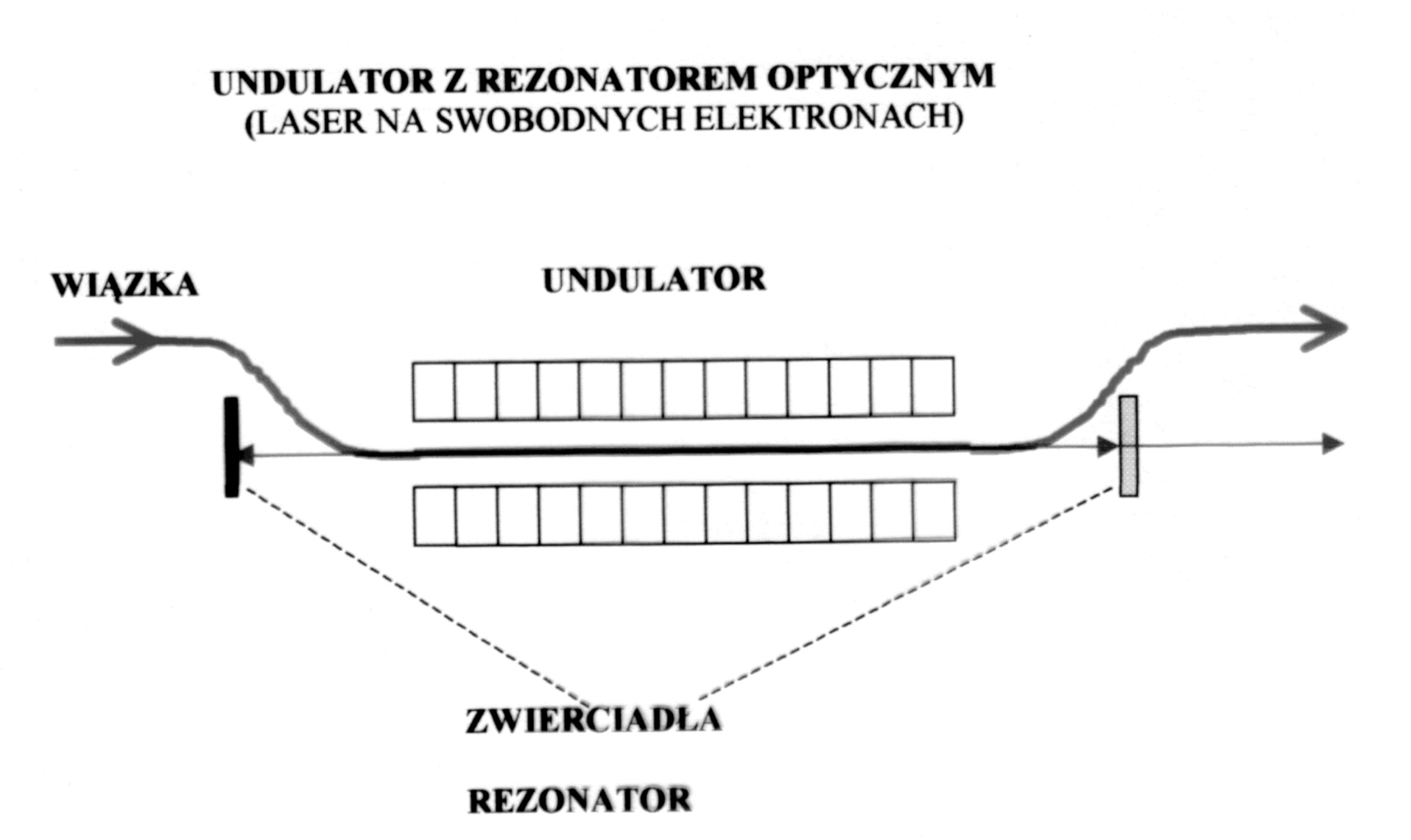

FREE ELECTRON LASERS

LOCATION	NAME	WAVELENGTHS	TYPE
FELI (Japan)	3 2 1 4 5	0.23 - 1.2µm 1 - 6µm 5 - 22µm 20 - 60µm 50 - 100µm	linac
FOM (Netherlands)	FELIX1 FELIX2	5 - 35µm 20 - 110µm	linac
Vanderbilt TN (USA)	MK-III	2.2 - 9.6µm	linac
Duke NC (USA)	MK-III OK-4	1.5 - 9.5µm 340 nm	linac storage ring
Stanford CA (USA)	SCA-FEL FIREFLY	3-10µm 15-65µm	sc-linac
UCSB CA (USA)	FIR-FEL MM-FEL 30µ-FEL	63 - 340µm 340µm - 2.5 mm 30 - 63µm	electrostatic
LURE - Orsay (France)	CLIO Super-ACO	3 - 50µm 350 nm	linac storage ring
ENEA - Frascati (Italy)		1 mm - 600µm	linac
LANL NM (USA)	AFEL RAFEL	4 - 8µm 16µm	linac
Grumman/Princeton NJ (USA)	CIRFEL	8 - 20µm	linac
CEA - Bruyeres (France)	ELSA	18-24µm	linac
ETL - Tsukuba (Japan)	NIJI-IV	350 nm	storage ring
IMS - Okazaki (Japan)	UVSOR	300 nm	storage ring
ILE - Osaka (Japan)		47µm	linac
ISIR - Osaka (Japan)		40µm	linac
Darmstadt (Germany)	IR-FEL	6.8 - 7.8µm	sc-linac
IHEP (China)	Beijing FEL	10µm	linac

ZASTOSOWANIE LASERÓW RENTGENOWSKICH

- Diffraction
  - Magnetism
  - Surface and Interface Science
  - High Pressure Work
  - Material Science
  - Soft Matter
  - Biology
- Nuclear Resonant Scattering
  - Expected Impact
  - Biology
  - Nuclear Physics
- Spectroscopy
  - X-ray Absorption Spectroscopy
  - X-ray Standing Waves
    - Surface Studies
    - Extremely Dilute Systems
  - Atomic Physics
- Scattering
  - Inelastic Scattering from Surfaces, Interfaces and Thin Films
    - Phonons in Thin Films
    - Surface Melting
    - Surface Layering in Liquid Metals: Phonon Spectrum
    - Surface-related Inelastic Precursor of Structural Phase Transitions
  - X-ray Scattering from Laser-induced Charge Densities
  - Inelastic X-ray Scattering Spectroscopy
- Spectroscopy with Coherent X-Rays
  - Status and Applications
    - Dynamics of Disordered Systems
    - Dynamic Structure Factor of Liquids
    - Crystal growth and surfaces
    - Rapid Solidification
    - Structural Studies of Disordered Biological Systems
  - Expected Impact
- Microscopy and Imaging with Coherent X-rays
- Quantum Optics
  - Introduction
  - Examples of Applications
    - Precise Frequency Shifts of X-rays
    - Spontaneous Parametric Conversion of X-ray Photons, Bell's Inequality, Two-photon Interference
    - Spectroscopy on Muonic Hydrogen
    - Nonclassical States of Light
    - Atom Beam Interferometry

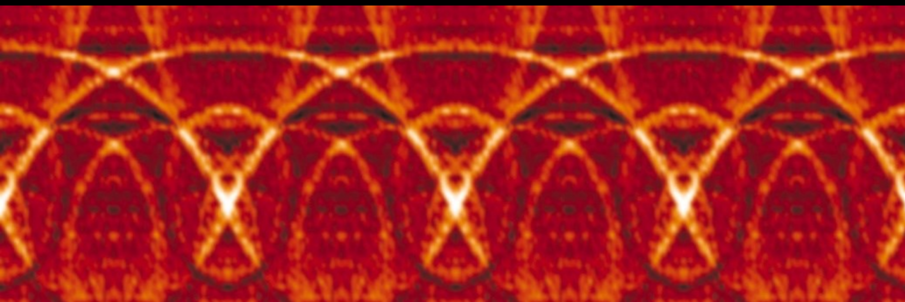

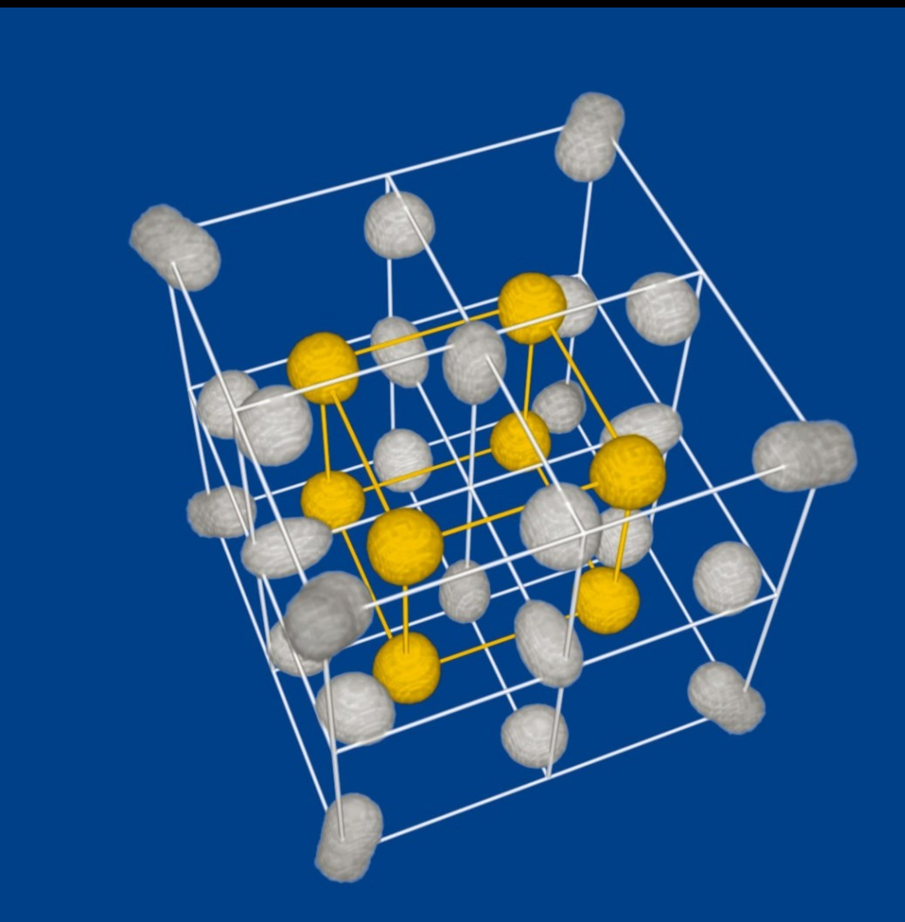

Electron beam
X-ray radiation
Magnetic structures

Storage ring

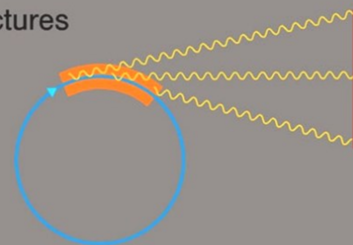

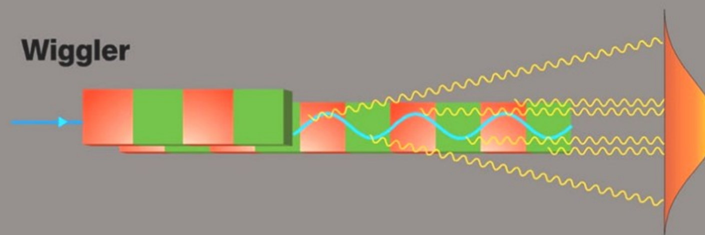

Undulator

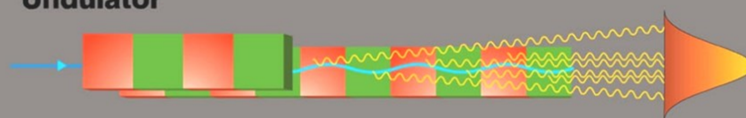

Free electron laser

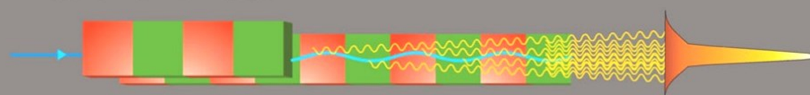

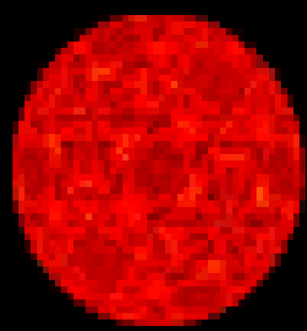

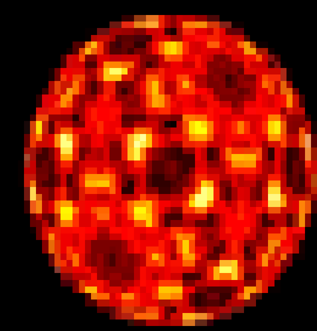

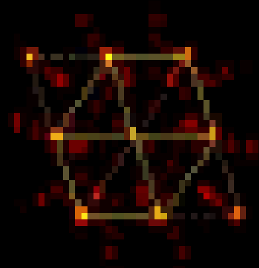

Bibliografia do wykładów

James, R.W. (1954).
The Optical Principles of the Diffraction of X-Rays. London: Bell and Sons Ltd.

Cullity, B.D. (1978).
Elements of X-Ray Diffraction. 2nd Ed., Addison Waseley Publ.Comp.Inc., London, Amsterdam, Don Mills, Sydney,
Podstawy dyfrakcji promieni rentgenowskich. tłum z j. ang., PWN (1964), Warszawa

Bunge, H.J. (1982).
Texture Analysis in Materials Science. Mathematical Methods. Butterworths Publ. London

Sonin, A.S. (1982).
O krystalografii, PWN, Warszawa.

Bojarski, Z., Łągiewka, E. (1988).
Rentgenowska analiza strukturalna, PWN, Warszawa.